STUDIES OF THE SECONDARY COMPONENTS
OF COSMIC RAYS

Thesis presented

by

KALYAN PRASAD SINGHAL

to the

Gujarat University
for the Ph.D. Degree

FEBRUARY 1973

PHYSICAL RESEARCH LABORATORY
AHMEDABAD — 380009,
I N D I A.

STATEMENT

The subject of the time variations of the secondary components of cosmic rays has been extensively studied by a number of workers over the last several years. The nucleonic component is measured by neutron monitors, while the mesonic component at different zenith angles is measured by means of G.M. counter or scintillation counter telescopes.

The coupling constants introduced by Dorman (1957) play a vital role in relating the secondary particles to the primary cosmic rays. Since most of the cosmic rays recorded deep in the atmosphere are secondaries, the precise knowledge of coupling constants is essential to relate any variation in these secondary intensity observations to the corresponding changes in the primary cosmic radiation intensity.

Uncertainties connected with atmospheric nuclear interactions make theoretical estimation of coupling constants rather difficult. However, coupling constants can be derived with the help of geomagnetic (latitude) effects, which are well obtained experimentally. Vertical cut-off rigidity of about 15 GV at equator puts an upper limit for such experimental deter-mination of coupling constants. Beyond 15 GV coupling constants are estimated by extrapolation formulae. The differential response of a neutron monitor falls off quite rapidly beyond 8 GV (Webber and Quenby, 1959; Lockwood and Webber, 1967); consequently the errors due to extrapolation beyond 15 GV are likely to be small. However, the maximum of the response curve of a meson monitor as obtained from the latitude effect data may lie in the region of 15-20 GV. Therefore, the extrapolation beyond 15GV may lead to serious errors (Kane, 1962).

The azimuth effect data recorded by meson telescopes at different azimuth angles corresponding to a fixed zenith angle assumes greater significance because of its ability to provide coupling constants in the range 10-25 GV. However, it must be kept in mind that for the same location coupling constants for vertical and inclined directions are not directly comparable, as the latter correspond to muons having traversed more air material and consequently will have a flatter coupling constant-rigidity plot. Nevertheless, such measurements can provide a direct clue to the shape of the response curve for the 10-25 GV range. Kane (1962) showed that the azimuth effect data available till then were not sufficiently accurate for this purpose and there was a need for more accurate azimuth effect measurement.

An experiment to study azimuthal variation of cosmic ray muon intensity has been conducted at Ahmedabad. The apparatus consisted of two independent triple coincidence G.M. counter telescopes. The telescopes were inclined at 45° to the zenith and were 180° apart in azimuths. The whole apparatus was mounted on a turn-table, capable of rotating about a vertical axis. Thus, the telescopes could be kept at any desired azimuth angle.

The author took the complete responsibility of running the azimuth effect experiment in 1968. The observations were taken on a continuous basis during the period 1967-69 for fourteen different directions well spread over all azimuths. The data have been analysed by the author on an IBM 1620 computer at the Physical Research Laboratory, Ahmedabad. The results obtained are presented in the thesis and their implications discussed.

A theoretical attempt based on a model of secondary meson production in the atmosphere by high energy primaries has been made by the author to get a best fit for all the experimental data on latitude and azimuth effect available so far for several zenith and azimuths (part of these obtained by the author as mentioned above) and atmospheric depths. It must be noted that at any latitude nearly 26% of the primary nucleons are alpha particles (or heavies) and have a cut-off only at $E_C/2$, where E_C is the cut-off (in terms of momentum per nucleon) for protons; hence, an appropriate correction for this effect is also incorporated in our calculations. Theoretical calculations have been carried out and coupling constants thus obtained for several zenith angles and atmospheric depths are also presented in the thesis.

Experimental determination of the _charge_ ratio of cosmic ray muons at different energies is also of considerable interest; because such measurements reflect the nature and multiplicities of the parent particles produced in the primary interactions. Such measurements at high energies are of greater significance because the information gained by these measurements cannot be obtained with the present day accelerators. However, the intensity falls quite fast with the energy and the statistically significant observations become rather difficult. At low energies ($E_\mu < 1$ GeV), the usual method of magnetic momentum spectrograph for the determination of the spectrum and the charge ratio of cosmic ray muons cannot be applied because of the large percentage of electrons present in the observed radiation. However, the method of delayed coincidence can be used to distinguish muons from other ionizing radiation and to separate positive muons from negative ones.

An experiment to determine the charge ratio of muons based on the method of delayed coincidences has been conducted by the author at Ahmedabad. The apparatus consists of three scintillation counters. Muons in a certain momentum range are brought to rest in an absorber and their decay products electrons are registered in different time channels. The distribution of electrons registered in different time channels serves as a check on the operation of the equipment, since the mean life of muon is known to be about 2.2 microsecond. Two different absorbers, one of high atomic number (lead) and another of low atomic number (graphite), were used as stopping materials. Both positive and negative muons decay freely in the latter absorber while only positive muons decay in the former absorber. The observations were taken during the period 1971-72. The author was responsible for the fabrication, setting-up and maintenance of the muon telescope for the determination of the charge ratio. The author was mainly responsible for the development of the entire electronics circuitry associated with the experimental set-up.

The data reduction was done by the author on IBM 1620 and System/360 computers at the Physical Research Laboratory, Ahmedabad. The results of charge ratio, differential spectrum and integral spectrum of cosmic ray muons in the momentum range (0.2-0.8 GeV/c) obtained by the author are also included in the thesis. Muon momentum has been calculated by the author using the energy loss expression of Sternheimer (1956).

The thesis is divided into six chapters as follows:-

The first chapter contains a brief review of the present knowledge about the primary and the secondary cosmic rays. The concept of coupling

constants and estimation of coupling constants from latitude effect and azimuth effect data are also dealt briefly. The significance of the charge ratio measurements is also shown.

The second chapter gives the experimental details for (a) the azimuth effect experiment, and (b) the charge ratio experiment carried out at Ahmedabad. Various electronic circuits used are described briefly. The operational procedure has also been described for both the experiments.

The third chapter describes the methods used in processing the data and the results obtained from the experiments. The results are mainly the azimuth effect recorded with inclined telescopes and coupling constants derived from it. The muon telescope for the charge ratio measurement was useful in providing new results on differential and integral momentum spectra, charge ratio and mean life of muons. Also included in this chapter is a brief description of the models of charge ratio of muons.

The method of estimating coupling constants theoretically is described in detail in the fourth chapter. Integration limits and implications of some of the parameters are also discussed.

Coupling constants theoretically derived are presented in the fifth chapter for different zenith angles and different atmospheric depths. Our theoretical results are compared with the latitude effect and azimuth effect data available so far.

The sixth chapter summarises the results obtained and the conclusions drawn from the present investigation.

The thesis, presents new results on the coupling constants for several zenith angles and atmospheric depths, gives a theoretical method to obtain coupling constants (for all energies) which would prove useful for a proper interpretation and understanding of the phenomenon of time variation of cosmic ray intensity.

(R.P. KANE)

24-2-1973

(K.P. SINGHAL)

ACKNOWLEDGMENTS

I am also thankful to all others who helped me directly or indirectly to bring this work in the present shape.

The financial support received from the Ministry of Education and Dept. of Atomic Energy, Government of India and recently from Department of Space, Government of India is gratefully acknowledged.

Last, but not the least, I greatly appreciate the cooperation and the moral support of my wife throughout this work and also I am deeply indebted to my parents for their constant interest and encouragement.

(K.P. Singhal)

C O N T E N T S

C H A P T E R - I

I N T R O D U C T I O N

1.1 Composition of the primary cosmic rays

Cosmic rays, since their discovery in 1913, have been studied primarily as a natural beam of high energy particles. Cosmic rays are found to be highly isotropic and contain fluxes of energetic nuclei with energies ranging from 10^8 eV to 10^{20} eV.

A number of experiments have been carried out to determine the charge spectrum of the primaries i.e. the relative number of protons, alpha-particles, Li-nuclei etc. Nuclear emulsions, cloud chambers, scintillation and proportional counters have been extensively used for such experiments. The detector determines the ionization of the primary, from which the charge of the nucleus is found. Since most of these particles are relativistic, the ionization is simply proportional to z^2 i.e. the square of the atomic number.

These measurements have shown that these particles are atomic nuclei belonging to various chemical elements (Bradt and Peters, 1948; 1950 a, b). These nuclei are completely ionized much before they enter the earth's atmosphere. The primary cosmic radiation is mainly composed of about 90 per cent protons, 9 per cent helium nuclei and about 1 per cent heavier nuclei. Electrons of energies greater than 1 GeV constitute about 1 per cent of the primary cosmic rays.

Chemical composition of the nuclear part of the cosmic radiation has been measured at several energies. The relative abundance of different

elements appears to be independent of energy upto at least a few hundred GeV per nucleon. Recent observations are included in the reviews by Webber (1967), Shapiro and Silberberg (1970).

1.2 The secondary cosmic rays

The earth's atmosphere is being continuously bombarded by an almost isotropic flux of highly energetic primary cosmic ray particles. The earth's atmosphere consists mainly of the gases nitrogen and oxygen which exert a pressure at sea level of about 1000 gm/cm^2. The primary cosmic radiation undergoes both electromagnetic and nuclear interactions in the atmosphere.

When a nucleon strikes a nucleus, many possibilities arise, the actual process depending on the energy of the nucleon, the size of the nucleus etc. The various possible processes are divided into two categories.

(a)   Absorption, and

(b)   Scattering.

The latter can be subdivided into elastic and inelastic scattering. In elastic scattering, momentum and kinetic energy are conserved, while in the case of inelastic scattering some of the kinetic energy of the incident nucleon is absorbed by the nucleus thereby raising the nucleus to an excited state, which, when reverting back to the ground state, emits this energy in the form of γ-rays, α-particles etc. by the so-called evaporation process. If the energy of the incident nucleon is sufficiently high, new particles (mesons) may be generated in a collison with an individual nucleon in the nucleus. Mesons are

charged as well as neutral and consist predominantly of π -mesons with a small percentage of K-mesons.

The π -mesons are unstable and rapidly decay into other particles. Neutral π -mesons decay, within a very short life time ($\sim 2 \times 10^{-16}$ sec), predominantly into two photons which by creation of electron-positron pairs initiate an electromagnetic cascade.

$$\pi^0 \rightarrow 2\gamma$$
$$\gamma \rightarrow e^+ + e^-$$

The charged π -mesons decay mostly into a muon and a neutrino with a life time of about 2.55×10^{-8} sec.

$$\pi^+ \longrightarrow \mu^+ + \nu_\mu$$
$$\pi^- \longrightarrow \mu^- + \overline{\nu_\mu}$$

Muons are produced in several of K-meson decays too. In the rarefied material of the atmosphere the decay of $\pi^{\pm}$-mesons is much more likely than a nuclear interaction. Only if the life time is greatly dilated by relativistic effects will nuclear interactions occur with appreciable probability. For a given energy this probability is larger in the dense lower regions of the atmosphere than in the rare upper regions.

Muons have no specific nuclear interaction with matter. At low energies ($E_\mu < 100$ GeV) ionization energy loss predominates. A muon decays with a mean life of about 2.2 microseconds into an electron (or positron) and two neutrinos.

$$\mu^+ \rightarrow e^+ + \nu_e + \overline{\nu_\mu}$$
$$\mu^- \rightarrow e^- + \overline{\nu_e} + \nu_\mu$$

However, the life time is greatly dilated by relativistic effects for muons of a few GeV energy resulting in a very small probability of muon decay before reaching the earth's surface. The decay probability increases at larger angles to the zenith (vertical) because of the increased path length available.

The main component of cosmic rays in the atmosphere are (see Figure 1.1):

(a)   A Nuclear component containing particles capable of producing nuclear collisions. This component contains mostly nucleons; the fraction of pions in it increases with increasing depth in the atmosphere. Nucleonic component is detected with a neutron-monitor.

(b)   An Electron-photon (or soft) component which arises mainly from the decay of neutral pions which are produced in nuclear collisions. It attains a maximum at about 13 km altitude; most of it dies out, however, before reaching earth's surface. This component is detected by extensive air shower arrays.

(c)   A Muon (or penetrating) component which owes its origin mainly to the production of $\pi^{\pm}$-mesons in nuclear collisions. Muons do not multiply like electrons. At sea level muons account for about 80 per cent and electrons about 20 per cent of charged particles. This component is detected by meson telescopes.

(d)   A Neutrino component which arises from the decay of unstable particles in the atmosphere, mostly pions and muons. Neutrinos have only weak interaction with matter and are capable of passing through the earth without any appreciable attenuation.
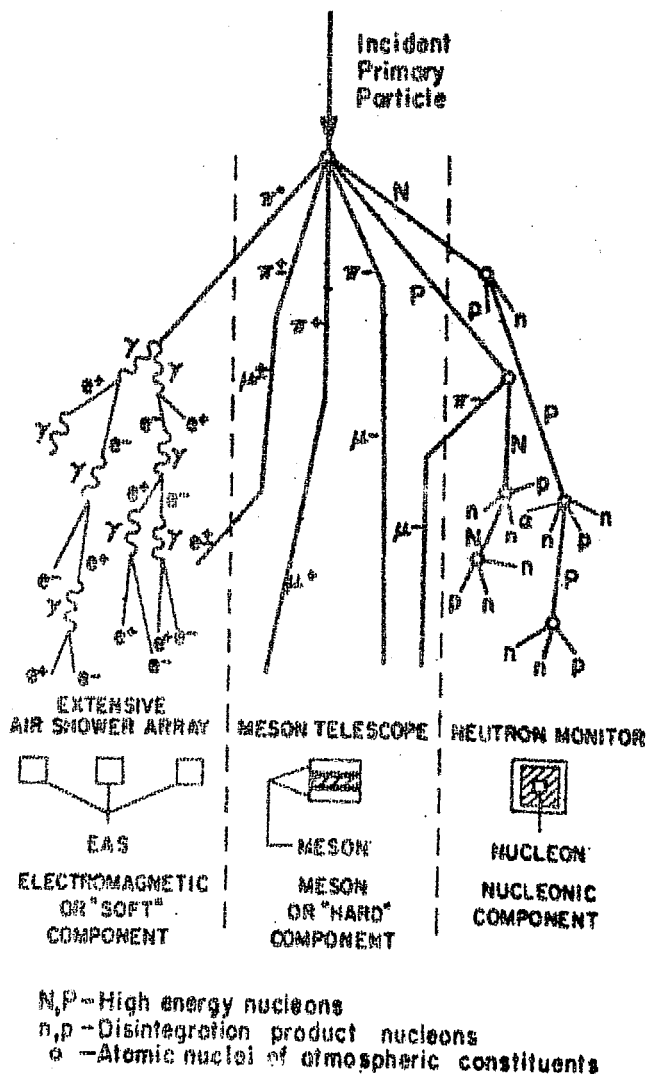
Figure 1.1   Schematic representation of the various modes, whereby an incident cosmic ray primary propagates its effects through the atmosphere down to ground level. The three types of detector respond to primaries with increasingly higher energies from right to left in this diagram. (After Pomerantz, 1970).

1.3   The influence of the earth's magnetic field

Charged cosmic ray particles are affected by the earth's magnetic field long before they enter the atmosphere. To a first approximation earth's magnetic field can be represented by a dipole of magnetic moment $M = 8.1 \times 10^{25}$ gauss-cm^3, situated at the centre of the earth and tilted such that the magnetic axis intersects the earth's surface at a geographical latitude of $78.2^{\circ}N$ and a geographic longitude of $69.0^{\circ}W$. A better approximation is that of a shifted dipole. In 1955, the eccentric dipole was situated 433 km from the centre of the earth at $15.3^{\circ}N$ latitude and $151.1^{\circ}E$ longitude (Webber, 1958).

The magnetic rigidity of a particle is the ratio of its momentum to charge i.e. pc/ze and has the dimensions of voltage. It is usually written in units of GV, equal to 10^9 volts. It is numerically equal to p/z if p is expressed in GeV/c.

1.3.1 The threshold rigidity

Störmer (1955) has made an extensive study of the motion of charged particles in a dipole field in connection with his work on auroral particles, and his approach has been applied to the motion of charged cosmic ray particles in the geomagnetic field. Negatively charged particles having different rigidities are shot from the earth and their motion in the earth's magnetic field is followed analytically. Particles which succeed in escaping to "infinity" correspond to positive particles approaching the earth from great distances. At a given point on the earth, for a given direction, the minimum rigidity for which the orbits connect with infinity is the threshold rigidity.

Störmer found the following analytical integral of the equation of motion which describes particle trajectories in the meridian plane containing the moving particle and the dipole axis:

$$2\gamma = R \cos\lambda \, \sin\xi + \frac{\cos^2\lambda}{R} \qquad \ldots\ldots(1.1)$$

where γ is a constant proportional to the particle impact parameter about the dipole axis at large distance, λ is the geomagnetic latitude and ξ is the angle between the velocity vector and the meridian plane and is taken positive if this plane is crossed from east to west. R is the radial distance measured in Störmer units where one Störmer unit is defined as $\sqrt{\frac{M}{p}}$ (M = the dipole moment). Thus, the scale of distance is rigidity dependent.

For a given λ and ξ, the minimum value of R is obtained by putting $\gamma = 1$ and this is

$$R_m = \frac{\cos^2\lambda}{1 + \sqrt{1-\sin\xi \, \cos^3\lambda}} \qquad \ldots\ldots(1.2)$$

The cutoff rigidity P_c is obtained by putting R_m equal to the radius of the earth (measured in Störmer units), which gives

$$P_c = \frac{M}{a^2} R_m^2 = 59.6 \frac{\cos^4\lambda}{\left[1 + \sqrt{1-\sin\theta \, \cos\phi \, \cos^3\lambda}\right]^2} GV \qquad \ldots\ldots(1.3)$$

In equation (1.3), a is the radius of the earth and $\sin\xi$ has been replaced by $\sin\theta \, \cos\phi$, where θ and ϕ are the conventional zenith and azimuthal angles of incidence.

The vertical threshold rigidity is obtained from (1.3) as,

$$P_c = 14.9 \cos^4\lambda \, GV \qquad \ldots\ldots(1.4)$$

According to Störmer theory, all particles above the threshold rigidity can reach from infinity to the given point from the given direction. If the cosmic ray intensity is isotropic at infinity, then from Liouville's theorem all these particles will arrive with their full intensity.

The simple theory outlined so far takes no account of the effect of the impenetrable earth. Vallarta and his colleagues have shown after detailed integration of trajectories of particles just above the threshold, that some trajectories intersect the earth elsewhere before arriving in a direction allowed by Störmer theory (Vallarta, 1961). These penumbral trajectories contain loops representing a turning away from and a turning towards the dipole. An appropriate correction to the threshold can be applied knowing the penumbral width.

An additional effect of the solid earth is that even uncomplicated trajectories, arriving at zenith angles close to the horizon, may be intercepted. This effect gives rise to the simple shadow correction and has been investigated for sea level and satellite altitudes by Kasper (1960). Kodama et al. (1957) have calculated the Störmer thresholds appropriate to the eccentric dipole.

1.3.2 Higher order terms correction to the threshold rigidities

In a neutron monitor latitude survey, Rose et al. (1956) noted that at a longitude of $30^{\circ}W$ the minimum in cosmic ray intensity was 9° north of its expected position on the geomagnetic equator. Other experiments further confirmed the discrepancy between the observed cosmic ray intensity and that expected from the dipole representation of the

geomagnetic field. It was originally suggested by Simpson et al.(1956) that the interaction between the geomagnetic field and the interplanetary plasma results in the distortion of the field which may account for the discrepancy. However, Rothwell and Quenby (1958) showed that these discrepancies are due to the non-inclusion of the non-dipole part of the geomagnetic field.

The geomagnetic potential V may be represented by a series of spherical harmonics.

$$V(r, \theta, \phi) = a \sum_{n=1}^{\infty} \sum_{m=0}^{n} (a/r)^{n+1} (g_n^m \cos m\phi + h_n^m \sin m\phi) P_n^m (\cos\theta) \quad \ldots\ldots(1.5)$$

where a is the radius of the earth, r is the distance from the centre of the earth, θ is the geographic co-latitude, ϕ is the geographic longitude, g_n^m and h_n^m are Gauss coefficients and $P_n^m (\cos\theta)$ are associated Legendre functions. The term n = 1 in this series corresponds to the centered dipole, tilted relative to the geographic axis. Quenby & Webber(1959) corrected the Störmer threshold rigidities by including non-dipole terms upto sixth harmonic. Using these revised thresholds a better fit was obtained to the measured cosmic ray equator. Quenby & Wenk (1962) further improved the rigidity calculation by including a penumbral correction. McCracken (1962) has developed a widely used programme for trajectory integration. Using this programme, Kondo et al. (1963) have obtained a still better fit between the nucleonic intensity and the thresholds. Shea et al. (1965) calculated the cutoff rigidities for different stations using McCracken's programme.

1.4 Relationship between primary cosmic rays and their secondary components

Time variations in the intensity of cosmic radiation arriving at the earth's surface have been extensively studied over the last several years. Most of the cosmic rays observed deep in the atmosphere are of secondary origin. Therefore, it becomes necessary:

(a) to understand how to relate these secondary particles to the primary cosmic rays, and

(b) to be able to follow the primary particles along their trajectories through the geomagnetic field out into interplanetary space.

Various attempts have been made for relating the secondary particles to the primary cosmic rays. Neher (1952) introduced the concept of "overall multiplicity" M(E,h) that gives the number of secondary particles produced at a depth h due to a primary particle of energy E. Treiman (1952) and Simpson et al. (1953) extended the idea to calculate the specific yield function for the nucleonic component. These were used by Fonger (1953) to connect the variations in the secondary components with variations in primary intensity.

1.4.1 Coupling constants

The idea of coupling constants was introduced by Dorman (1957). Dorman expressed the intensity N_λ^i (h) of a secondary component of type i (nucleons, mesons) at a latitude λ and at an atmospheric depth h as

$$N_\lambda^i (h) = \int_{E_\lambda^c}^{\infty} D(E) M^i(E,h) dE \qquad \ldots\ldots (1.6)$$

where D(E) is the primary spectrum and $M^i(E,h)$ is the multiplicity function that gives the number of secondary particles of type i produced at an atmospheric depth h due to a primary particle of energy E. E_λ^c is

the minimum energy necessary for the arrival of primaries at a latitude λ. It is a function of zenith and azimuth angles also.

Varying $N_\lambda^i(h)$ with respect to the parameters appearing on the right hand side of (1.6) we get

$$\delta N_\lambda^i(h) = -\delta E_\lambda^c \, D(E_\lambda^c) \, M^i(E_\lambda^c, h) + \int_{E_\lambda^c}^{\infty} \delta D(E) M^i(E,h) \, dE$$
$$+ \int_{E_\lambda^c}^{\infty} D(E) \, \delta M^i(E,h) \, dE \qquad \ldots\ldots(1.7)$$

dividing by $N_\lambda^i(h)$, we get

$$\frac{\delta N_\lambda^i(h)}{N_\lambda^i(h)} = -\delta E_\lambda^c \, W_\lambda^i(E_\lambda^c, h) + \int_{E_\lambda^c}^{\infty} \frac{\delta D(E)}{D(E)} W_\lambda^i(E,h) dE$$
$$+ \int_{E_\lambda^c}^{\infty} \frac{\delta M^i(E,h)}{M^i(E,h)} W_\lambda^i(E,h) \, dE \quad \ldots\ldots(1.8)$$

where
$$W_\lambda^i(E,h) = \frac{D(E) \, M^i(E,h)}{N_\lambda^i(h)} \qquad \ldots\ldots(1.9)$$

is called the "coupling constant",

so that
$$\int_{E_\lambda^c}^{\infty} W_\lambda^i(E,h) \, dE = 100 \text{ per cent} \qquad \ldots\ldots(1.10)$$

The "coupling constant" gives the percentage contribution of primaries of energy E to the secondary component of type i at an atmospheric depth h at a latitude λ. Hence, the precise knowledge of the coupling constants is essential in predicting the response of a detector deep in the atmosphere to any variation in the primary energy spectrum.

The first term on the right hand side of equation (1.7) represents secondary variations due to variations in the cut-off energy E_λ^c. The second term gives the variation of secondary intensity due to variations

in the primary spectrum $D(E)$. The third term gives changes due to variations in the multiplicity function which may be due to meteorological factors.

The role, which coupling constant W of equation (1.9) plays in connecting variations of a secondary component with those of primary intensity, is thus obvious. W is a function of the primary spectrum $D(E)$ and the multiplicity function $M(E,h)$. Hence, to estimate W theoretically these functions should be known. Multiplicity function $M(E,h)$ is difficult to calculate because of uncertainties connected with secondary processes. Hence a theoretical calculation of W is rather difficult.

1.4.2 Estimation of coupling constants from latitude effect

Coupling constants can be estimated from geomagnetic effects that relate N^i_λ with E^c_λ. Thus, rewriting (1.6) for a latitude λ and differentiating partially with respect to the lower limit of integration, we get

$$\frac{\delta N^i_\lambda (h)}{\delta E^c_\lambda} = -D(E^c_\lambda) \, M^i (E^c_\lambda, h) \qquad \ldots\ldots (1.11)$$

combining (1.9) and (1.11)

$$W^i_\lambda (E^c_\lambda, h) = -\frac{1}{N^i_\lambda (h)} \cdot \frac{\delta N^i_\lambda (h)}{\delta E^c_\lambda} \qquad \ldots\ldots (1.12)$$

The right hand side of (1.12) represents geomagnetic effects that are approximately known for secondary components (mesons, nucleons) for vertical intensity at sea level as well as at high altitudes. However, W can be calculated upto about 15 GeV energy only, which is the maximum cut-off energy for vertical intensity at the equator. For energies more than 15 GeV, Dorman suggests an extrapolation by the formula

$$W = K \left(\cfrac{E}{\overline{E}} \right)^{-a + b \frac{\overline{E}}{E}} \qquad \qquad ....(1.13)$$

where the constants K, a, and b are determined by normalization conditions and tying in at the point $\overline{E}$ = 15 GeV.

Secondary cosmic rays recorded by various detectors located deep in the atmosphere are mainly the products of primary radiation incident near the vertical at the top. Thus, although the cut-off rigidity at any given point is a function of zenith and azimuth angle, the vertical cut-off rigidity is a reasonably good approximation to the lower limit of the primary rigidity spectrum contributing to a detector at that point. This approximation improves as the depth of the detector in the atmosphere increases (Webber and Quenby, 1959)

Coupling constants for meson and neutron components can be calculated using latitude effect data upto 15 GV and by formula (1.13) for higher rigidities. In the case of neutron component this method works quite well. Because the differential response of a neutron monitor falls off quite rapidly beyond 8 GV rigidity (Webber & Quenby, 1959; Lockwood & Webber, 1967) and thus extrapolation of the response curve beyond 15 GV is unlikely to produce significant errors. In the case of mu-meson detectors the extra-polation by formula (1.13) to obtain the coupling constants beyond 15 GV may cause serious errors (Kane, 1962) because the maximum of the response curve of a meson detector may lie in the region of 15-20 GV as discussed below.

Fig. 1.2 shows the coupling constants for meson intensity calculated by Dorman using latitude effect data upto 15 GeV and formula (1.13) for higher energies. The top curve in Fig. 1.2 represents the differential primary energy spectrum estimated by Neher (1951).

It can be seen from this Figure that for larger atmospheric depths, the downward slopes of the log W versus log E curves steadily decrease. At sea level, the W values for mesons actually increase with energy for low energies, attain a maximum at about 25-30 GeV, and then decrease for higher energies. This implies a mean energy response toward higher primary energies for increasing atmospheric depths.

Webber & Quenby (1959) have revised the vertical cut-off energies E^C_λ by taking into consideration quadruple, and higher order terms. Using these revised values of E^C_λ and data on latitude effects (Rose et al., 1956; Meyer & Simpson, 1955) they have calculated the coupling constants W, which are shown in Fig. 1.3.

It is to be noted from Fig. 1.2 and Fig.1.3 that there is considerable difference between Dorman's and Quenby & Webber's coupling constants. Thus, for sea level mesons, Quenby & Webber's W curves attain a maximum at much lower energies, about 15 GeV, in contrast to Dorman's maxima at 20-30 GeV.

Dorman's and Quenby & Webber's coupling constants are based on experimental data only for energies upto 15 GeV. For higher energies, both have used extrapolation formulas like (1.13). Thus substantial portion of the (log W) versus (log E) curves are obtained by extrapolation methods that need independent justification.

1.4.3 Estimation of coupling constants from azimuth effect

Now, the experimental limit of 15 GV is applicable to latitude effects of vertical intensities only. This limit can be pushed to about 60 GV, at least in principle, by making use of the variation of threshold rigidity with zenith angle in the east-west plane at the geomagnetic equator. However, such measurements cannot yield the coupling constants necessary
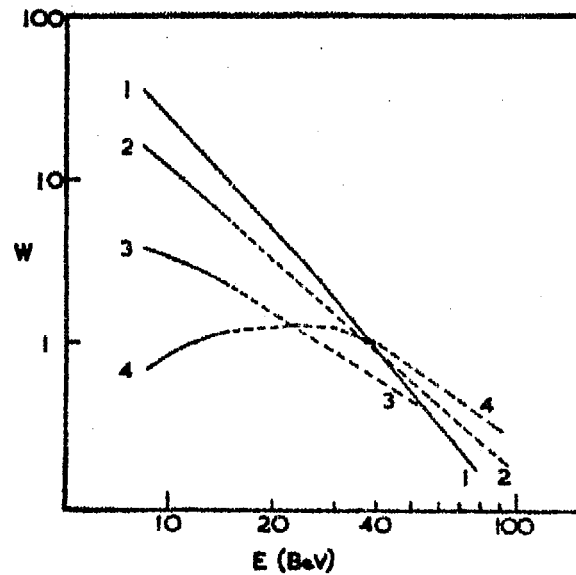
Figure 1.2   Dorman's coupling constants for meson component at
various atmospheric depths. 1. Neher's primary spe-
ctrum.   2. Ionizing component at top of atmosphere.
3. Ionizing component at 4300 meters.   4. Hard com-
ponent at sea level.
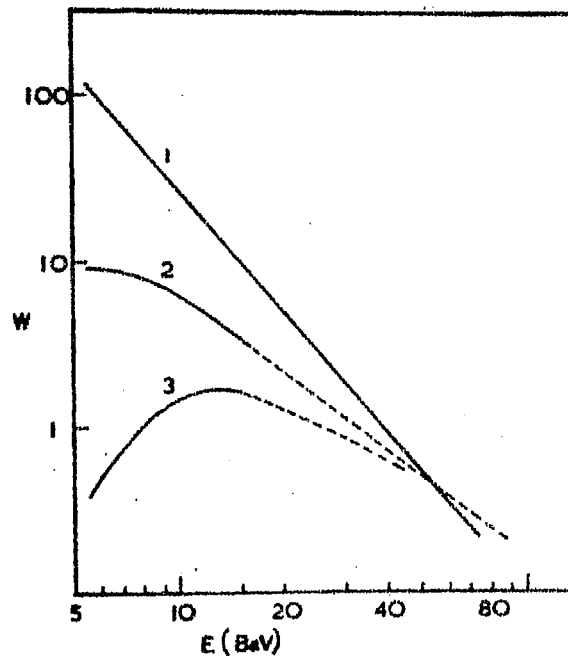
Figure 1.3   Quenby and Webber's coupling constants for meson component.
1. Webber's primary proton spectrum.   2. Meson intensity at
312 g cm^{-2}.   3. Meson intensity at sea level.

for a sea level vertical detector, because the variation in counting rate with zenith angle depends not only on the differences in threshold rigidities, but also on the absorption of mesons in the varying amount of air mass in the direction of the telescope axis and the varying proba-bilities for the decay of pi-and-mu-mesons in this varying mass (Mathews and Sivjee, 1967). These atmospheric effects can be kept constant by taking the counting rates of telescopes at different azimuth angles but at a fixed zenith angle. Kane (1962) calculated coupling constants from the data of various azimuthal surveys carried out near the equator in the past and showed that the experimental data available till then were not sufficiently accurate for this purpose and there was a need for more accurate data.

It is to be noted that for the same location, coupling constants for vertical and inclined directions are not directly comparable, as the latter refer to a greater atmospheric depth and hence will have a flatter W-E plot, the maximum of W values occurring at higher energies. However, such calculations will give a direct clue to the shape of the W-E. curves for the region 10-30 GeV. Mathews and Sivjee (1967) have measured the counting rates at three locations at three different zenith angles such that effective overlying air masses as well as the threshold rigidities are equal. Comparison of these rates showed that values are not signi-ficantly different implying thereby that effects of any changes in pi-and-mu-meson decay rates are not noticeable within the accuracy of their experiment. Coupling constants for inclined directions at high altitudes could therefore be compared with those of vertical intensity at sea level, as both would involve roughly similar atmospheric paths.

1.5   The spectrum and the charge ratio of cosmic ray muons

Precise measurements of the sea level spectrum and charge ratio of cosmic ray muons are important because these measurements are the main sources of information on the interactions of primary cosmic rays with air nuclei. Such measurements, at high energies, where muon decay and energy loss factors are minimum reflect the nature and multiplicities of the parent particles produced in the primary interactions which are not accessible by the present day accelerators.

The presence of an excess of positive particles over negative particles in the hard component of the cosmic radiation at sea level was noticed as soon as magnetic deflection methods were used for measuring particle momenta (Blackett, 1937; Jones, 1939). The excess still remains even after correcting for the contribution due to protons ($\sim$1 per cent of the hard component is composed of protons) and it is concluded that there are more positive than negative muons in the sea level flux.

Since the major target nuclei in the atmosphere (oxygen and nitrogen) contain protons and neutrons in equal numbers, this positive excess among muons should be attributed to the excess of protons over neutrons in the primary cosmic radiation. At a given energy per nucleon, the primary nucleons consist of 87% protons and 13% neutrons (Waddington, 1960).

This extreme positive excess in primary cosmic radiation is transmitted to the π-mesons produced in the nuclear interactions and hence to their decay products, the mu-mesons. Since the primary nucleons are absorbed in the upper atmosphere in several collisions, the sea level mu-mesons arise from the pions produced in several generations. However, the positive excess is reduced considerably after the first generation collision.

Most of the low energy muons are produced by the decay of pions, whereas, in the case of high energy muons, contribution due to Kaons becomes quite appreciable. This happens because the mean life of charged Kaons is shorter than that of charged pions and their mass is greater. Therefore, at a given energy, the probability of decay before interacting in the atmosphere is larger for a Kaon than for a pion. Thus in the high energy region where pion interaction becomes more probable than decay, an increasing fraction of muons arises from the decay of charged Kaons. Kaon contribution does not become significant until a primary energy of several hundred GeV is reached. This has been indicated both by accelerator experiments and on theoretical grounds (Hagedorn and Ranft, 1968; Maeda, 1964).

The experimental results of positive excess are sometimes presented as the positive excess and sometimes as the positive-nagative ratio. These quantities are defined as follows:

If $N(\mu^+)$ and $N(\mu^-)$ are the respective numbers of positively charged and negatively charged mesons, the positive excess, η, is given by

$$\eta = \frac{N(\mu^+) - N(\mu^-)}{N(\mu^+) + N(\mu^-)}$$

and the positive-negative ratio, or the charge-ratio as

$$R = \frac{N(\mu^+)}{N(\mu^-)} \quad (\text{i.e.} \quad R = \frac{1 + \eta}{1 - \eta})$$

The energy dependence of the charge-ratio is governed by the following considerations.

(a)   Some muons are produced in the lower atmosphere where the charge composition of interacting nucleons is more symmetric.

(b)   In the low regions of the atmosphere pion production by pions becomes important and contributes symmetrically to the positive and negative muons.   The charge ratio thus decreases.

(c)   In the case of high energies the relative contribution of charged Kaons becomes appreciable and, because of the large K^+/K^- ratio at production, tends to increase the charge ratio of muons.

As noted in the beginning the measurements of the charge ratio of cosmic ray muons is much more significant at high energies where it can provide valuable informations.   But the intensity falls too rapidly in high energy region and statistically significant observations become rather difficult.   However, many measurements have been performed in high energy range starting from a few GeV to 1 TeV or possibily much more (Ashton et al., 1963; Aurela et al., 1966; Flint and Nash, 1970; Appleton et al., 1971; Allkofer et al., 1971b; Kamiya et al., 1971; Ayre et al., 1971b).

The variation of ultra high energy muon intensities with zenith angles is closely related to the production mechanism of muons.   In the conventional picture of high energy interactions these muons are mainly produced in the decay of pions and Kaons (Mackeown et al., 1965).   An enhancement of the muon intensity at large zenith angles is a direct consequence of the competition between decay and capture of the parent particles.

Utah group has, however, given the evidence that an appreciable fraction of the muons above 1 TeV does not show this enhancement. Bergeson et al. (1967) attributed this to a new possible mechanism for muon production.   Keuffel et al. (1970) indicated that their data could be

interpreted in terms of a production process involving 2 per cent of X-production; observations of Krishnaswamy et al. (1968), Stockel (1969), and Sheldon et al. (1970), favour muon production processes involving long lived parent particles pions and Kaons and there is little direct support from intensity measurements for the X-process.

1.6   Statement of the problem

The purpose of the investigation described in this thesis is two-fold. Firstly, as mentioned earlier, the coupling constants can be derived from experimental data of latitude effect as well as azimuth effect. Whereas data for latitude effect are well obtained, those for azimuth effect were rather in a poor shape (Kane, 1962). Similarly, data on charge ratio of muons also were not well known for all energy ranges. Hence from the experimental point of view, an attempt has been made to derive the azimuth effect and charge ratio of muons accurately.

Having obtained these, an analytical attempt has been made to see whether by choosing an appropriate model of secondary meson production in the atmosphere (K. Ästrom, 1966), and fixing some parameters in the same, one could derive a theoretical formulation which would give the best fit for all the experimental data on latitude and azimuth effect, available so far, for various zenith and azimuths (part of which is obtained by us) and atmospheric depths. With this best fitting formulation, which essentially gives the coupling constant W as a function of energy E, one could obtain W versus E for all higher energies too. This has been achieved and W versus E curves for several zenith angles and atmospheric depths are presented.

EXPERIMENTAL SET-UP

2.1 Experimental study of azimuthal variation of cosmic ray muons

2.1.1 Apparatus

The study of azimuthal variation of the cosmic ray mesons at Ahmedabad (23°N, 72.6°E) was started in 1967 to obtain the coupling constants. The observations were taken during the period 1967-1969.

The apparatus consisted of two independent triple coincidence G.M. counter telescopes/of semi-angles 18° x 22°. The zenith angle was fixed at 45° and the two telescopes pointed to directions 180° apart in azimuth. The arrangement was capable of rotating about a vertical axis. Thus the telescopes could be kept at any desired azimuth angle.

Each telescope consisted of three trays of counters. Each tray had six G.M. counters/of diameter 4 cm and length 30 cm. An absorber of 15 cm of iron plates was interposed between the middle and bottom trays to cut-off the soft component. The vertical distance between successive trays was 37 cm. The trays subtended a semi-angle of 18° in the east-west plane and 22°in the north-south plane. Figure 2.1 shows the arrangement of the apparatus.

The counter trays were enclosed in a plywood box. The observations were recorded in a specially built air conditioned room with thin walls and roof.

2.1.2 The Geiger Muller Counter

Geiger Muller counter is essentially a diode, consisting of a cylindrical cathode and a thin wire passing along the axis as the anode. A gas like argon fills the entire space between the anode and the cathode. Passage of an ionizing particle through the counter results in the ionization of some gas atoms. Electrons thus produced are accelerated towards the central wire, while the positive ions drift towards the cylindrical cathode. As the electrons approach the central wire the field strength increases and the electrons gain sufficient energy to ionize some more gas atoms. The secondary electrons thus produced also gain energy and further ionization takes place until an "avalanche" is formed. During this process, the positive ions being heavier drift very slowly towards the cathode.

The electrons interact with gas atoms and also with the surface of the anode. In this process photons are emitted. Some photons have sufficient energy to eject electrons from the gas or from the cathode surface. The behaviour of an ejected electron is similar to that of a single electron from a primary ion-pair. Now, since even a single free electron is capable of triggering the discharge mechanism, it becomes necessary to quench the discharge.

The following two methods are generally used to quench the discharge.

(a)   External quenching

In this method the quenching is achieved by reducing the electric field during the period immediately following an avalanche to such an extent that a further discharge cannot take place. This is achieved by employing a suitable electronic circuit.

(b)   Internal quenching

In this method the spurious discharge is avoided by adding a polyatomic vapour to the counter gas to absorb the photons. A vapour such as ethyl-acetate, whose molecules dissociate on excitation, is generally used for this purpose. Photons present in the gas are thus absorbed by the quenching vapour and further discharge is avoided to a large extent.

Generally both internal and external quenching are used to minimise the spurious discharge. G.M. counter has an important property of providing a uniform magnitude of discharge independent of the specific ionization of the incident particle. Counters generally have a threshold voltage in the region of $\sim$ 1000 V and a plateau width of $\sim$ 200 V.

2.1.3 Electronic circuits

The block diagram of the electronic circuits used for each tele-scope is shown in Figure 2.2.

(a)   Quenching Unit

The quenching unit (Figure 2.3) consists essentially of a mono-stable multivibrator which feeds a negative rectangular voltage pulse of ($\sim$ 300 V) and duration ($\sim$ 140 μsec) to the central wire after every discharge due to the traversal of a charged particle through the counter. All the six counters in each tray are connected in parallel and their outputs are fed to one quenching unit.

(b)   Coincidence circuit

The circuit in this experiment for recording triple coincidences (Figure 2.4) is originally due to Rossi. In this circuit, plates of all the pentodes are connected together and fed through a common-load
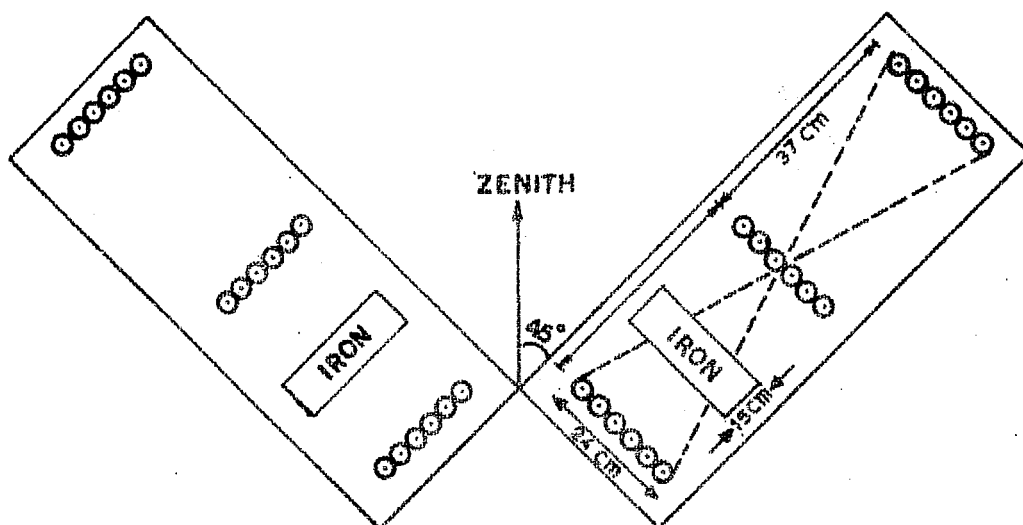
Figure 2.1   Apparatus for the study of the azimuth effect.
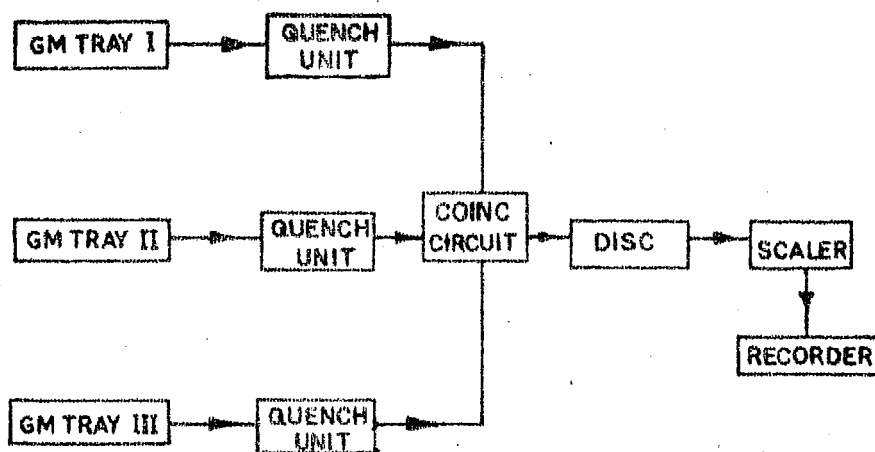
Figure 2.2   Block diagram of electronic circuits for counter telescopes.
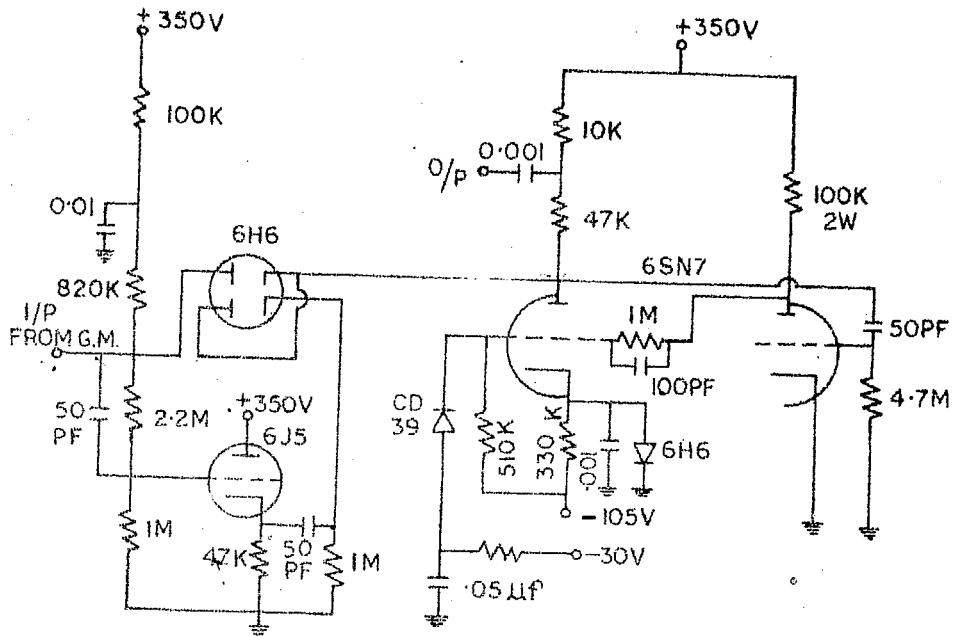
QUENCHING UNIT

Figure 2.3
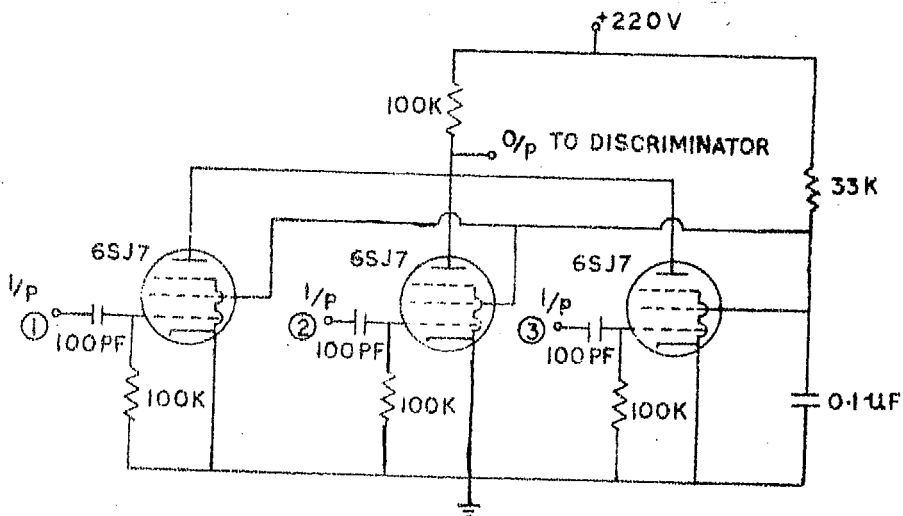
COINCIDENCE CIRCUIT

Figure 2.4

resistance. D.C. conditions are such that when all the grids get a negative pulse simultaneously, the current through the common plate-load resistance R is cut-off and a positive pulse appears. If input signal does not appear on any one of the grids, the current through the load resistance does not change significantly from the normal condition of conduction.

(c)   Discriminator circuit

Whenever all the grids of coincidence circuit receive signals simultaneously, a sufficiently high voltage positive pulse appears at the output. However, there may appear some small pulses due to partial coincidences. These small pulses are eliminated by discriminator circuit (Figure 2.5) the bias of the pentode being so adjusted as to make it insensitive for the small pulses generated by partial coincidences.

(d)   Scaler

For high counting rate measurements, it becomes essential to scale it down to such an extent that a mechanical recorder can work effectively. The circuit used in the present experiment is based on the Eccles-Jordan trigger circuit. It is a bi-stable multivibrator and is a basic scale of two circuit. Any scaling factor 2^n can be obtained by connecting n such scale of two circuits in cascade.

The scale of two circuit is shown in Figure 2.6. In this bi-stable multivibrator the two sections V_1 and V_2 of the twin-triode 6SN7 are used. Circuit has two stable states of operation. One state has V_1 conducting and V_2 non-conducting while the other state has reverse configuration i.e. V_1 non-conducting and V_2 conducting. Let us assume that the multivibrator is in the first state so that the grid
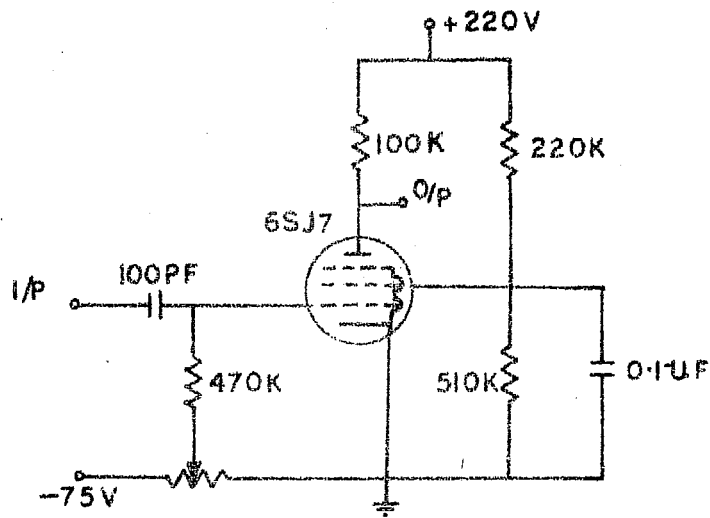
DISCRIMINATOR CIRCUIT
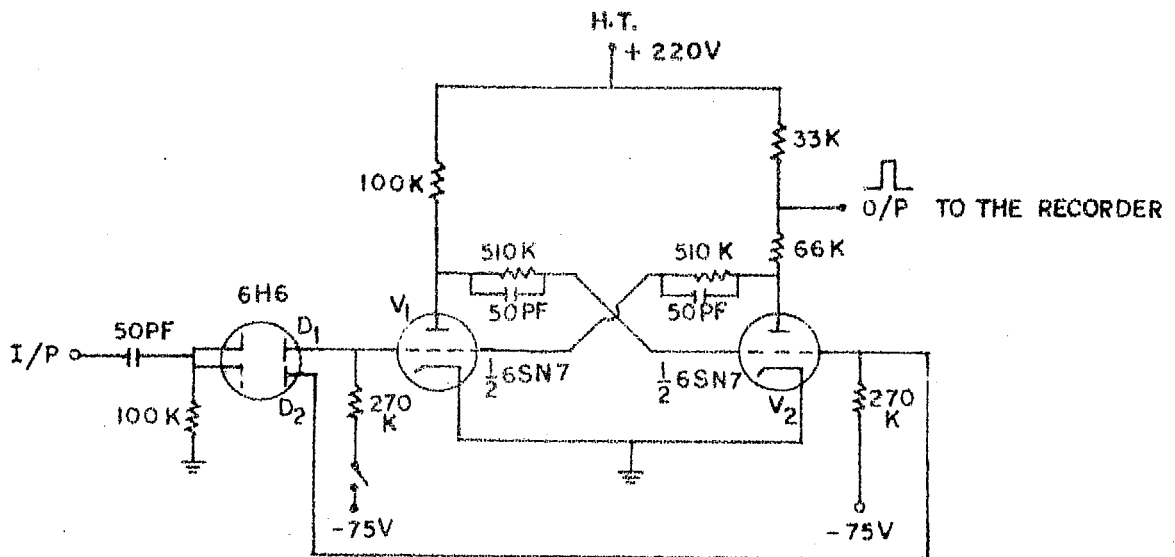
Figure 2.5

SCALE OF TWO

Figure 2.6

of V_1 is at a higher potential than that of V_2. This makes the diode D_1 only conducting. If a negative pulse appears at the input, it is fed to the grid of V_1 which becomes non-conducting. Now plate-to-grid coupling makes V_2 conducting. Similarly, it can be shown that another negative pulse arriving at the input will bring the circuit back to its first state and the tube V_2 will give a positive pulse which can be used to trigger mechanical recorder circuit. Thus a scaling factor of two is obtained. Resetting of the scaler is achieved by applying -75 V to one of the grids through a microswitch as shown in Figure 2.6.

(e)   Recorder

Electromechanical recorders are used for final recording of the data. Electro-mechanical recorder is connected to the plate of a power amplifier. Amplifier tube 6F6 is normally much below cut-off. Positive pulses from the scaler to the grid of the tube causes it to conduct and actuate the recorder.

2.1.4 Operational considerations

Two independent triple-coincidence-telescopes with the same geometry were used in the present investigation. Satisfactory operation of the apparatus can be judged by comparing the results obtained with these identical telescopes in the same direction.

All the counters were tested for their plateau characteristics and operated for a period of nearly 24 hours in the middle of their plateau region. Counters which exhibited good plateau after this process of ageing were selected for use in the instrument.

Since, different counters have different threshold voltages, the voltage divider has been designed in such a way as to apply the most appropriate voltage to each counter. The plateau characteristics of a

counter may change after some use. Counters used in the instrument should be operated in the middle of their plateau for reliable counting rate. Therefore, rates for different trays were checked everyday for constancy. Each counter of the tray giving improper tray rate were tested and bad counters were replaced.

Self-quenched counters have very limited useful life. Therefore, electronic circuits are used for external quenching. This lengthens the life of the counter and also makes it more stable.

Stabilisation of voltage against line voltage fluctuations and load variations becomes necessary for the satisfactory operation of various electronic circuits. All the power supplies used in the present investigation were thus designed properly. The A.C. voltage supplied to these power supplies was also regulated by a constant voltage transformer.

2.1.5 Mode of operation

The azimuth experiment was performed first for four azimuths, viz., East, West, North and South. The rotation of the telescope was arranged in such a way that each telescope scanned West, North, East and South directions in sequence over a period of four days. About 5 minute dead time was allowed in the counting while the telescopes changed position. The two telescopes pointed to directions 180° apart in azimuth. Therefore, when one of the telescopes was pointing East another was pointing West and so on. This procedure was continued for these four azimuths (N, S, E, W) till an accuracy of about 0.4% for each azimuth was obtained. Generally observations extending over a period of two to three months were found to be sufficient to achieve this accuracy.

Having obtained the counting rates for East, West, North and South azimuths, the last two azimuths namely, North and South were replaced by

several pairs of diametrically opposite azimuths keeping East and West

as reference directions. Observations were continued for a sufficiently

long period to get accuracies of about 0.4% for each azimuth. Azimuth

angles were measured with respect to the North. In all 7 pairs of azimuths

$(10^\circ, 190^\circ)$, $(35^\circ, 215^\circ)$, $(60^\circ, 240^\circ)$, $(83^\circ, 263^\circ)$, $(130^\circ, 310^\circ)$, $(153^\circ, 333^\circ)$

and $(173^\circ, 353^\circ)$ were scanned during the period 1967-69.

Scale of 4 was used to record the triple coincidence counts. Readings

of the electromechanical recorders were recorded manually every day.

2.2 Experimental determination of the spectrum and the charge ratio of cosmic ray muons

2.2.1 Methodology of the Experiment

There are only few charge ratio measurements at low energies i.e.,

muon energy less than 1 GeV (Conversi, 1950; Fukui et al,1955; Allkofor

et. al., 1968; Allkofer and Clausen, 1970 and Allkofer and Dau, 1972).

One of the main difficulties in the experimental determination of the

spectrum and the charge ratio of cosmic ray muons is that of distin-

guishing muons from other cosmic ray particles such as protons and

electrons.

The spectrum and the charge ratio of cosmic ray muons are usually

determined by the magnetic momentum spectrograph. The charged particle

trajectory before and after traversing the magnetic field is determined

either by neon flash tubes and G.M. counters or by spark chambers.

The deflection of charged particles by a magnetic field helps to decide

the charge of the particle and the momentum. In this method a part of

the positive excess may be due to protons. It is not easy to extend

this method to low energies because of the large percentage of electrons

present in the observed radiation when observations are made under little or no shielding material.

Advantage may be taken of the following two properties of muons to distinguish them from other ionizing radiation:

(a)   muons are unstable and when free, decay with a characteristic mean life of about 2.2 microseconds;

(b)   their interaction with matter is weak. Positive muons always decay while negative muons also have a finite probability of being captured by the nucleus of the absorber material in which they are brought to rest. Nuclear capture has but a small probability in absorbers of low atomic number but predominates in high z absorbers.

Rossi et al. (1947) and Sands (1948), utilizing above mentioned properties and the method of delayed coincidence, separated muons from other ionizing particles. Shamos et al. (1948) used this method for the first time for separating positive muons from negative muons. Later, Conversi (1950) and Fukui et al. (1955) utilized the delayed coincidence method for determining the charge ratio of low energy cosmic ray muons.

As stressed earlier precise measurement of charge ratio is important because of its direct connection with the understanding of the nature and multiplicity of the parent particles produced in the inter-actions of the primary radiation with the air nuclei. However, the results obtained from earlier experiments were statistically poor and different measurements did not show any positive indication towards the variation of the charge ratio with momentum. Hence, the present investigation was carried out.

2.2.2 Apparatus.

In the present investigation the method of delayed coincidence has been used to distinguish muons from other ionizing cosmic ray particles.

As shown in Figure 2.7 the scintillation telescope AB (semi-angle 19°) is formed by the scintillation counters A and B each having dimensions 23.2 cm x 23.2 cm x 1.3 cm and separated by a vertical distance of 67.7 cm. Scintillator C is 46.4 x 46.4 cm^2 and 5 cm thick. Counter C is placed about 32.7 cm below scintillation counter B, so that it completely covers the solid angle defined by counters A and B.

Particles incident in a small cone of directions about the vertical are chosen by this telescope. The absorber S' placed between counters A and B sets a lower limit to the energy of the muons which can actuate the telescope. Muons which traverse the telescope AB meet the absorber S placed between the counters B and C. C is placed in prompt anti-coincidence with the telescope AB. Hence, for the event ABC no count is recorded. However, some muons which have traversed the AB telescope but do not have sufficient energy to emerge from the absorber S will be brought to rest in the absorber S. Thus an event $AB\overline{C}$ would be recorded. These stopped muons decay and since, the mean life of muons is about 2.2 microseconds, nearly 97.4% muons will be able to decay within 8 micro-seconds. The $AB\overline{C}$ pulse triggers different monostable circuits of different pulse durations, the longest being 8 microseconds. Some of the decay electrons will pass through C and will be detected by the coincidence between C and the monostable pulse. Thus, the counter C is in prompt anti-coincidence and at the same time in delayed coincidence with respect to the coincidences AB.

By performing this experiment with two different absorbers S, one of high atomic number, i.e. lead, (in which only positive muons decay, negative ones being captured), and the other of low atomic number, i.e. graphite, (in which both types of muons decay), the charge ratio can be determined. By changing the thickness of the absorber S' the energy of the muons incident on S can be changed and the spectrum over the required band of energies can be scanned as shown later in the methods of analysis.

2.2.3 Detectors and associated electronics

The block-diagram of the electronic circuits used is shown in Figure 2.8. Photomultiplier pulses are first amplified by preamplifier and then by main amplifier. Amplified pulses thus obtained are discriminated against the noise by discriminator circuit and a rectangular pulse is obtained at the output of each discriminator corresponding to each scintillation counter. $A B \overline{C}$ circuit then provides a pulse corresponding to a muon which is being brought to rest in the absorber S. These $A B \overline{C}$ pulses are shaped and then used to trigger various univibrators (of different pulse durations). The positive pulse from the monostable circuit provides one input to the delayed coincidence circuit while the other input comes from the C pulse. Delayed coincidence output is then fed to the electromechanical recorder through emitter follower for final recording.

(a) Scintillators and photomultiplier tubes

Plastic scintillation counters are now accepted internationally as standard equipment. The plastic scintillator can be given any desired shape. Furthermore, the practically unlimited life-time favours the
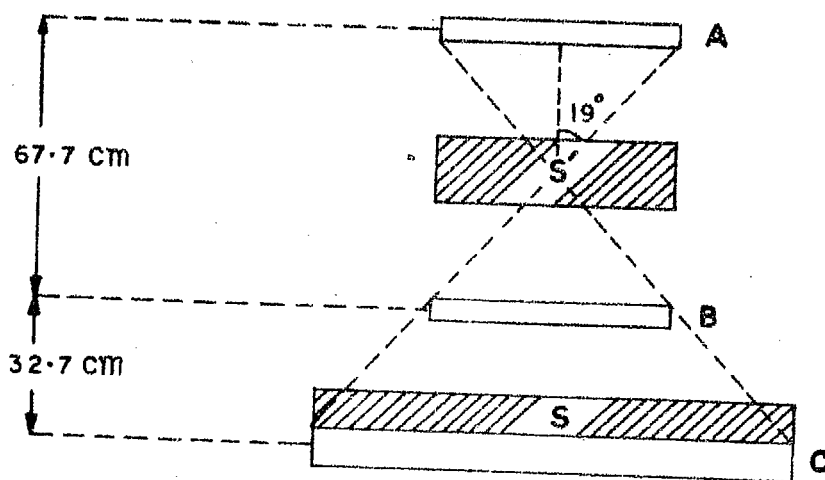
Figure 2.7 Schematic diagram of the muon telescope for the charge ratio measurement.
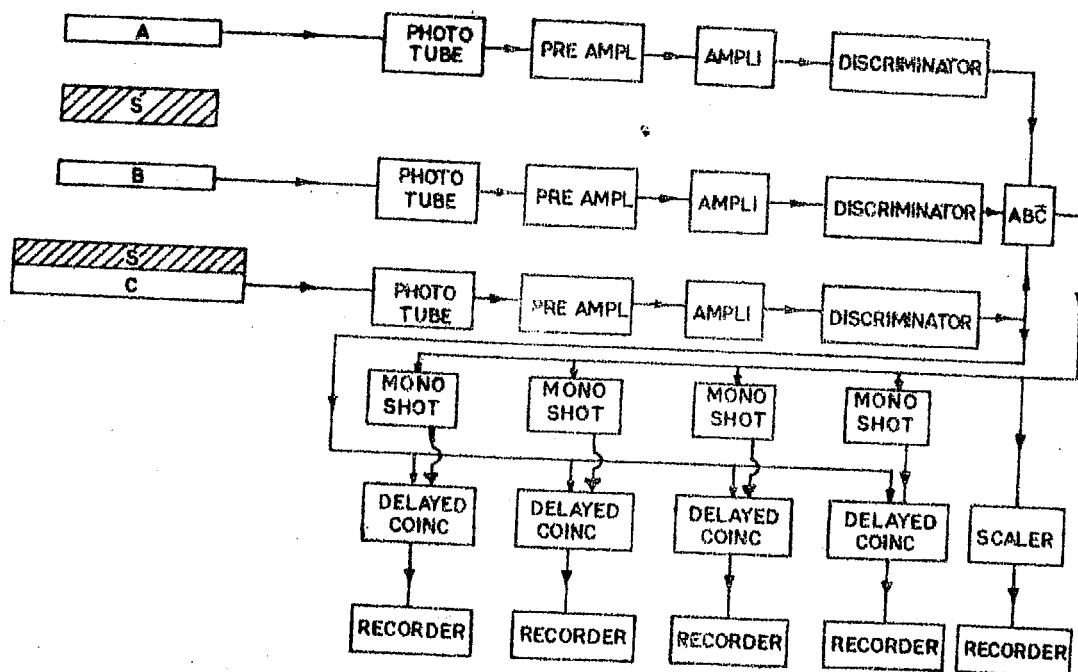
Figure 2.8 Block diagram of electronic circuits for the charge ratio experiment.

choice of scintillators for the studies wherein the observations are to
be taken for a very long time. Also, plastic scintillators have short
decay times of the order of 4×10^{-9} second and therefore, are most useful
for the fast coincidence work with charged particles. Plastic scinti-
llators used in the present investigation were supplied by the Department
of Atomic Energy, Government of India. Photomultiplier tubes are mounted
at the centre of the scintillators A and B such that phototube is in direct
contact with the scintillator, while in the case of scintillation counter C,
the phototube is placed at a distance below the scintillator. Light-pipe
has been used in this case to have the optical coupling of the phototube
to the scintillator.

RCA 6655A photomultipliers have been used in the present investigation.
The photocathode size is 1.69 inch and there are 10 dynodes. The spectral-
response of the Sb-CS cathode lies in the range of $4000\text{Å} - 5000\text{Å}$ which is
well matched to the fluorescent emission of the plastic-scintillator.

(b)   High-voltage connection to the photomultiplier

High-voltage connections to the phototube are shown in Figure 2.9.
The dynodes are connected to a common voltage divider from a high-voltage
regulated power-supply. The voltage divider for the dynodes and the cathode
is mounted inside the photomultiplier case. To minimise the ripple component,
a filter network is used and the phototubes are decoupled. Voltage difference
between the first dynode and the photocathode is larger compared to the
others so that the electrons emitted from the photocathode undergo larger
acceleration. The last three dynodes carry high signal current which can
cause fluctuations in the anode potential and so these have been bypassed
with capacitors.

5325

(c) Preamplifier and linear amplifier

Preamplifier is mounted near the photomultiplier to reduce noise and cable lengths. The circuit is shown in Fig. 2.10 and has a gain of 5. Amplified pulses are fed to main amplifier. The linear amplifier (Fig. 2.11) consists of a single ended differential amplifier driving a common-emitter amplifier. Gain is stabilized by giving negative feed-back.

(d) Discriminator

The discriminator is used to cut-off the background noise and the dark current noise from the photomultiplier. The circuit is shown in Figure 2.12. It consists of a differential amplifier, common-emitter amplifier and a monoshot. Base voltage of one differential amplifier transistor can be adjusted by a potentiometer and the pulses from the main amplifier are fed to the other base. The discriminator level is adjusted experimentally by plotting the counting rate versus the discriminator level and then finally adjusting the discriminator level corresponding to the flat portion. The discriminated pulses are amplified and then shaped by a monoshot.

(e) $A B \bar{C}$ circuit

The circuit is shown in Figure 2.13. The A and B pulses from discriminators are fed to the AND gate comprising of D_1, D_2 and R_3. The AB pulse thus obtained is fed to the linear gate transistor T_1. The C pulse is applied to the base of T_1 so that whenever C pulse is present, T_1 shorts the AB pulse appearing at T_1 collector to the ground. So a pulse at T_2 collector is obtained only when A and B are present simulta-neously but C is absent.

(f) Coincidence circuit for counting decay electron

The $A B \bar{C}$ pulse is used to trigger four monoshots (shown in Fig. 2.14) of 2, 4, 6 and 8 microsecond durations. The output pulse from each monoshot is fed to a coincidence circuit, the other input to the coincidence circuit

HIGH VOLTAGE CONNECTIONS
TO THE PHOTOTUBE
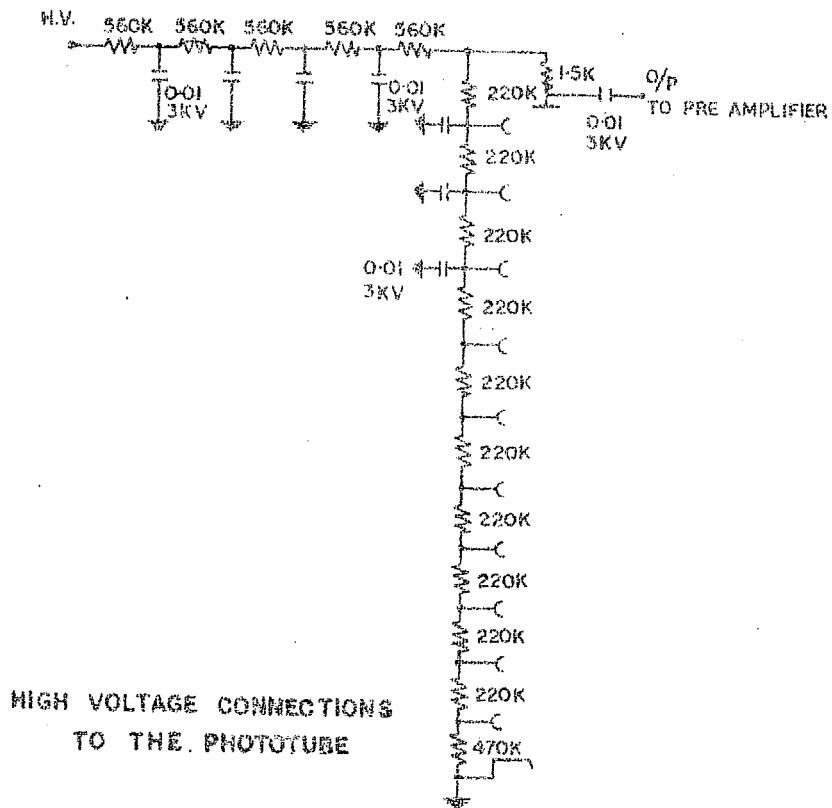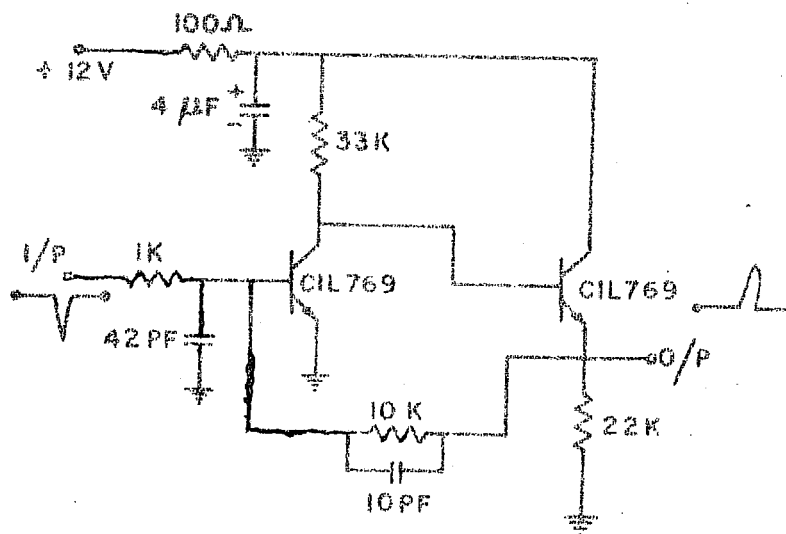
Figure 2.9

PRE AMPLIFIER
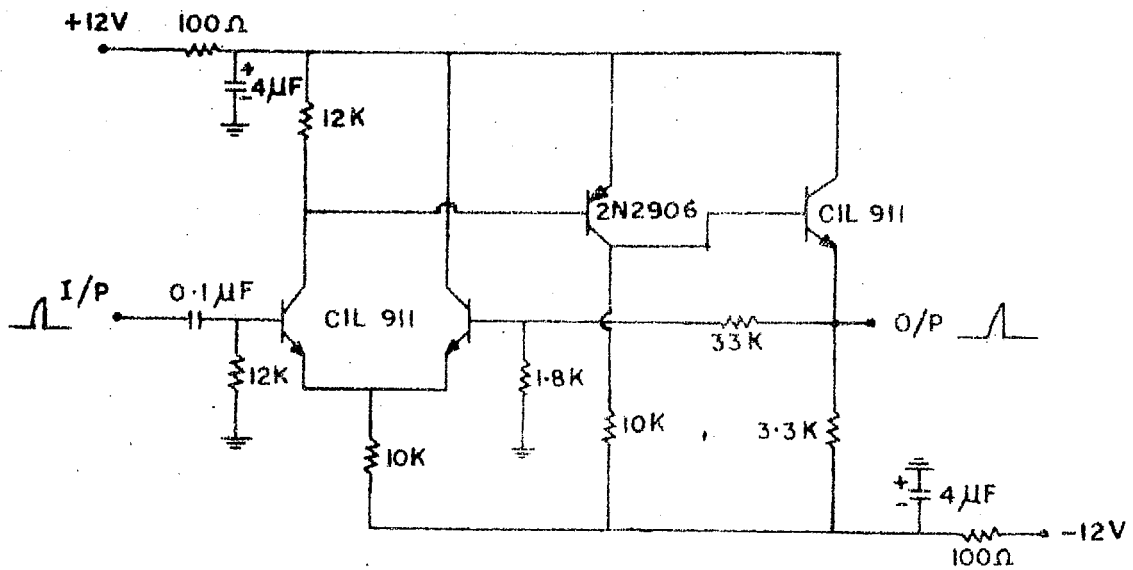
Figure 2.10

MAIN AMPLIFIER

Figure 2.11
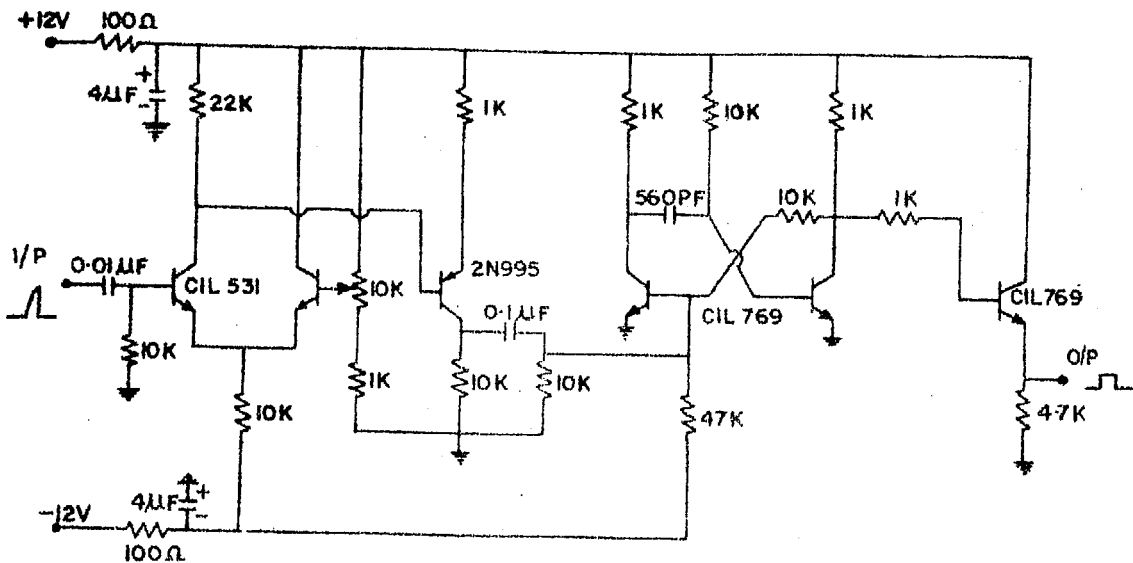
DISCRIMINATOR

Figure 2.12
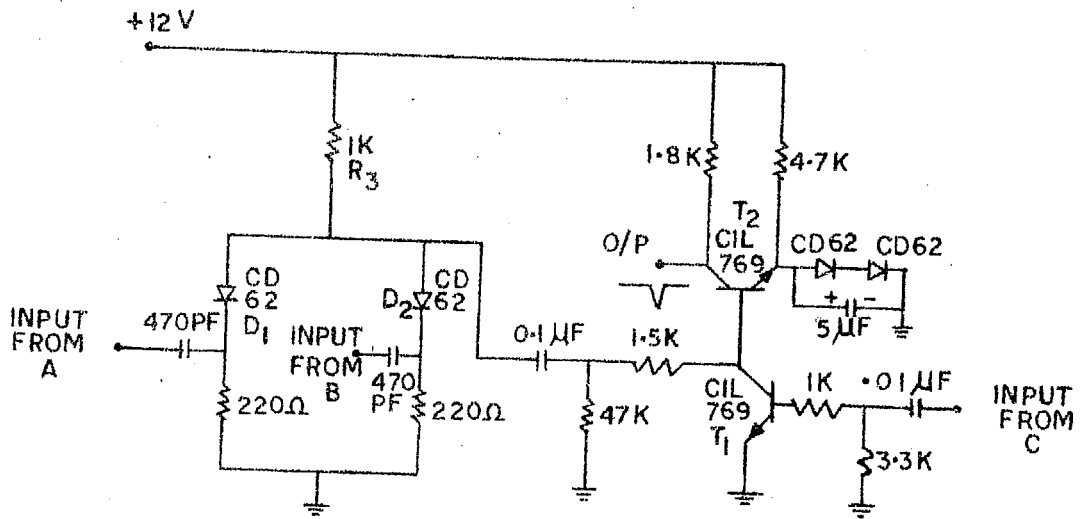
ABC̄ CIRCUIT

Figure 2.13
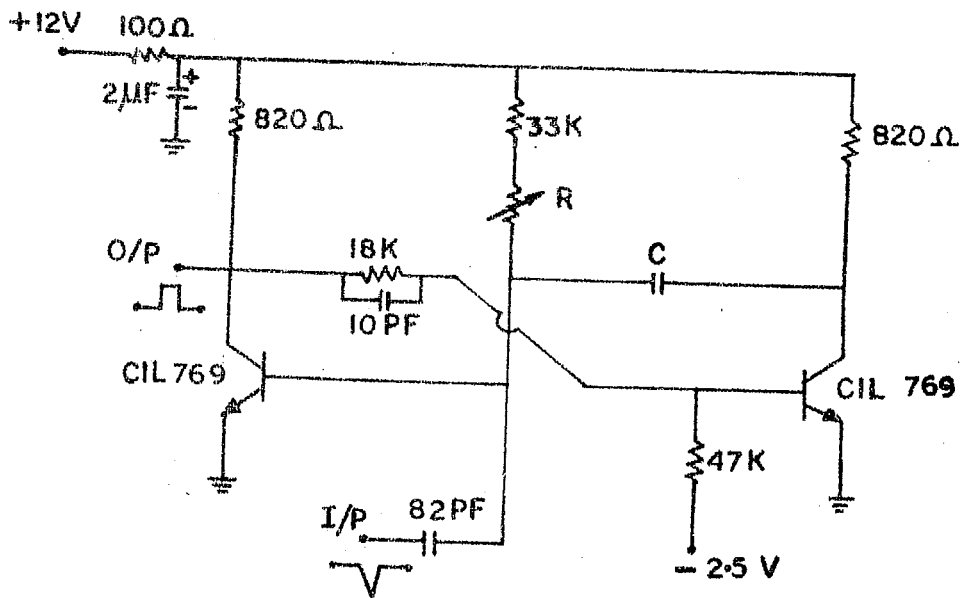
Figure 2.14. The Monoshot Circuit.

being the C pulse (shown in Figure 2.15). This C pulse now corresponds
to the electrons which are produced in the decay of the muons following
their stoppage in the absorber S. Thus we get decay events corresponding
to times of 2, 4, 6 and 8 microseconds. These pulses are then fed to the
electromechanical recorders for final recording. The recorder circuit is
shown in Figure 2.16.

2.24   Tests and checks

Charged particles lose energy in traversing the scintillation
media and this energy is converted into photons. These photons in turn
produce photoelectrons at the photocathode. Electrons are then multiplied
nearly a million times by the photomultiplier. Actual gain of the photo-
multiplier depends upon the applied voltage.

The output pulse height is proportional to the energy lost by the
charged particles. Phototube pulses show a spectrum. Small voltage pulses
are mainly due to noise and can be eliminated by the discriminator.

The photomultiplier voltage and the discriminator level are the main
parameters which control the performance of the scintillation counter
telescope. The characteristic dependence of the counting rate on these
parameters must be investigated. The following behaviour were studied
experimentally for this purpose.

(a)   Counting rate of each detector vs photomultiplier voltage

(b)   Coincidence counting rate vs photomultiplier voltage

(c)   Differential pulse height spectrum, and

(d)   Integral pulse height distribution.

Thus, the photomultiplier voltage and the discriminator level
were adjusted so as to separate the cosmic ray peak from the background
noise.
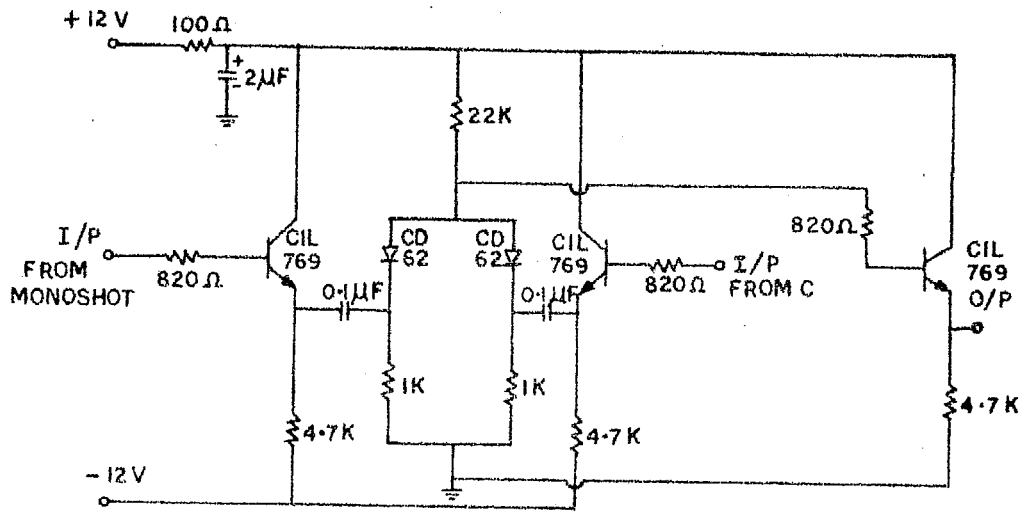
DELAYED COINCIDENCE CIRCUIT

Figure 2.15
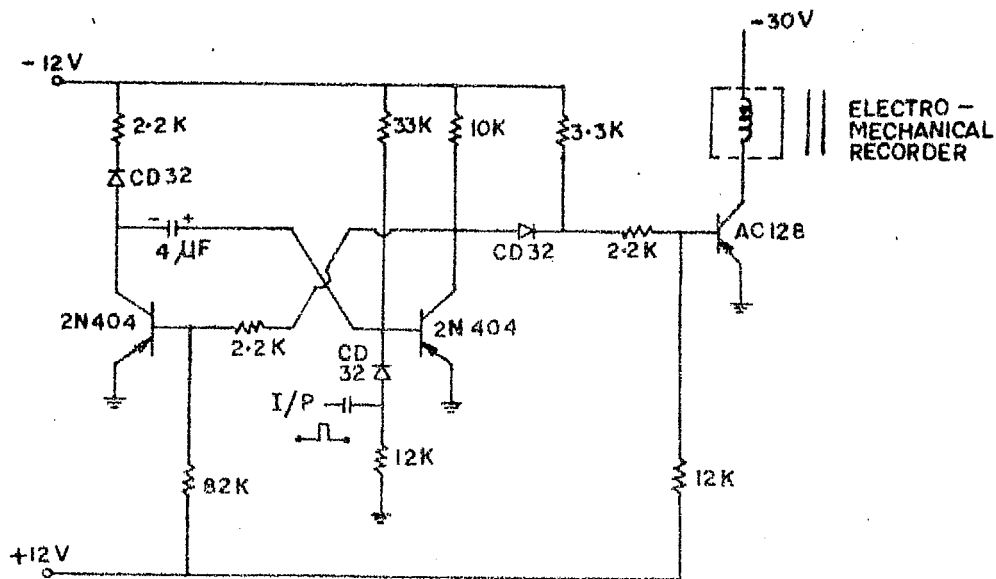
RECORDER CIRCUIT

Figure 2.16

Scintillation counters of the telescopes are periodically tested for the plateau characteristics. Changes in the photomultiplier voltage and the discriminator level are made whenever found necessary.

2.2.5 Mode of operation of charge ratio experiment

Charge ratio measurements have been performed under different thicknesses of absorber S'. The thickness of absorber S' and thicknesses of scintillators A and B set a lower limit to the energy of the muon which can actuate the telescope. Thus, charge ratio measurements for different muon energy ranges have been made possible.

A part of the absorber S' is placed between the counters A and B and the remaining material (if any) is placed above the apparatus in the solid angle of the counter telescope. A meson traversing the counter telescope AB and stopping in the absorber had a maximum permitted zenith angle of about 26°.

Measurements have been taken alternately with and without the absorber S. Thus observations were taken in the sequence (a) without absorber (b) with graphite absorber (c) without absorber and (d) with lead absorber to eliminate systematic errors. Thus, while changing the absorber an observation was always taken without absorber. Many such sets of observations were taken for a particular muon momentum range to get a better statistical accuracy.

Measurements without an absorber were usually taken for a comparatively short period. The anticoincidences and delayed coincidences were recorded simultaneously in all these measurements as is evident from the block diagram of the apparatus (Figure 2.8).

Observations with any one of the absorber S or without absorber were generally taken for a day or two. Delayed coincidence counts and anticoincidence counts were recorded manually by reading various electro-mechanical recorders quite frequently during the period of observation.

Measurements were carried out in an air-conditioned room with thin walls and roof. Observations for each momentum range were generally taken for a period of two to three months. Pulse durations for delayed coincidence measurements were checked regularly. All the electronic circuits and regulated power supplies were also checked for realiable operation.

METHOD OF ANALYSIS AND RESULTS OF EXPERIMENTS

3.1   Method of analysis and results of the azimuth effect experiment

3.1.1 Processing of Data

Hourly counting rate for each observation is obtained by dividing the total triple coincidence counts by the number of hours. Four azimuths were selected at a time as explained earlier. Hourly counting rates obtained for various days and for each azimuth are checked for reliable counting rate. If by inspection any individual observation is found to be far from the approximate average hourly rate, i.e. if any observation is found to be out by more than twice the standard deviation, that observation is rejected for further analysis. The data thus obtained form the basis of further analysis.

Data for these four azimuths is then arranged in different sets, each set containing at least one observation for each azimuth. If a set contains more than one observation for an azimuth, all these observations are combined to get an hourly counting rate for that particular azimuth.

Hourly counting rates are normalized such that the rate becomes 100 for West direction. Normalized rates, standard errors and normalized standard errors are determined as follows:

Let θ_1, θ_2, θ_3 and θ_4 be the four azimuths under consideration, West is always chosen as θ_1. Let n_1, n_2, n_3 and n_4 be the hourly rates (in scale of 4) and let t_1, t_2, t_3 and t_4 be the corresponding durations in hours. Normalization factor f is determined such that

$$f = 100/n_1$$

Then n_1, n_2, n_3 and n_4 are multiplied by f (normalization factor) to get normalized hourly counting rates as

$$N_i = n_i \times f \qquad \dots (3.1)$$

The standard error of the hourly rate is obtained as

$$\Sigma_i = \sqrt{\frac{n_i}{4 \times t_i}}$$

and the normalized standard error corresponding to the normalized rate (eqn. 3.1) as

$$\sigma_i = \Sigma_i \times f$$

All the sets are now thoroughly checked. If a set is found to contain more than one observation which are unreliable under the statistical limits, that set is completely rejected. However, if there is only one unreliable observation then that observation is rejected and other observations of that set are combined with the next set.

Finally, weighted mean is obtained from all the normalized rates as follows:

Let N_1, N_2, N_3 ...., N_r be the normalized rates for a particular azimuth where r is the number of sets and let σ_1, σ_2, σ_3, ..., σ_r be the corresponding standard errors. Then weighted mean is given by

$$\langle N \rangle = \frac{\Sigma (N_i / \sigma_i^2)}{\Sigma (1 / \sigma_i^2)}$$

Thus, each observation N_i is given a weight proportional to the reciprocal of the square of its standard error, and the standard error of the mean is given by

$$\sigma_{\langle N \rangle} = (\Sigma 1 / \sigma_i^2)^{-\frac{1}{2}}$$

This procedure is repeated for all the azimuths and for both the telescopes. Thus we have obtained normalized rates for all the azimuths with their standard errors for both the telescopes.

The observations were recorded in the sequence mentioned earlier to minimize meteorological effects. Frequent observations were taken for each of the fourteen directions studied and thus averaging out as far as possible intensity variations due to pressure or temperature changes. Mostly observations for complete days were utilised for final analysis to avoid any effect of daily variation inherent in the meson flux.

3.1.2   Determination of threshold rigidities for various azimuths at Ahmedabad

Since the cosmic ray intensity decreases with zenith angle, the effective direction of the telescope will not be the same as the geometrical axis of the telescope. This difference depends on the opening angle of the telescope as well as on the variation of intensity with the zenith angle.

Kane and Rao (1960) have shown that for a telescope, inclined to the vertical at 45° and having a semi-angle 20°, the mean inclination of all radiation recorded is at 42.5^O and 50% of the recorded radiation is incident within a range of $\pm 5.5^O$ of this mean value.

Daniel and Stephens (1966) have calculated the threshold rigidities by a sixth degree simulation of the geomagnetic field (Finch and Leaton, 1957). They have kindly provided us threshold rigidities at Ahmedabad at every 10° interval in zenith and every 15° interval in azimuths.

From these values we obtained cut-off rigidities at every 15° interval in azimuths corresponding to a fixed zenith of 42.5^O. Rigidity

values thus obtained are shown in Figure 3.1. Threshold rigidities corresponding to all the azimuths, experimentally studied by us, were then obtained from Figure 3.1.

3.1.3 Azimuthal effect recorded by the counter telescopes at Ahmedabad

As mentioned earlier two independent triple coincidence G.M. counter telescopes, inclined at an angle of 45° to the vertical and pointing to directions 180° apart in azimuths, were in operation at Ahmedabad during the period 1967-1969. Fourteen directions were studied experimentally and normalized rates for all the azimuths and for both the telescopes were obtained by analysing the data as explained in section 3.1.1.

Azimuths versus normalized rates thus obtained are shown in Fig.3.2. Two points for each azimuth refer to measurements taken with two independent telescopes. The error flags show one standard deviation.

It can be seen from this figure that the rates recorded by the two telescopes corresponding to each azimuth are similar within statistical limits for most of the azimuths studied, indicating thereby that both the telescopes worked satisfactorily during the whole period of operation. Statistical accuracies of East and West directions as seen from Fig. 3.2 are good as expected because these, being reference directions, were monitored for most of the time.

Threshold rigidities (as obtained from Figure 3.1) versus normalized rates are shown in Figure 3.3, where rates of both the telescopes are shown with their standard deviations.

3.1.4 Determination of coupling constants from azimuthal experiment

Rates of both the telescopes for each azimuth are combined by the method of weighted means to obtain the normalized intensity as a
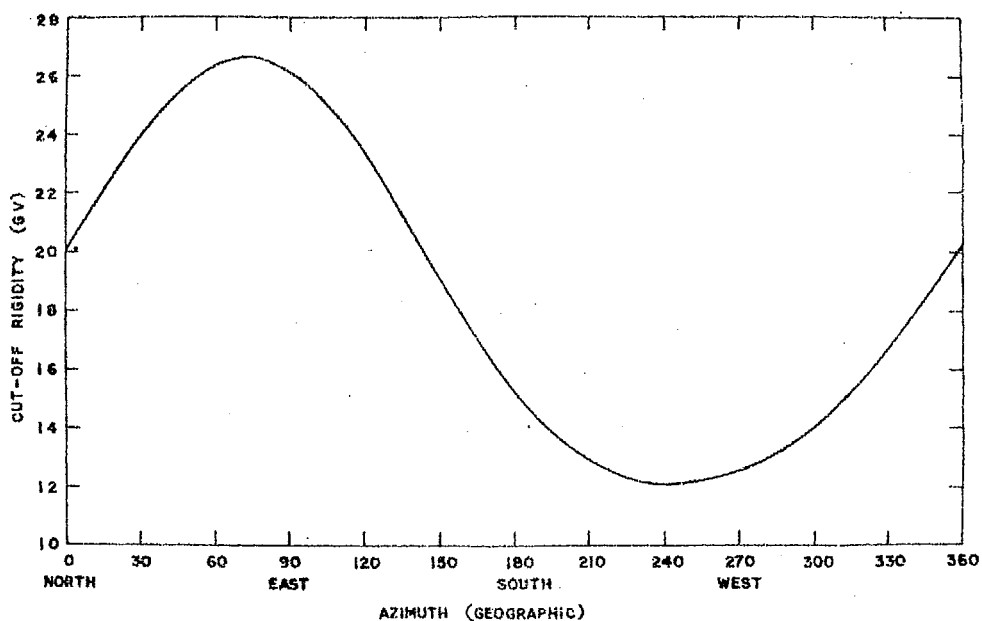
Figure 3.1   Geomagnetic cut-off rigidity as a function of
azimuth for 42.5° zenith angle at Ahmedabad.
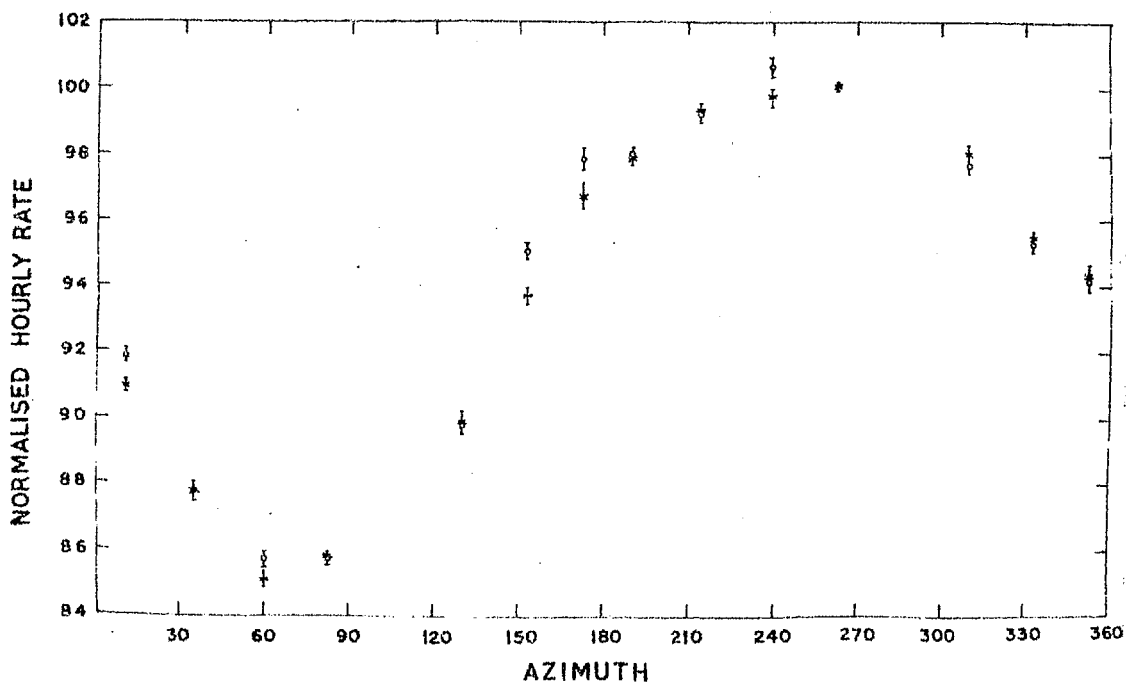
Figure 3.2   Azimuthal effect recorded by the counter telescopes at
Ahmedabad for 42.5° zenith angle.   Two points for each
azimuth refer to observations taken with two independent
telescopes and the error flags show one standard deviation.
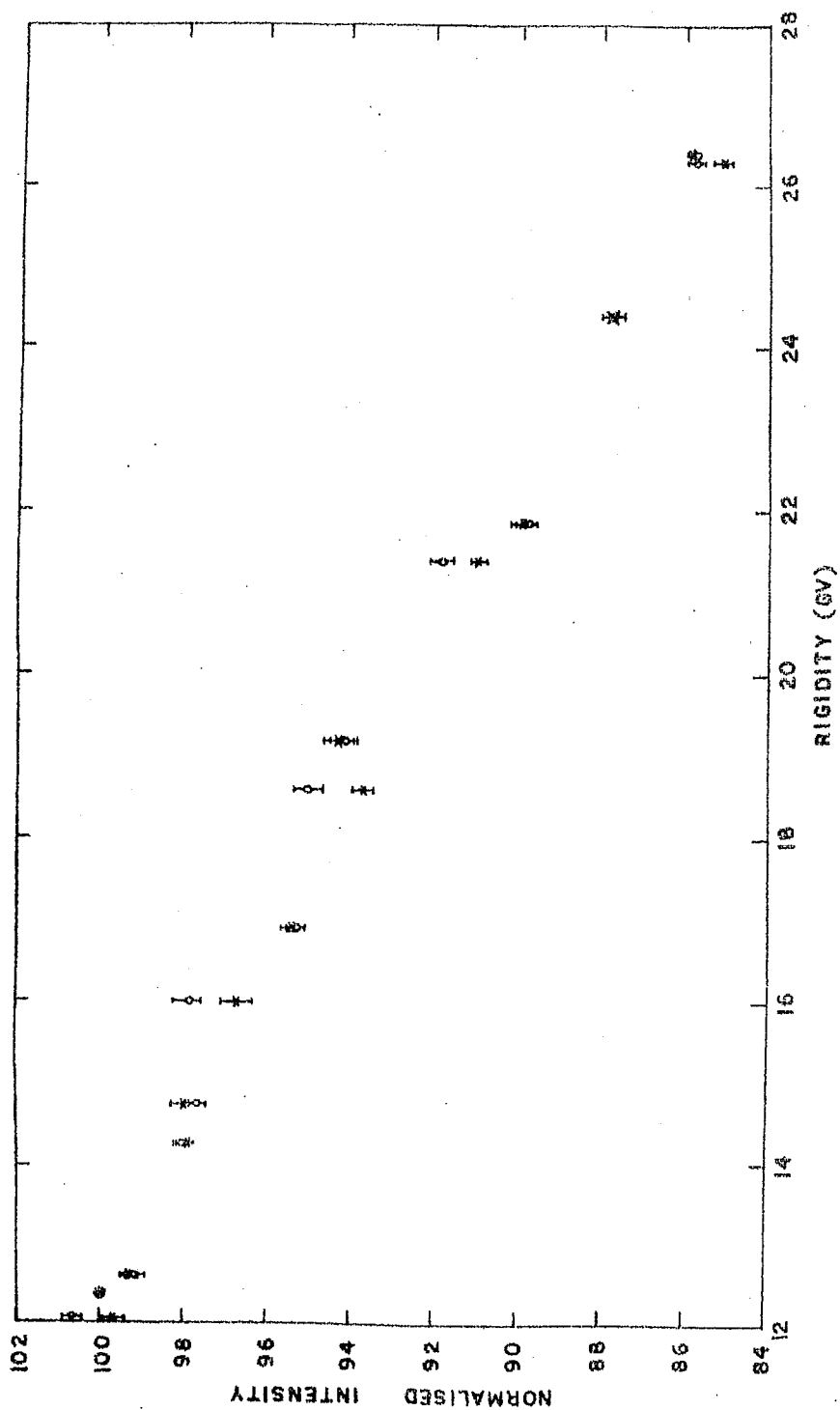
Figure 3.3   Meson intensity as a function of threshold rigidity at Ahmedabad as obtained by two independent triple coincidence telescopes inclined to the vertical at 42.5°.

function of rigidity.

It was felt that for some points the rigidities were very close to each other and therefore weighted means of rigidities and intensities were taken for these points. Mean normalized intensities thus obtained are shown in Fig. 3.4 as a function of mean rigidity.

Coupling constants are then derived in the usual manner from the increment in meson flux with geomagnetic cut-off. Coupling constants thus obtained are shown in Figure 3.5 for the 12-26 GV rigidity range. The experimental observations indicate a maximum at about 21 GV. However, the variation in W is not large in the 12-26 GV range. Some possible sources of inaccuracy must be kept in mind as follows:-

(a)   Opening angle of the telescope

Coupling constants have been derived by us using cut-off rigidities corresponding to a fixed zenith 42.5° and appropriate azimuths, but in fact primary particles do arrive in a cone of directions (allowed by the opening angle of the telescope) centered around the mean direction. This might have introduced errors. A very narrow angle telescope is therefore necessary for such investigations to obtain coupling constants very accurately. However, the counting rates would then be smaller unless very large areas and a very long period of operation are used.

(b)   Contributions from heavier nuclei

In deriving the coupling constants we have used the cut-off rigidity values pertaining to protons incident on the top of the atmosphere in the respective directions. However, nearly 26% of the primary nucleons are alphas and heavies and hence, do not have the cut-off at a value
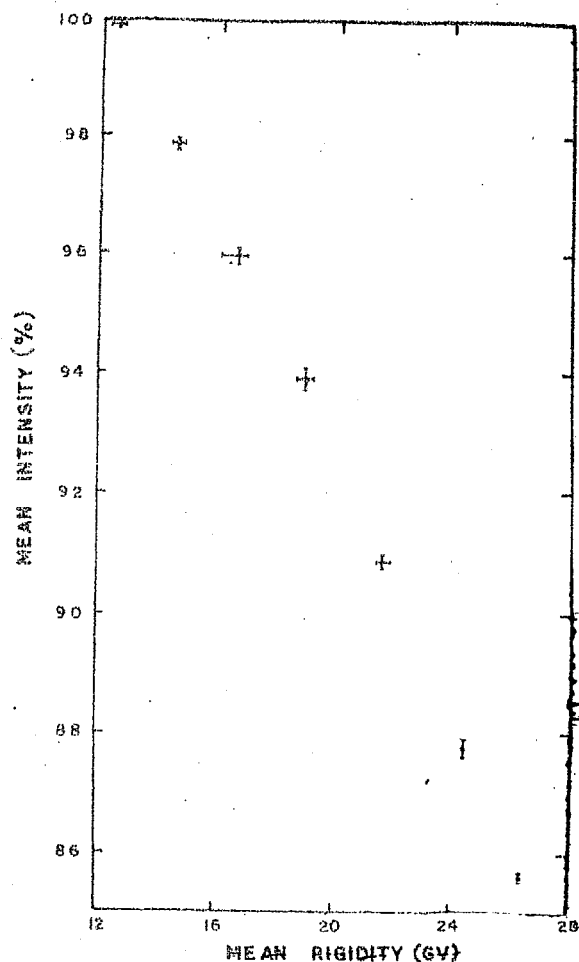
Fig. 3.4   Meson intensity at Ahmedabéd as a
function of rigidity recorded by
inclined telescopes.
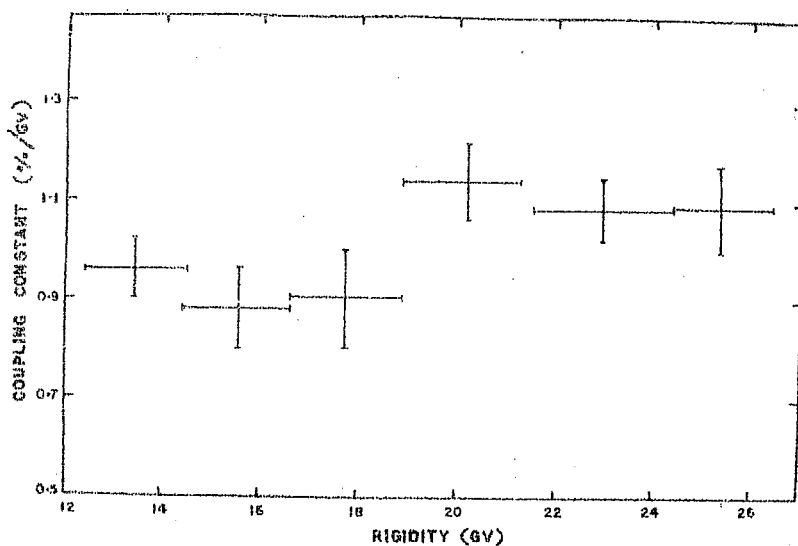
Fig. 3.5   Coupling constants for the meson component, as
derived from the azimuthal effect recorded at
Ahmedabad as a function of rigidity for 42.5°
zenith angle.

corresponding to that of primary proton but only at half of that value
(in terms of momentum per nucleon). This also needs to be taken into
account for an accurate estimation of the coupling constants. In our
theoretical calculation we have taken this into account.

Comparison with results obtained by other authors is shown in
Chapter V.

3.2   Method of analysis and results of the charge ratio experiment

3.2.1   Method of determination of the charge ratio from the experimentally measured quantities

Conversi (1950) has given the details of relating the experimentally
obtained quantities to get the charge ratio of cosmic ray muons.

Let us suppose that we choose muons having an energy in the range
E and E + $\triangle$ E and stop them in the absorber S. For a moment, let us
neglect the possibility of the capture of negative muons, the muons will
decay with their characteristic mean life and some of the decay electrons
will trigger the counter C. Let p be the probability that a muon brought
to rest in the absorber S decays into an electron which triggers the
counter C.

For all time measurements, we choose, as the origin, the instant
at which the muon is brought to rest in the absorber S. Suppose we record
the delayed coincidence events in n time channels as follows:

The first channel records those decay events which take place
after a certain minimum delay t_m and/a time t_m + t' (t' being the time
                                    before
width of the channel). We keep the channels equally spaced in time so
that the (r + 1) th channel records those decay events which take place
between times t_m + rt* and t_m + rt* + t', t* being the time difference
between the adjacent channels.

If M muons are brought to rest in the absorber at $t = 0$, then the rate of decay at any subsequent time t is given by

$$\frac{dN}{dt} = -(1/\gamma) \, Me^{-t/\gamma} \qquad \dots\dots(3.2)$$

where γ is the mean life of the muon.

The number of muons decaying between times t and $t + t'$ is given by

$$\int_t^{t + t'} dN = -(1/\gamma) M \int_t^{t + t'} e^{-t/\gamma} dt$$

therefore, $\quad N(t) - N(t+t') = Me^{-t/\gamma} \, (1-e^{-t'/\gamma}) \qquad \dots\dots(3.3)$

As noted previously p is the probability that a muon decay in the absorber S results in a decay electron which triggers the counter C. Hence, if N_{tc} is the number of counts recorded in the channel starting at time t, the actual number of decay events occurring in the time width t' of the channel would be

$$N_{tc}/p = M \, e^{-t/\gamma} (1-e^{-t'/\gamma})$$

therefore, $\quad \ln N_{tc} = -(t/\gamma) + \ln \left\{ Mp(1-e^{-t'/\gamma}) \right\} \qquad \dots\dots(3.4)$

The last term in the above logarithmic relation is constant for given M, t' and p.

A semi-logarithmic plot of N_{tc} versus t is a straight line of slope $-1/\gamma$. The intercept on the ordinate gives the number of muons that would have been recorded had there been a channel for recording the number of electrons passing through C in the time interval between $t = 0$ and $t = t'$.

Let us denote this number by N_c. Then,

$$N_c = Mp(1-e^{-t'/\mathcal{J}})$$

$$\text{i.e., } M = (N_c/p)(1-e^{-t'/\mathcal{J}})^{-1} \qquad \ldots\ldots(3.5)$$

Thus, if we know p and $\mathcal{J}$, we can estimate M, the number of muons brought to rest in the absorber at time $t = 0$. We have estimated p in the following way, since it is not possible to calculate p for arbitray geometrical arrangement of the absorber and counters.

If we measure the number of events I_a in which a muon is known to have come to rest in S, but which does not result in a decay electron which triggers the counter C between times t_m and $t_m + nt^* + t'$.

Then,

$$I_a = (1-p)M \qquad \ldots\ldots(3.6)$$

or

$$M = I_a/(1-p) \qquad \ldots\ldots(3.7)$$

combining (3.5) and (3.7), we get

$$I_a/(1-p) = (N_c/p)(1-e^{-t'/\mathcal{J}})^{-1}$$

or

$$\frac{1}{p} = 1 + (I_a/N_c)(1-e^{-t'/\mathcal{J}}) \qquad \ldots\ldots(3.8)$$

Thus, p can be determined by eqn. (3.8) and use of this value of p in eqn. (3.5) enables us to estimate M. Note that if I_a is measured as a rate, then M is the rate at which the muons are being brought to rest in S. Now, if the energy of the muons incident on the absorber S is varied by changing the thickness of the absorber S', the number of muons in the incident beam having energies between E and E + $\triangle$E is obtained as a function of E. In other words, we get the muon spectrum.

To determine the charge ratio, the experiment must be performed with two different absorbers, one of high atomic number and the other of low atomic number. We assume for the time being that both positive and negative muons decay freely in the latter absorber while only positive muons undergo decay in the former.

Let p_a and p_b be the probabilities that a decay electron triggers C when the low z and high z absorbers are placed above C and let N_a and N_b be the corresponding extrapolated counting rates (the difference between p_a and p_b may arise only due to possible differences in the geometry of the two settings). Also, let M_a and M_b be the rates of muons stopped in the low z and high z absorbers respectively. Knowing that both positive and negative muons decay freely in the low z absorber and only positive muons decay in the high z absorber, it can be shown that

$$\frac{M_+ + M_-}{M_+} = \frac{(N_a/p_a)/M_a}{(N_b/p_b)/M_b} = \frac{N_a\, p_b\, M_b}{N_b\, p_a\, M_a} \qquad \ldots\ldots(3.9)$$

or

$$\frac{M_+}{M_-} = \frac{1}{(\mathcal{P}\cdot N_a / N_b - 1)} \qquad \ldots\ldots\ldots(3.10)$$

where
$$\mathcal{P} = (p_b\, M_b)/(p_a\, M_a) \qquad \ldots\ldots\ldots(3.11)$$

3.2.2 Parameters of the muon telescope

Four channels were used for registering the delayed coincidence events, so that four points of the decay curve corresponding to the muons stopped in the absorber were obtained.

Experimental dependence of the capture probability of negative muons upon the atomic number is such that only 3 to 4% of the negative muons stopped in lead decay with a mean life of about 0.075 microsecond while the rest get captured (Feinberg and Lederman, 1963). The minimum delay for which a coincidence was recorded in the first channel in the

present experiment was chosen to be 0.2 microsecond. Thus the assumption

that all negative muons are captured in lead seems to be reasonable. On

the other hand, for graphite, the main process will be decay rather than

capture; for both positive and negative muons.

Decay events were recorded simultaneoulsy in four time channels

viz. 0.2 to 2.2 microseconds, 0.2 to 4.2 microseconds, 0.2 to 6.2 microseconds

and 0.2 to 8.2 microseconds, in the integral manner. The differences between

the successive channels were obtained to get N_{tc} to be used in equation

(3.4). Thus, for the present experiment:

n,	no. of channels	= 4
t_m,	minimum delay for registering a delayed coincidence event	= 0.2 microsecond
t',	time width of the channel	= 2 microsecond
t*,	time difference between the adjacent channels	= 2 microsecond

A comparison of the number of events registered in these four time

channels also served as a check on the operation of the equipment since

the mean life of the muon is known to be about 2.2 microsecond.

The geometrical factor of the experimental arrangement has been

calculated by the method described by Kane and Rao (1958) using the

dimensions of the counters and their separation. The geometrical factor

thus calculated comes out to be 56.65 cm^2 sr.

Random events may give a contribution to the delayed coincidences

registered in each channel. Therefore, an accurate estimate of spurious

events occurring in each channel becomes essential for correcting the

corresponding delayed coincidences recorded experimentally. Only then

the decay curve of the stopped muons can be obtained accurately.

Events, in which a particle producing a double coincidence AB
but failing to trigger the counter C (let $n_{AB\overline{C}}$ be the counting rate of
these events) was followed after a short time by a triggering of counter
C, could cause the random delayed coincidences. If n_c is the background
counting rate of the counter C, then we have

$$N_r = 2 \, n_{AB\overline{C}} \, \mathbf{n}_c \, t'$$

.....(3.12)

where $t' = $ time width of the channel

N_r, the rate of random delayed coincidences is small at sea level.
However, the correction can be applied with sufficient accuracy because all
the quantities needed for the estimation of N_r can be measured with great
accuracy.

3.2.3 <u>The method of obtaining the extrapolated delayed coincidence rate
and the mean life of mu-mesons</u>

Equation (3.4) relates N_{tc}, the number of decay events occurring in
a particular channel to t, the start of the channel. A semi-logarithmic
plot of N_{tc} against t is a straight line with a slope of $-1/\tau$, where τ
is the mean life of muons at rest.

Replacing $\ln N_{tc}$ by y, eqn. (3.4) can be re-written as

$$y = at + b$$

.....(3.13)

If we now substitute different values of t in the above relation,
values of y thus obtained will not be in general equal to y_s (obtained
experimentally) as there will be an "error" of magnitude

$$at_s + b - y_s$$

We now, try to obtain the linear relation which best fits the
experimental data using the usual statistical "least square" method i.e.

by choosing a and b in such a way that the sum of the squares of the errors is least, that is,

$$\sum (at_s + b - y_s)^2 \text{ is least.}$$

Differentiating the above relation partially with respect to a and b we obtain the conditions

$$\sum t_s(at_s + b - y_s) = 0$$

and

$$\sum (at_s + b - y_s) = 0$$

These conditions yield a and b after simplification as

$$a = \frac{n[ty] - [t][y]}{n[tt] - [t][t]}$$

$$b = \frac{[y][tt] - [t][ty]}{n[tt] - [t][t]}$$

where,   n = number of data points i.e, number of time channels, and

$[yt]$ denotes the summation $\sum_{s=1}^{n} y_s t_s$

Next step is to estimate the accuracy of the coefficients a and b derived by the above method.

We can calculate the residuals d_s, given by $at_s + b - y_s$, using the values $y_1, y_2 \ldots \ldots, y_n$, and $t_1, t_2, \ldots \ldots, t_n$; and the most probable values of a and b. Then the mean square error σ^2 in the expression $at_s + b - y_s$ is given by

$$\sigma^2 = [dd]/(n-2)$$

If standard errors in the values of a and b are denoted by σ_a and σ_b, then we have

$$\sigma_a^2/n = \sigma_b^2/[tt] = \sigma^2/\triangle$$

where $\triangle$ is the determinant

$$\left| \begin{array}{cc} \left[tt \right] & \left[t \right] \\ \left[t \right] & n \end{array} \right| = n \left[tt \right] - \left[t \right]^2$$

Having thus obtained a, σ_a, b and σ_b, we can derive $\mathcal{T}$, the

mean life of muons, and N_c (the extrapolated delayed coincidence events)

as follows:

since,
$$\mathcal{T} = -1/a$$

therefore,
$$\sigma_{\mathcal{T}} = \sigma_a \Big/ {a}^2$$

and
$$b = \ln N_c$$

therefore,
$$N_c = e^b$$

and
$$\sigma_{N_c} = N_c \sigma_b$$

Thus, we obtain $\mathcal{T}$, $\sigma_{\mathcal{T}}$, N_c and σ_{N_c}.

3.2.4 The determination of the probability p

We have mentioned earlier that eqn. (3.8) can be used for the

experimental determination of p, where I_a is the true anticoincidence rate.

The events are registered as anticoincidences when no pulse appears from

the counter C within 8.2 microseconds after the time of occurrence of a

coincidence AB.

An assumption was made in writing eqn. (3.6) that only muons contribute

to the anticoincidence rate I_a. However, any ionozing particle traversing

the telescope AB and stopping in the absorber S will give an additional

contribution, x, to the anticoincidence rate I_a, so that we shall write,

in general

$$I_a = (1-p) M + x \qquad \qquad \ldots\ldots(3.14)$$

The intensities of muons and of X-particles can be determined from equations (3.5) and (3.14) if the value of p is known. The hard component of cosmic rays is known to be composed mainly of muons at large atmospheric depths, protons accounting only for a small percentage of the hard component. The momentum spectrum of the sea level protons is now well studied (Brooke and Wolfendale, 1964). Therefore, we can perform measurements in such experimental conditions in which the contribution of x in eqn. (3.14) is negligible in comparison with (1-p)M. In such cases only eqn. (3.6) is valid and p can be determined from eqn. (3.8).

Two series of measurements were performed and the results obtained are shown in Tables 3.1 and 3.2. The measurements being referred to as series No. 1 and 2 and the amount of material being also specified there. A graphite absorber of thickness 22.95 gm cm^{-2} was used in these measurements.

The delayed coincidences registered in all channels have been corrected for the random coincidences and corrected events are shown in Table 3.1. The extrapolated delayed coincidences shown in Table 3.1 have been obtained by the method described in the previous section (3.2.3). Anticoincidence rates, obtained without any absorber between counters B and C and reported in Table 3.2, are attributed to those low energy muons which lose almost all their kinetic energy in scintillator B and fail to emerge out of it with any appreciable energy. Anticoincidences reported in Table 3.2 have been obtained simultaneously with the delayed coincidences reported in Table 3.1.

It is to be noted that ratio I_a/N_c between "true anticoincidences" and "extrapolated delayed coincidences" for both series of measurements is the same within statistical limits. If particles other than muons

(X-particles) were present in significant percentage in the case of series No.1, we should expect in passing from the first to the second series a decrease of the ratio I_a/N_c due to their absorption in the additional amount of material available in series No.2.

TABLE 3.1

Results of measurements of delayed coincidences for the determination of p

Series No.		1	2
Material above the absorber S (g/cm^2)		313	495
Duration of observations (minutes)		20940	24030
Corrected delayed coincidences registered in channel:	1	293	340
	2	119	138
	3	43	·53
	4	20	23
Total extrapolated delayed coincidence events		316 $\pm$ 21	369 $\pm$ 12
Extrapolated delayed coincidences per hour		0.91 $\pm$ 0.06	0.92 $\pm$ 0.03
Mean life of muons Υ in microsecond		2.205 $\pm$ 0.082	2.213 $\pm$ 0.040

On the basis of our results, therefore, contribution of x seems to be negligible. Then eqn. (3.6) is valid and we obtain the values for p given in Table 3.2. σ_p, the standard error in the probability p, has been calculated by the relation

$$\sigma_p^2 = p^4 \left[(\frac{1}{p} - 1)^2 \left\{ (\frac{\sigma_I}{I})^2 + (\frac{\sigma_N}{N})^2 \right\} + (\frac{2I^2}{N \Upsilon^2}) e^{-2t'/\Upsilon} \sigma_\Upsilon^2 \right]$$

where,

I = True anticoincidence rate

N = Extrapolated delayed coincidence rate

t' = Time width of the channel

$\mathcal{T}$ = Mean life of muons at rest

and σ_I, σ_N and $\sigma_{\mathcal{T}}$ are the corresponding standard errors.

TABLE 3.2

Results of measurements of anticoincidences for the determination of p

Series No.	1		2	
Material above the absorber S (g/cm^2)	313		495	
Absorber S (Graphite)	On	off	on	off
Duration of observations (minutes)	20940	25800	24030	21330
Anticoincidences per minute	3.27 ± 0.013	2.82 ± 0.011	3.02 ± 0.011	2.56 ± 0.011
True anticoincidence per minute, I_a	0.45 ± 0.016		0.46 ± 0.016	
I_a/N_c	29.9 ± 2.3		29.8 ± 1.4	
p	0.0531 ± 0.0040		0.0534 ± 0.0024	
$\langle p \rangle$ Weighted mean		0.0533 ± 0.0021		

Weighted mean of these two values of p is taken and mean p thus obtained is shown in the last line of Table 3.2. We obtain, then, from eqn. (3.5)

$$M \approx 31.4 \ N_c \qquad \qquad \ldots\ldots(3.15)$$

since, $t' = 2.0$ microsecond

Value of p experimentally derived is very low indeed as was expected because a large percentage of electrons produced by the decay of muons either get reabsorbed in the absorber S or scatter out. A better value of p could have been achieved by putting a number of scintillation counters around the absorber S and thereby reducing the effect of scattering.

3.2.5 The integral intensity of vertical muons

The integral intensity is usually defined as the intensity of all particles with momentum greater than a certain minimum momentum. Better statistical accuracy can be achieved in determining the integral intensity than the differential intensity. A relatively simple arrangement, consisting mainly of a counter telescope with an absorber (to define the minimum momentum), is needed for the measurement of the integral intensity.

In the present experiment, rates of double coincidences AB have been taken with different thicknesses of lead absorber to obtain the integral intensity corresponding to different minimum momentum. The energy loss expression of Sternheimer (1956) has been used for the computation of the minimum momentum required for muons to traverse the telescope AB, formed by the counters A and B and the absorber S' placed between them and thus, to give a double coincidence AB.

The results obtained are shown in Table 3.3. Also shown are the amount of material in each case. The double coincidence rates have been corrected for the random coincidences. The integral intensity obtained by us of muons of momentum greater than 320 MeV/c is presented in Table 3.4 together with the results of other workers. The integral intensity

measured by us at 320 MeV/c is found to be about 3.3% lower than the value given by Allkofer et al. (1968). This reduction of intensity can be explained on the basis of different geomagnetic cut-offs at two different places.

TABLE 3.3

The measured integral intensities of
muons at Ahmedabad

Lead Absorber (g/cm^2)	Minimum momentum (MeV/c)	Duration of observations (minutes)	Integral intensity $(10^{-3}cm^{-2}s^{-1}sr^{-1})$
167	320	2880	7.01 ± 0.027
313	495	3990	6.64 ± 0.022
404	603	2510	6.32 ± 0.027
495	715	2880	6.06 ± 0.025

TABLE 3.4

The integral intensity of muons $(p_\mu \geqslant 320\ MeV/c)$

Author	Geomagnetic Latitude (°N)	Cut-off (GV)	Integral intensity $(10^{-3}cm^{-2}s^{-1}sr^{-1})$
Present experiment	13.7	16.0	7.01 ± 0.027
Allkofer et al. (1968)	9	14.1	7.25 ± 0.1
Bhattacharyya (1970)	12	13.7	7.30 ± 0.15
Fukui et al.(1957)	24	12.6	7.35 ± 0.2
Kitamura and Minakawa (1953)	25	12.6	7.2 ± 0.1
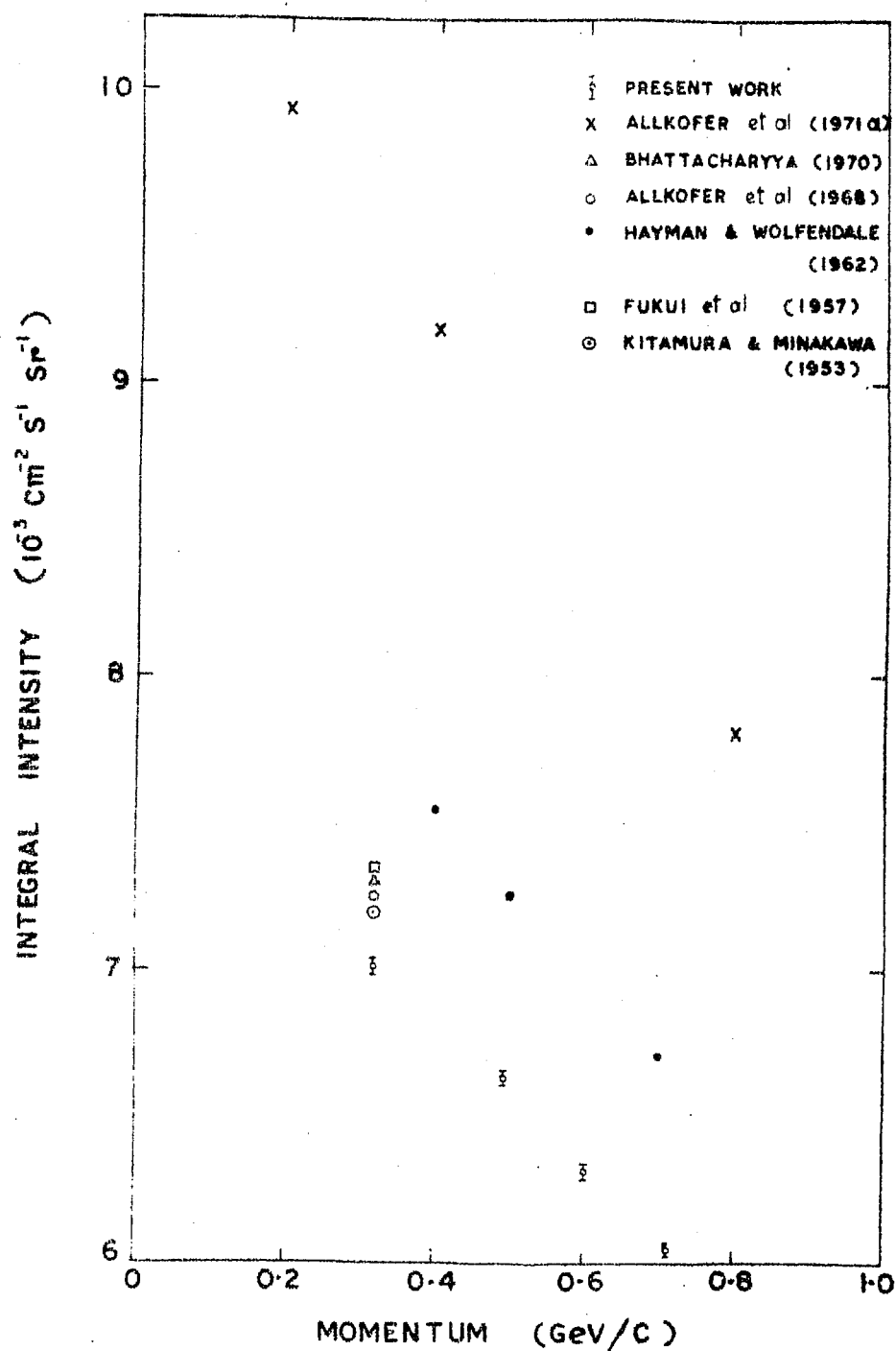
Figure 3.6   Integral spectrum of the vertical cosmic
ray muons at various latitudes.

In Figure 3.6 we have shown results obtained by us together with the results obtained by other workers in the same momentum range. The measured intensities by us are in good agreement with the results of other workers. However, the integral intensities obtained by us are significantly lower than those of Hayman and Wolfendale (1962) and Allkofer et al. (1971 a). This is in conformity with the existence of the latitude effect of low energy muons because the latter experiments were performed at geomagnetic latitudes $55.0^{\circ}N$ and $57.5^{\circ}N$ respectively and hence refer to measurements at low cut-off rigidity.

3.2.6 The differential intensity of the vertical muons:

As mentioned earlier both types of muons brought to rest in the absorber of low atomic number decay with a mean life of about 2.2 microseconds because the capture probability for the negative muons in graphite is very low indeed. This fact enables us to determine the differential intensity of muons from the delayed coincidence events registered experimentally.

Four series of measurements were performed with different thicknesses of lead absorber S'. Thus four points of the muon momentum spectrum were obtained corresponding to four momentum ranges. The thickness of the graphite absorber (S) was 22.95 g/cm^2.

Extrapolated delayed coincidence rates were obtained from the decay events registered in four time channels as explained in section 3.2.3. Delayed coincidence events registered in all channels were corrected for random coincidences. M, the rate at which the muons are being brought to rest in absorber S, is then obtained by eqn. (3.15). The muon momentum has been computed in each case using the energy loss expression

of Sternheimer (1956). Knowing the momentum difference, the geometrical factor of the telescope and the rate of muons stopped in the graphite absorber the differential intensity can be obtained.

Results of our measurements are shown in Table 3.5. The amount of lead absorber in g/cm^2 has also been given in column 1 of the Table 3.5.

TABLE 3.5

The measured differential intensities
of vertical cosmic ray muons

Lead Absorber (g/cm^2)	Momentum group (GeV/c)	Mean momentum (GeV/c)	The differential intensity $(10^{-4}cm^{-2}s^{-1}sr^{-1}(GeV/c)^{-1})$
78	0.21-0.26	0.235	33.2 $\pm$ 1.1
143	0.29-0.34	0.315	31.0 $\pm$ 0.6
313	0.49-0.54	0.517	29.8 $\pm$ 2.0
495	0.71-0.76	0.740	29.4 $\pm$ 0.9

The measured differential intensities of muons in the momentum range (0.2-0.8) GeV/c are shown in Figure 3.7 together with those measured by Allkofer et al. (1968) and Bhattacharyya (1970) near the geomagnetic equator. Also shown are the results obtained by Hayman and Wolfendale (1962) at 55°N and Allkofer et al. (1971 a) at 57.5°N.

In most cosmic ray experiments at sea level the muon spectra are not measured absolutely but adapted at a normalization point of 1/GeV/c to the intensity of $2.45 \times 10^{-3}cm^{-2}s^{-1}sr^{-1} (GeV/c)^{-1}$. This value was obtained by Rossi (1948). Rossi spectrum itself is being normalized at 0.3 GeV/c to the spectrum obtained by Greisen (1942).
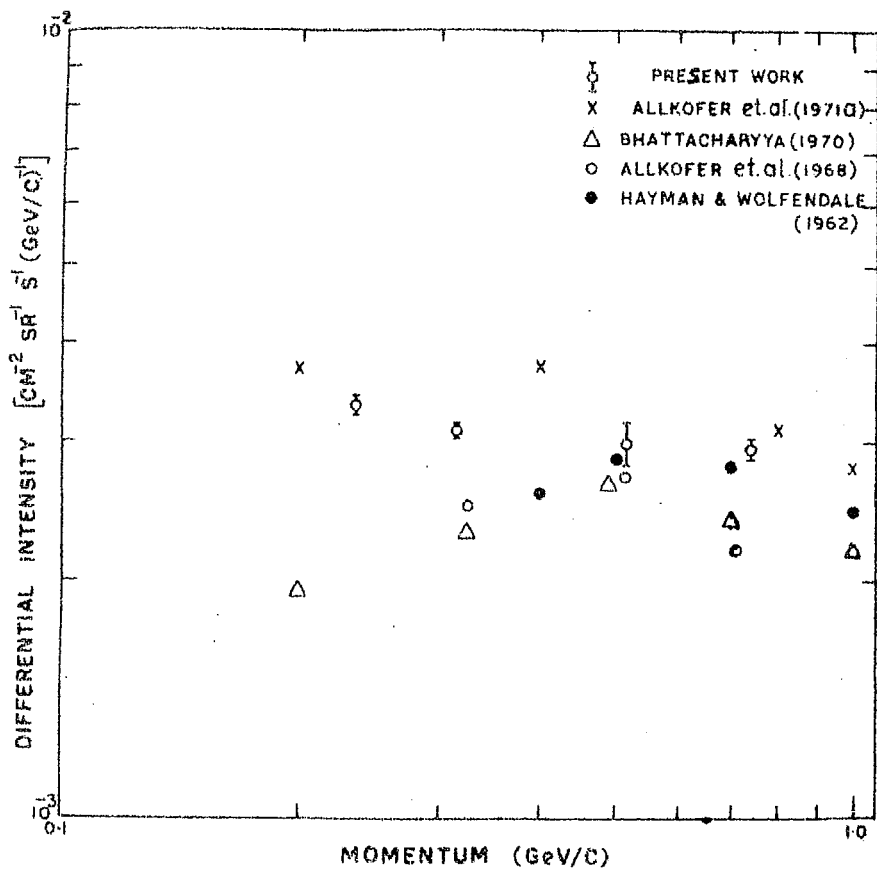
Figure 3.7   Differential momentum spectrum of
vertical cosmic ray muons at various
latitudes.

Recently Allkofer et al. (1970) remeasured the intensity at the momentum of 1 GeV/c and found it to be about 26% higher than the Rossi value at the same latitude. Also recent measurements of De et al. (1972), Ayre et al. (1971 a), Bateman et al. (1971) and Crookes and Rastin (1971) showed the evidence of higher vertical muon intensities near and above 1 GeV/c muon momentum. Consequently doubt has been cast on the validity of those spectra which were normalized to the Rossi value.

It can be seen from Figure (3.7) that Hayman and Wolfendale values (which are normalized to Rossi value) seem to be too low despite the fact that these values were obtained at 55°N. However, the muon intensities obtained by us at different momentum are significantly lower than the corresponding values of Allkofer et al. (1971 a) which is to be expected on the basis of the latitude effect of the low energy muons. But the differential intensities obtained by us are higher than those obtained by Allkofer et al. (1968) and Bhattacharyya (1970) at low latitude stations.

3.2.7 <u>Measurements for the determination of the charge ratio of cosmic ray muons at sea level</u>:

(a) <u>The thickness of the stopping material</u>:

The measurements of the change ratio of cosmic ray muons were performed by the method of delayed coincidences. It has already been noted that some of the low energy muons are stopped in the middle scintillator (B) and the energy lost by these muons in scintillator B is sufficient to give a detectable pulse B. These stopped muons will also decay and some of the decay electrons have a reasonable probability of traversing the counter C and thereby registering themselves in different time channels for recording delayed coincidence events. This would make the

charge ratio measurements uncertain upto a great extent because the decay events registered by the delayed coincidence circuit should allow electrons corresponding to muons which were brought to rest in the absorber S. However, this uncertainty can be removed by choosing the thickness of the absorbers according to the range of decay electrons in them. Electrons from the muon decay can have a maximum energy of about 52 MeV (Barlow et al., 1964) and the range of 52 MeV electron in graphite is nearly 23 g/cm^2. Therefore, a graphite block of this thickness was chosen to stop all the electrons produced in the counter B lest they might trigger the counter C.

The probability of registering a decay event p, can be determined experimentally from eqn. (3.8). However, this expression can be used when graphite is used as a stopping material. In lead absorber, negative muons are captured and therefore eqn. (3.8) cannot be used as it is. However, if sizes of the two stopping material are chosen in the ratio of the ranges of the decay electrons in them, then equal probability for detection can be assured (Shamos et al., 1948). The thickness of the lead absorber was thus chosen appropriately as 14.4 g/cm^2.

(b) X-events

The true anticoincidence rate, I_a, is obtained by subtracting the anticoincidence rate without absorber (spurious anticoincidence rate) from the anticoincidence rate recorded with the absorber S.

The geometry of the apparatus and the small amount of material used as the stopping absorber make it very unlikely that a lateral shower, which in the absence of the absorber S would strike the scintillation counter C, produces an anticoincidence when the absorber S is on. Other causes of spurious anticoincidence events such as random events etc. are

not appreciably affected by the presence of the absorber S. These

considerations suggest that the method of obtaining true anticoincidences

outlined above is the appropriate one.

We have mentioned earlier in section 3.2.4 that the two series of

measurements were performed in which the contribution of x was negligible

as compared to $(1-p)M$ of eqn. (3.14). However, if the thickness of the

absorber S' is reduced then this may not be so. Nevertheless, we can

estimate the rate of X-events in such cases as $I_a - (1-p)M$.

So far we have not said anything specifically about the nature of

these X-particles. There are some possibilities about the nature of

particles contributing to these X-events. The various possibilities are:

(i) X-particles must be ionizing particles arriving from the atmosphere

and either stopping in the absorber S after traversing counters A and B,

or producing other ionizing particles (in the lead between counters A and B),

of which at least one traverses counter B, stopping in the absorber S, and

none of which strikes the counter C.

(ii) After they or their secondary particles have been stopped in the

absorber S, no emission of secondary ionizing rays striking the counter C

has to take place within 8.2 microseconds.

Anticoincidence observations with about 7 cm and about 13 cm of

lead material between counters A and B are shown in Table 3.6. Also shown

are the rates of X-events estimated by the above considerations.

It is very unlikely that any appreciable percentage of such events

could be due to electrons. A large electron shower capable of traversing

13 cm of lead can hardly end in the absorber S without triggering the

counter C. Contribution due to locally produced π-mesons also seems

to be insignificant.

TABLE 3.6

The results of measurements of anticoincidences and the X-events

Series No.	1		2	
Material above the absorber S (g/cm^2)	78		143	
Absorber S (Graphite)	On	Off	On	Off
Duration of observation (minutes)	22190	16180	14380	14060
Anticoincidences per minute	3.787 ± 0.013	3.120 ± 0.014	3.242 ± 0.015	2.688 ± 0.014
True anticoincidences per minute, I_a	0.667 ± 0.019		0.554 ± 0.020	
X-particles per minute $(I_a - (1-p)M)$	0.14 ± 0.026		0.09 ± 0.019	

This led us to believe that the majority of ionizing particles contributing to the X-events must be protons. Protons, capable of penetrating 13 cm of lead placed between counters A and B and stopped in the graphite absorber, must have momentum in the range of 0.914 to 1.006 GeV/c if they lose energy only by ionization. The intensity of protons derived from the rates of X-particles is at least twice of that given by Brooke and Wolfendale (1964) even after taking into consideration the statistical limits.

However, with 7 cm of lead interposed between counters A and B, protons contributing to the X-events must have momentum in the range 0.75 to 0.86 GeV/c. The intensity of protons derived in this case comes

out to be at least 60% higher than those obtained by Brooke and
Wolfendale (1964).

3.2.7.1   Results of the charge ratio measurements

We have mentioned earlier that p can be determined experimen-
tally in the case of the graphite absorber and also that the sizes of
the two absorbers were chosen in the ratio of the ranges of the decay
electrons in them to ensure equal probability. However, in addition to
this the geometry must also remain the same in both the settings. The
thickness of the lead and graphite absorbers were quite different. The
lead absorber was kept,therefore,on 3 plywood strips each of thickness
~ 6 g/cm^2 between counters B and C in such a way that the geometry
remains roughly the same in both the settings.

All the 3 plywood strips together covered nearly 11% of the area
of the counter C. Some of the muons will decay in this material and this,
being nearer to the counter C and also having smaller capture probability
for negative muons, would give spurious delayed coincidence events.
Unfortunately, there seems to be no way to correct for this effect.

Assuming for the moment $p_b/p_a = 1$ and taking appropriate "true
anticoincidence rates" for lead and graphite absorbers the charge ratio
has been estimated using the expression (3.10). The results obtained are
shown in Table 3.7. However, p_b/p_a can be determined if we know the charge
ratio accurately. We have, therefore, normalized our results to those of
Allkofer et al. (1968) at a muon momentum 0.71 GeV/c; p_b/p_a thus derived
comes out to be 1.153, i.e., the probability of detecting a delayed
coincidence from lead absorber is nearly 15% more than the analogous
probability for the graphite absorber for the present experimental set-up

TABLE 3.7

The results of the charge ratio of cosmic ray muons

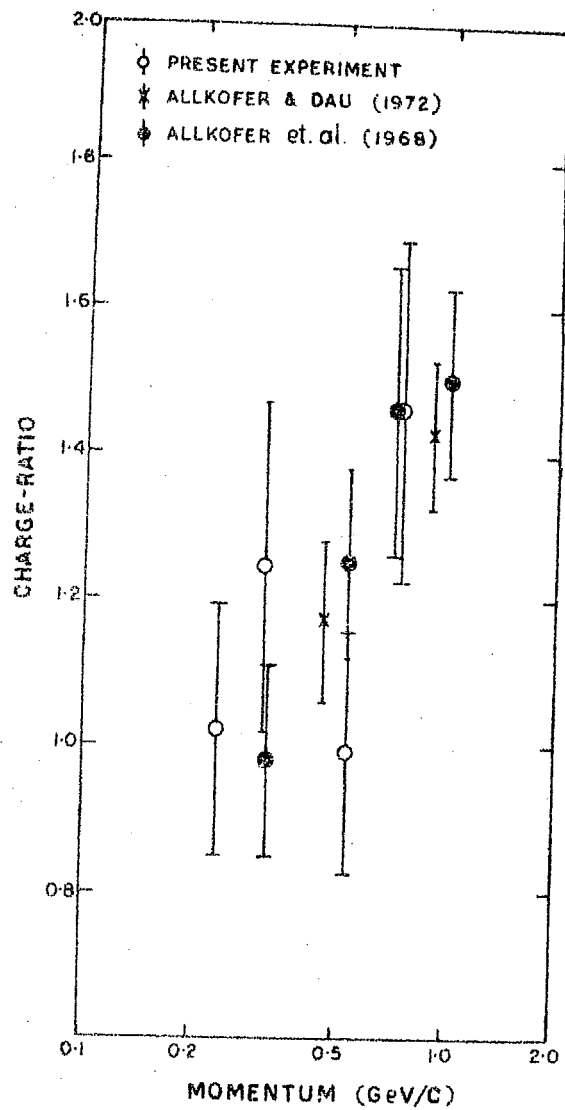| 1	2	3	4	5	Delayed coin. regi-stered in channel:				10	11	12
Sr. No.	Material above absorber (g/cm²)	Mean momentum (GeV/c)	Absorber S	Duration of obs. (Min.)	1	2	3	4	N_c per hour	Charge ratio	Normalized charge ratio (see text)
					6	7	8	9			
1.	78	0.235	Gr	22190	363	142	62	24	1.064±0.034	1.40±0.28	1.02±0.17
			Pb	25490	240	93	39	16	0.606±0.014		
2.	143	0.315	Gr	14380	208	82	35	14	0.939±0.019	1.77±0.40	1.25±0.23
			Pb	26710	254	98	43	17	0.613±0.020		
3.	513	0.517	Gr	20940	293	119	43	20	0.905±0.060	1.35±0.27	0.99±0.17
			Pb	35880	255	105	41	17	0.469±0.007		
4.	495	0.740	Gr	24030	340	138	53	23	0.922±0.030	2.17±0.45	1.46±0.24
			Pb	25690	184	76	30	12	0.476±0.006		

Figure 3.8   The sea level charge ratio as a function
of muon momentum in vertical direction
near the geomagnetic equator.

which seems to be quite reasonable in view of the above discussion.

The results of vertical muon charge ratio measurements thus obtained by us at Ahmedabad in the momentum range 0.2-0.8 GeV/c are shown in Figure 3.8. Also shown in this figure are the results obtained by Allkofer et al. (1968) and Allkofer and Dau (1972) near the geomagnetic equator at sea level.

It can be seen from Figure 3.8 that the present results are in good agreement with those of Allkofer et al. (1968) and Allkofer and Dau (1972). The charge ratio below 0.7 GeV/c muon momentum comes out to be nearly unity from the present experiment which is to be expected on the basis of following theoretical considerations:

(a)   In low energy range, because of the diminished survival probability of muons from first collision, a greater fraction of the muons recorded at sea level arrive from lower atmosphere where the interacting nuleons are likely to be charge symmetric.

(b)   The median primary energy for such low energy muons is likely to be around 15 GeV per nucleon, in which case the primaries will be heavies at our latitude, since the vertical cut-off (in energy per nucleon) for heavies is about half that for protons   (Pal, 1971).

(c)   Kaon contribution, which tends to enhance the charge ratio, is negligible in the low energy range.

3.2.8   The mean life of the mu-mesons

Some of the results of the measurements of delayed coincidences for different momentum ranges reported in Table 3.7 have been graphically represented in Figure 3.9. It may be noted from this figure that all the decay curves are consistent with a mean life $\mathcal{T}$ of approximately 2.2 microsecond. The delayed coincidence measurements were analysed
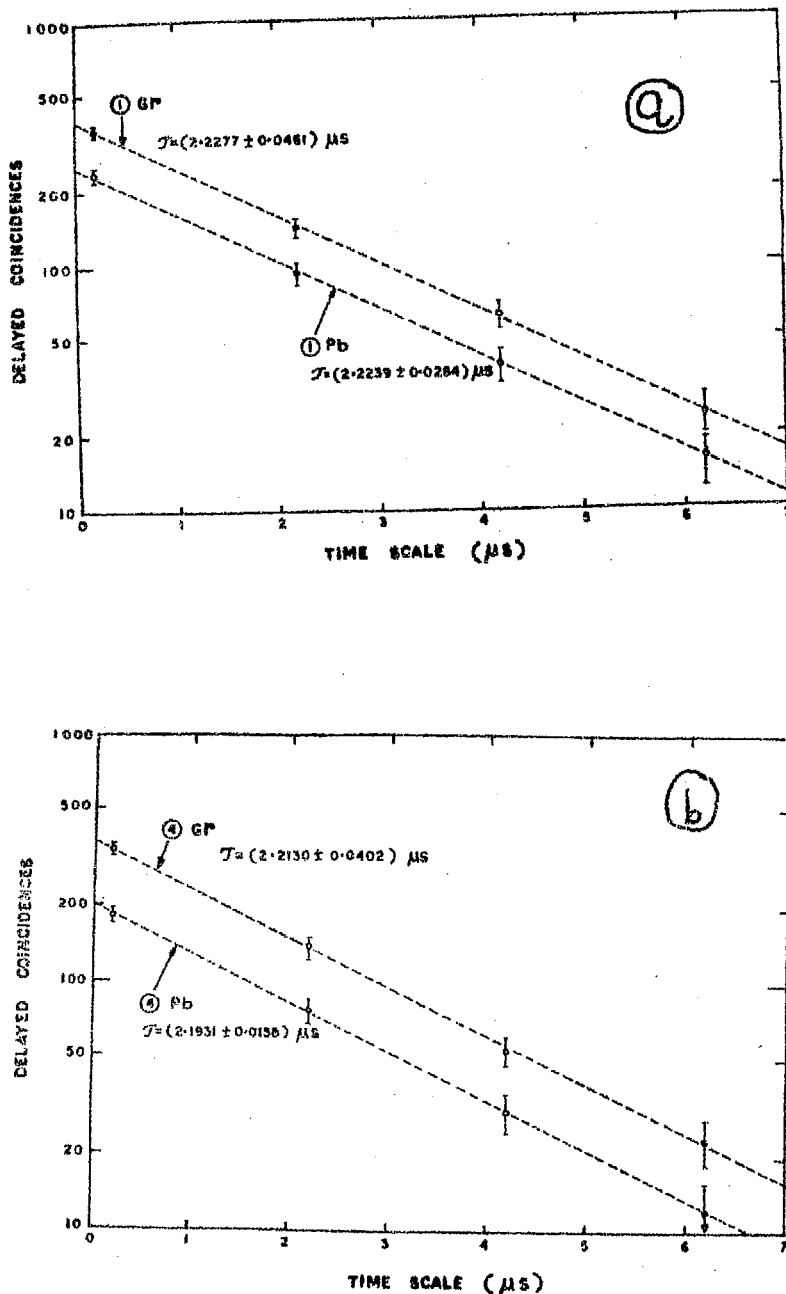
Figure 3.9   Decay curves obtained for the different momentum
ranges.   Each point of the decay curve represents
the number of muons disintegrating between the in-
stant t of the corresponding abscissa and t + t'
(t' = 2.0 μs.)
(a)   Series No. 1 of the Table 3.7
(b)   Series No. 2 of the Table 3.7

separately for each of the momentum ranges and each of the absorbers.

The values of Υ obtained were found to be not much different from individual measurements, therefore, all the observations pertaining to different momentum ranges were combined together to get a value of Υ for each absorber. The values obtained are :

$$\Upsilon = 2.2167 \pm 0.0102 \ \mu S \text{ with lead absorber}$$

$$\Upsilon = 2.2197 \pm 0.0205 \ \mu S \text{ with graphite absorber}$$

Both these values, being similar within the statistical limits, were combined to get

$$\Upsilon = 2.2185 \pm 0.0135 \ \mu S$$

Mean life Υ thus obtained is in agreement with the values obtained by other workers. This shows that the equipment worked satisfactorily during the/period of its operation.
entire

3.2.9 <u>The interpretation of the charge ratio of cosmic ray muons</u>

Several attempts have been made to explain theoretically the variation of the charge ratio with momentum.

Earlier attempts were mainly by Caldiroli and Loinger (1950), Cini and Wataghin (1950) and Yeivin (1955). Since then further data on the charge ratio have been accumulated and also more information on high-energy interactions has become available. Both these factors made it possible to make refinements in the theoretical calculations.

Mackeown and Wolfendale (1966) have given an excellent review of the theoretical work done to explain the charge ratio data prior to 1966. Hence, we would simply attempt to describe; (a) the isobar model of meson production by Pal and Peters (1964), and (b) a recent model proposed by

fragmentation or scaling hypothesis and the knowledge of primary cosmic ray spectra. They have then used the accelerator data to explain the observed charge ratio of cosmic ray muons.

3.2.9.1 The isobar model

A model based on the strong coupling of the π -meson -nucleon system has been given by Pal and Peters (1964). The pion-nucleon coupling results in a series of nucleon isobaric levels. In the nucleon-nucleon collision one or both of the nucleons is excited from nucleon ground state to one of such isobaric levels. Subsequent de-excitation of nucleon isobars result in the emission of low energy π -mesons. Pal and Peters used the observed charge ratio of muons to determine some of the characteristics of a general isobar model.

However, besides the contribution of pions by their decay to muon flux, certain non-strange isobars can also decay by various modes into kaons and these kaons by their decay also contribute to the observed flux of muons.

The kaon contribution becomes significant in the high energy range because the mean life of charged kaons is significantly shorter than that of charged pions and their mass is greater. Therefore, in the energy range where pion interaction becomes more probable than decay, a large fraction of muons arises from the decay of charged kaons, because at a given energy the decay probability before interacting in the atmosphere is larger for a kaon than for a pion.

The various decay modes contributing to kaons are:

$$N^* \rightarrow K + Y \qquad (M > 1610 \text{ MeV})$$

$$N^* \rightarrow (K\overline{K}) + N \qquad (M > 1960 \text{ MeV})$$

and

$$N^* \rightarrow K + Y^*, \quad Y^* \rightarrow \overline{K} + N \quad (M > 2010 \text{ MeV})$$

where the symbols K, Y and N represent kaons, hyperons and nucleons respectively, and N* represents a nucleon in an excited isobaric state.

The first decay mode dominates in the production of kaons because it has the lowest threshold energy for the production of/kaons. Further, this mode can produce positive but not negative kaons. Also, the large positive excess among kaons (Lal et al., 1953) follows directly from the assumption that most of the excited isobars have strangeness number zero.

Pal and Peters, therefore, expressed the ratio of positive to negative muons at sea level as

$$\frac{N(\mu^+)}{N(\mu^-)} = \frac{1 + \delta_\mu}{1 - \delta_\mu} + \frac{2}{1 - \delta_\mu} b_k \frac{F_{\mu k}}{F_\mu}$$

where F_μ is the muon flux arising from the decay of pions, $F_{\mu k}$ is the muon flux delivered from the decay of kaons, δ_μ is the positive excess of muons at sea level produced purely by pion decay and b_k is the branching ratio for the decay mode $N^* \rightarrow K + Y$.

Various curves were drawn to show the variation of the charge ratio with momentum (given by the above expression) corresponding to various values of b_k. A comparison of these curves with the experimental data allows b_k to lie between 0.05 and 0.2 for a satisfactory agreement. Each value of b_k corresponds to a definite value of the kaon to pion production ratio, K/π. A value of $b_k = 10\%$ corresponds to a K/π ratio of 20%.

Ashton and Wolfendale (1963) obtained an upper limit of 40% for the K/π ratio at about 70 GeV production energy from the variation of the sea level muon flux with zenith angle. Judge and Nash (1963) by a similar study concluded that the kaon contribution is less than 30%. Thus the upper limit of 20% for the K/π ratio derived by Pal and Peters is not inconsistent with the experimental results.

It can be concluded, therefore, that according to Pal and Peters model the observed charge ratio of high energy cosmic ray muons at sea level cannot be explained on the assumption of production by π -mesons only.

3.2.9.2   Scaling hypothesis and the charge ratio of cosmic ray muons

In the understanding of high energy multiparticle reactions the property of limiting fragmentation (Benecke et al., 1969) or scaling (Feynman, 1969) has played an important role.

Frazer et al. (1972), in order to obtain the charge ratio of cosmic ray muons theoretically, illustrated how to correlate the cosmic ray data with accelerator data by combining the scaling hypothesis with the steep decline of the primary cosmic ray flux with increasing energy. By this method one can check (i) whether scaling hypothesis and accelerator data can explain the observed charge ratio of muons, and (ii) whether the observed constancy of the charge ratio favours any particular model of high energy reactions.

Muons are produced by two mechanisms, fragmentation and pionization. In pionization mechanism, copious production of low energy particles takes place from a cloud which is at rest in the centre of mass system of the colliding nucleons, whereas in the fragmentation process particles are produced at low energy in the rest frame.

In some models, such as the multiperipheral model, only the fragmentation products reflect the charge of the incident particle; the pionization products are indepedent of the nature of the incident particles. As the energy of the incident particle increases the ratio of the number of pionization to fragmentation products increases logarithmically in such models, hence μ^+/μ^- ratio is expected to decrease asymptotically

to 1. However, as a consequence of the steeply falling primary spectrum, the contribution from high energy particles gets suppressed, whereas the contribution from particles near the threshold for producing a given energy pion gets enhanced. Since pions produced in the latter case are fragmentation products, it can be concluded in view of above discussion that fragmentation is the dominant process in the production of cosmic ray pions (and consequently of muons) of any given energy, despite the existence of pionization. It should be mentioned here, however, that the same result was obtained by Pal and Peters (1964).

Frazer et al. first started with an oversimplified model based on the following assumptions:

(i) The primary spectrum consists entirely of protons which interact once with the atmospheric nuclei.

(ii) All pions, produced in these interactions, decay into muons.

(iii) Kaon production is ignored for simplicity.

Following the general approach described by Bjorken et al. (1969) and making use of the hypothesis of limiting fragmentation, they arrived at the following conclusions:

(i) μ^+/μ^- ratio is independent of the muon energy.

(ii) The charge ratio (μ^+/μ^-) is greater than unity because the probability of fragmentating proton into π^+ is more than the analogous probability for π^-.

(iii) μ^+/μ^- depends on the exponent γ of the primary cosmic ray spectrum and consequently any variation in the exponent would result in the corresponding change in the ratio μ^+/μ^- .

(iv) The nature of the target nuclei in the atmosphere is unimportant.

(v) Pionization products have very little effect on the charge ratio.

After this simplified picture, they proceeded to calculate the charge ratio in a more realistic way by incorporating in it the neutron component of the primaries, and also the production of kaons and their contribution to muons. They followed the method described by Barrett et al. (1952) and used the property of scaling. They treated the pion, kaon, and muon fluxes by diffusion equations and obtained the resulting muon spectrum. To draw some quantitative conclusions they ignored the contributions from kaons and the pion charge-exchange fragmentation and arrived at the following conclusions:

(i)   The dependence of the nature of the atmospheric nuclei for the μ^+/μ^- ratio is fairly mild and is only through λ_π/λ_N.

(ii) $\mu^+/\mu^- > 1$ (always).

(iii)   Using presently available accelerator data μ^+/μ^- ratio comes out to be 1.56.

This seems to be somewhat higher than the observed charge ratio (which is known to be approximately 1.2-1.3 in the energy range of a few GeV to 1 TeV).

They attributed this discrepancy to the non-scaling behaviour of present accelerator data at $x \approx 0$ (where x is the usual Feynman scaled variable and in the case of very high energy interaction it becomes approximately the ratio of pion energy to the primary energy) and to the possible inaccuracy of their factorization assumption.

Finally, they showed that contributions from kaons and from the pion charge-exchange fragmentation tend to cancel each other, and μ^+/μ^- ratio is only slightly modified.

THEORETICAL ESTIMATES OF THE COUPLING
CONSTANTS OF THE COSMIC RAY MUONS

4.1 Introduction

The network of ground based neutron monitors and muon telescopes

provides a powerful tool in probing the solar modulation of primary cosmic

rays by the interplanetary medium. However, this can be effectively

accomplished if the coupling constants for a particular detector are

accurately known.

Coupling constants for the sea level meson detectors have been derived

from the observed latitude effect and using extrapolation methods (Dorman,

1957; Webber and Quenby 1959; Dorman et al., 1970; Cooke and Fenton, 1971).

However, the validity of these estimates were doubted (Kane, 1962) because

the maximum of the response curve of a meson detector lies near the upper

limit of the latitude effect.

Dorman (1957) suggested that the coupling constant of the sea level

muon telescopes after suitable scaling and renormalization could be used

to obtain the coupling constants applicable to the underground muon

detectors. Mathews (1963), using this method, derived the coupling constants

for the underground detectors.

The atmospheric temperature effect for the muon monitor is quite

serious and, therefore, the data obtained from the latitude surveys need

to be corrected for this effect before deriving the coupling constants.

This effect arises because the air temperature is lower at high latitudes

than at the equator; consequently the atmosphere become more compressed

resulting in an enhancement of the survival probability of the muons

because the muons will have to traverse a shorter path from the production

layer to the level of observation.

The correction factors for the muon monitor on account of atmospheric

temperature effect have been evaluated by Carmichael et al. (1969 a,b) for

various sites of the latitude surveys carried out by them. It is evident

from these correction factors that the atmospheric temperature effect

itself may contribute several percent to the observed latitude variation

of the muon component. This seems to be the reason that the earlier

workers reported about 13.5% latitude effect at sea level (without

applying temperature corrections because of the non-availability of the

upper atmospheric temperature data) whereas Carmichael and Bercovitch (1969)

and Dorman et al. (1970) obtained about 8.5% latitude effect after applying

temperature corrections, the difference (~5%) being accounted entirely

due to temperature effect.

There have been various attempts in the past to obtain the coupling

constants for muon monitors theoretically (Krimsky et al., 1965; Peacock,

1970; Ahluwalia and Ericksen, 1971; Bedewi and Goned, 1971 and Simpson

and Mathews, 1972).

4.2   Method of Calculation

K. Åström (1966) has given a model to calculate the muon energy

spectrum in the zenith direction based on the various processes in the

atmosphere. In the low energy range which accounts for the bulk of the

recorded intensity/good agreement with the measured spectra is obtained
                at the sea level

by fitting some parameters.

We have used this model to calculate the coupling constants

for the muon component for several zenith angles and several atmospheric

depths. We have also incorporated in our calculations the necessary

correction for the contribution of heavies. Coupling constants thus

obtained are in good agreement with all the experimental data on

latitude and azimuth effect available so far, as will be shown in

Chapter V.

Notations, Indices and Symbols

In what follows, we would use the following symbols, notations

and indices:-

m   rest mass of a particle (always accompanied by an index as

       m_p, m_π etc.)

β the velocity of a particle in terms of the velocity of light

$$\beta = v/c$$

γ the Lorentz factor

$$\gamma = \frac{1}{\sqrt{1 - \beta^2}}$$

     γ expresses the total energy of a particle in units of its rest

     energy (always accompanied by an index as γ_p, γ_μ, γ_π etc.)

p   momentum in units of the rest mass

$$p = \sqrt{\gamma^2 - 1}$$

E   total energy

τ_o mean life of a particle in its rest system

τ mean life of a particle in the laboratory system

α_p the zenith angle of the primary beam

ϕ_p the azimuth angle of the primary beam

α_s the zenith angle of the secondary particle

ϕ_s the azimuth angle of the secondary particle

θ the angle between the momenta of a primary and a secondary particle

dw   solid angle element

z   linear height above sea level

x   atmospheric depth in gcm^{-2}

x_o sea level pressure in gcm^{-2}

L   effective interaction mean free path of a primary particle in the atmosphere

λ attenuation length of primary nucleons in the atmosphere

l   scale height of the atmosphere

n   number of particles

Indices:

p   proton or primary

π π - meson

μ μ - meson

/   the center of mass system in a nucleon-nucleon collision

*   the rest system of a particle

Notations of functions

$N(0, E_p)$ the differential primary spectrum at the top of the atmosphere in units of $cm^{-2} \ s^{-1} \ sr^{-1} \ (GeV)^{-1}$

$\dfrac{d^2 N_\mu}{dw_\mu d\gamma_\mu}$ or $\dfrac{dN_\mu}{d\gamma_\mu}$ the differential muon spectrum in units of $cm^{-2} s^{-1} sr^{-1}$ (muon mass equivalent)$^{-1}$

M or M (γ_p) or M $(\gamma_p I^2)$ the mean multiplicity

I   the mean value of the inelasticity in the center of mass system

P_s or $P_s (E_\mu, \alpha_s, x)$ the probability that a muon produced at the level x will survive and reach sea level with an energy E_μ in a direction making an angle α_s to the vertical.

Π_μ or $\Pi_\mu(E_\mu, \theta, E_p)$ the normalized muon production spectrum, thus, $\Pi_\mu(E_\mu, \theta, E_p)dw_\mu dE_\mu$ is the probability that a muon is produced in the energy interval $(E_\mu, E_\mu + dE_\mu)$ and within the solid angle dw_μ. dw_μ makes the angle θ to the momentum of the primary particle having the energy E_p. The $\Pi-\mu$ decay is implicit.

4.2.1   Basic assumptions for the muon spectra calculations

The muon spectra have been calculated on the basis of the following assumptions:

(a)   The primary cosmic rays arrive isotropically at the top of the atmosphere and have a differential energy spectrum of the form

$$N(0, E_p)dE_p = A(E_p + B)^{-\gamma} dE_p \qquad \ldots\ldots(4.1)$$

where E_p is the total energy of the primary particle in GeV.

(b)   Primaries are assumed to interact once with the atmospheric nuclei. A number of pions are assumed to be produced in such interactions.

(c)   The number of primary nucleons is assumed to decrease exponentially with an attenuation mean free path λ in the atmosphere. The value of λ is assumed to be independent of the primary energy.

(d)   The inelasticity, which expresses the fraction of the incident energy available in the CMS (center of mass system) of the nucleon-nucleon collision for the production of mesons (Camerini et al., 1952), is also assumed to be independent of the primary energy.

(e)   The average multiplicity (one of the most important energy dependent parameters), which gives the number of mesons produced, is given by

$$M(\gamma_p) = C_1(\gamma_p I^2)^{C_2} \qquad \ldots\ldots(4.2)$$

where C_1 and C_2 are constants and the numerical values of these constants are given by Bradt et al. (1950).

(f)   Camerini et al. (1951; 1952) have studied the production spectrum of pions experimentally by nuclear emulsion technique. The pions are found to be produced isotropically in the CMS system and their differential energy spectrum can be represented by

$$\frac{dN_\pi}{d\gamma'_\pi} = A_\pi (E_p) \frac{\sqrt{(\gamma'_\pi)^2 - 1}}{(\gamma'_\pi)^3} \qquad \ldots\ldots(4.3)$$

(g)   The maximum energy with which a pion can be produced in the CMS is given by Bradt et al. (1950)

$$\gamma'_{\pi \, max} = \frac{2m_p}{m_\pi} (\gamma'_p - 1) - M(\gamma_p I^2) + 1 \qquad \ldots\ldots(4.4)$$

(h)   The number of charged pions produced is taken to be 2/3 of the total number of pions produced in accordance with the property of charge independence (Sitte, 1961).

(i)   The interaction of pions in the atmosphere is neglected i.e., they are assumed to decay almost instantaneously after their production (Rossi, 1952), with a mean life of about 2.5×10^{-8} sec. at rest into a muon and a neutrino.

$$\pi^\pm = \mu^\pm + \nu_\mu (\overline{\nu}_\mu)$$

Neutrino produced in this process takes away a part of the energy (Rossi, 1952; Ascoli, 1950). This has been taken into account.

(j)   The muons are produced isotropically in the rest system of the pions. However, the decay of the pions introduces a small spreading effect, so that the muon beam is slightly more divergent than the original pion beam (Ascoli, 1950; Puppi, 1956; Brunberg, 1958). This spreading is, therefore, neglected for the energy range of our interest i.e., the direction of propagation of the decay muon is assumed to be the same as that of its parent particle.

(k)   The ionization losses of the muons in their passage through the atmosphere are assumed to be energy independent.

(l)   The atmosphere is assumed to be static and isothermal with an effective temperature of -50°C (Åström, 1966, Figure 1 of this paper gives a comparison between the assumed atmosphere and the NACA atmosphere).

4.2.2   Deduction of the energy spectrum of muons:

We calculate the number of charged pions produced in an atmospheric layer of thickness dx at a depth x by the primaries in the energy interval E_p and $E_p + dE_p$. Here, the primaries entering the atmosphere within the solid angle dw_p make the angle α_p to the vertical.

The total number of such primaries at the depth x is given by

$$N(x, E_p)\ dE_p dw_p = N(0, E_p)\ \exp\left(-\frac{x}{\lambda \cos\alpha_p}\right)\ dE_p dw_p\ \ ....(4.5)$$

The number of charged pions produced by a primary in the layer $= 2/3\ M(\gamma_p)$ and the number of pion producing collisions in this layer $= dx/(L \cos\alpha_p)$. The curvature of the atmosphere is neglected. We get the number $d^3 n_\pi$ (where the number assigns the order of differential) of charged pions produced by combining the above quantities, as

$$d^3 n_\pi = N(0, E_p)\ dE_p dw_p\ \exp\left(\frac{-x}{\lambda \cos\alpha_p}\right)\ \frac{2}{3} M(\gamma_p)\ \frac{dx}{L \cos\alpha_p}\ \ ...(4.6)$$

The pions thus produced will decay into muons and let the number of muons thus generated with energies between $(\bar{E}_\mu, \bar{E}_\mu + d\bar{E}_\mu)$ and moving in a direction making an angle α_s to the vertical within the solid angle dw_μ be denoted by $\overline{d^5 N_\mu}$. We obtain the production spectrum of muons from the definition of Π_μ as:

$$\overline{d^5 N_\mu} = d^3 n_\pi \cdot \Pi_\mu(E_p, \theta, \bar{E}_\mu)\ dw_\mu\ d\bar{E}_\mu\ \ ......(4.7)$$

Some of the muons generated here will decay before reaching sea level. d^5N_μ, which denotes the number of muons surviving at sea level, is given by

$$d^5N_\mu = \overline{d^5N_\mu} \; P_s(E_\mu, \alpha_s, x) \qquad \ldots\ldots(4.8)$$

Earlier an assumption was made that the energy loss per unit path length of the muons is independent of the muon energy. Therefore, we obtain for E_μ at sea level

$$E_\mu = \bar{E}_\mu - \frac{1}{\cos\alpha_s} \cdot \frac{dE_\mu}{dx} \; (x_0 - x) \qquad \ldots\ldots (4.9)$$

Combining the above quantities we get

$$d^5N_\mu = \frac{2}{3} N(0,E_p) \; dE_p dw_p \; \exp\left(\frac{-x}{\lambda\cos\alpha_p}\right) M(\gamma_p) \; \frac{dx}{L\cos\alpha_p}$$

$$\cdot \Pi_\mu(E_p, \theta, \bar{E}_\mu) dw_\mu \; d\bar{E}_\mu P_s(E_\mu, \alpha_s, x) \qquad \ldots\ldots(4.10)$$

From (4.9) we get

$$dE_\mu = d\bar{E}_\mu \qquad \ldots\ldots(4.11)$$

Now, $\dfrac{d^2N_\mu}{dE_\mu dw_\mu}$, the differential muon spectra at sea level in a direction making an angle α_s to the vertical can be obtained by integrating over the primary energies, the upper hemisphere 2Π, and the atmospheric levels. Thus,

$$\frac{d^2N_\mu}{dE_\mu dw_\mu} = \int_{E_{pmin}}^{\infty}\int_0^{\Pi/2}\int_0^{x_0} \frac{2}{3} N(0,E_p)dE_p dw_p$$

$$\cdot \exp\left(\frac{-x}{\lambda\cos\alpha_p}\right) M(\gamma_p) \; \frac{dx}{L\cos\alpha_p} \cdot \Pi_\mu(E_p,\theta,\bar{E}_\mu)P_s(E_\mu, \alpha_s, x).$$

$$\ldots(4.12)$$

$$\ldots(4.13)$$

where $\displaystyle\iint \Pi_\mu(E_p, \theta, \bar{E}_\mu) \; dw_\mu d\bar{E}_\mu \equiv 1$

from the definition of Π_μ.

4.2.3   The derivation of the muon production spectrum

$d^2 n_\pi$, the number of pions produced in the energy interval $(\gamma_\pi, \gamma_\pi + d\gamma_\pi)$ within the solid angle dw_π making the angle θ to the primary direction, is given by

$$d^2 n_\pi = G(\gamma_p, \gamma_\pi, \theta)\, dw_\pi\, d\gamma_\pi \qquad \ldots\ldots(4.14)$$

where $G(\gamma_p, \gamma_\pi, \theta)$ denotes the differential energy spectrum of the pions produced by a primary of energy γ_p.

It has been mentioned earlier that the angular spread of the muons produced in the decay of pions is very small. Therefore, we may write

$$dw_\mu = dw_\pi \qquad \ldots\ldots(4.15)$$

However, the energy spread is not negligible. The muons will be produced with energies ranging from a minimum $\overline{\gamma_{\mu 1}}$ to a maximum value $\overline{\gamma_{\mu 2}}$. Also any energy in the interval between $\overline{\gamma_{\mu 1}}$ and $\overline{\gamma_{\mu 2}}$ is equally probable (Ascoli, 1950).

Thus, the number of muons produced in the energy interval $d\overline{\gamma_\mu}$ and moving within the solid angle dw_μ making the angle θ to the primary direction is

$$d^3 n_\mu = \frac{G(\gamma_p, \gamma_\pi, \theta)}{(\overline{\gamma_{\mu 2}} - \overline{\gamma_{\mu 1}})}\, d\gamma_\pi dw_\mu d\overline{\gamma_\mu} \qquad \ldots\ldots(4.16)$$

The total energy of the muons produced by the decay of pions is readily obtained by applying the laws of conservation of energy and momentum and is given by

$$\overline{\gamma_\mu} = k\,\gamma_\pi + k_1\sqrt{\gamma_\pi^2 - 1}\cdot\cos\theta^* \qquad \ldots\ldots(4.17)$$

where θ^* is the angle between the direction of the moving pion and the

direction of the muon in the rest system of the pion and k and k_1 are

constants given by

$$k = \tfrac{1}{2} \left(\frac{m_\pi}{m_\mu} + \frac{m_\mu}{m_\pi} \right), \quad k_1 = \tfrac{1}{2} \left(\frac{m_\pi}{m_\mu} - \frac{m_\mu}{m_\pi} \right) \qquad \ldots (4.18)$$

From (4.17) we obtain

$$\overline{\gamma_{\mu 1}} = k\gamma_\pi - k_1 \sqrt{\gamma_\pi^2 - 1} \qquad \ldots\ldots (4.19)$$

$$\overline{\gamma_{\mu 2}} = k\gamma_\pi + k_1 \sqrt{\gamma_\pi^2 - 1} \qquad \ldots\ldots (4.20)$$

Denoting by $\triangle$ the difference $\overline{\gamma_{\mu 2}} - \overline{\gamma_{\mu 1}}$, we get

$$\triangle = 2k_1 \sqrt{\gamma_\pi^2 - 1} \qquad \ldots\ldots (4.21)$$

From this expression it is evident that the energy interval of the muons

produced in the decay of pions increases with the pion energy.

The angle between the momenta of a primary and a secondary

particle θ is related to the direction of the primary beam (α_p, ϕ_p)

and the measuring direction of the telescope (α_s, ϕ_s). Thus, from Fig.4.1

$$\cos\theta = \sin\alpha_p \, \sin\alpha_s \, \cos(\phi_p - \phi_s) + \cos\alpha_p \, \cos\alpha_s \qquad \ldots\ldots (4.22)$$

According to the Lorentz transormation, the energy γ_p of

the incoming nucleon in the LS and its energy γ'_p in the CMS are related

by

$$\gamma_p = 2(\gamma'_p)^2 - 1 \quad \cdot \qquad \ldots\ldots (4.23)$$

As the transverse component of momentum is same in both the systems,

we get

$$p'_\pi \sin\theta' = p_\pi \sin\theta \qquad \ldots\ldots (4.24)$$

From the relativistic transformation of coordinates we obtain two
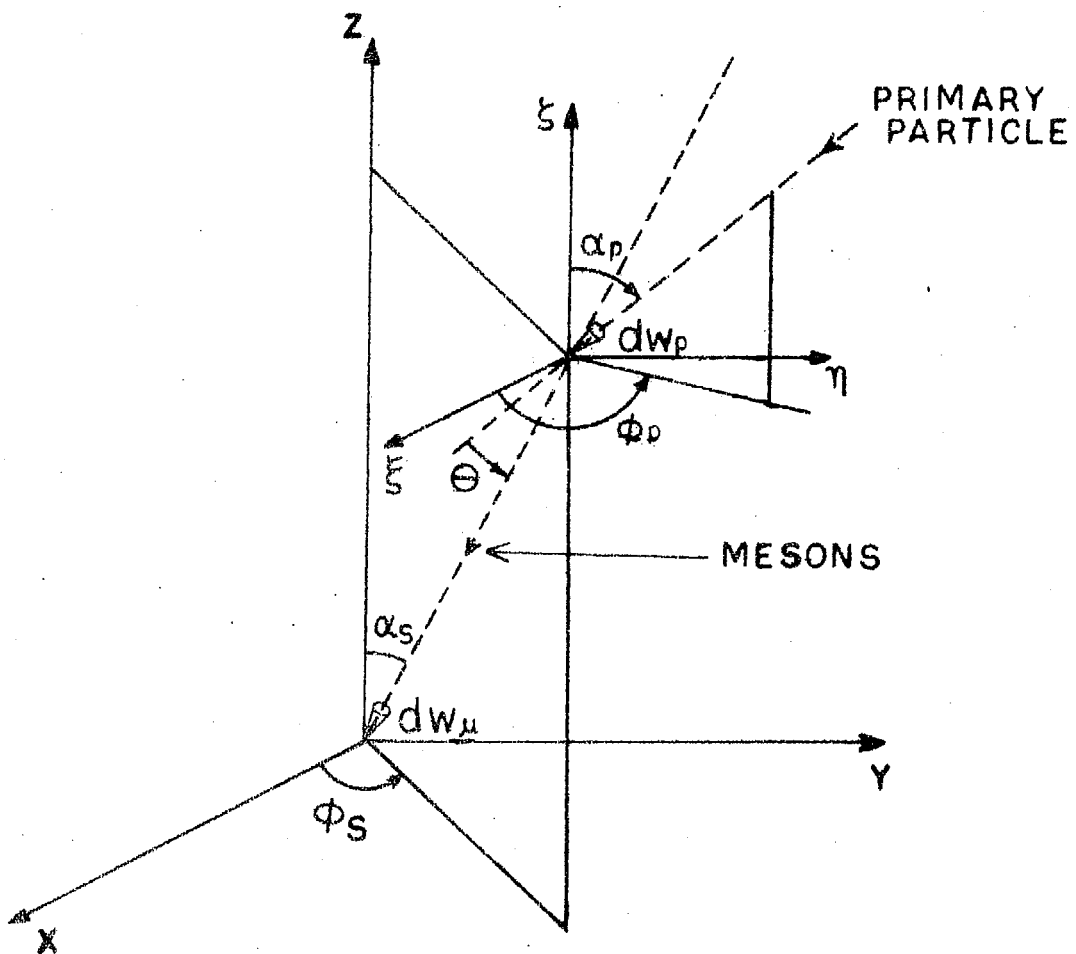
Fig. 4.1   A telescope at sea level with the infinitely small solid
           angle dw_μ records mesons arriving in the direction α_s, ϕ_s.
           The mesons are produced at the height z by primary
           particles coming from the direction α_p, ϕ_p.

relations between energy and angles of emission

$$F = \gamma'_p \tan \theta = \frac{\sin \theta'}{\cos \theta' + m} \qquad \ldots\ldots(4.25)$$

$$\gamma'_p \tan \theta' = \frac{\sin \theta}{(\cos \theta - \beta'_p/\beta'_\pi)} \qquad \ldots\ldots(4.26)$$

where

$$m = \beta'_p/\beta'_\pi . \qquad \ldots\ldots(4.27)$$

The energy of the pions in both the systems is obtained with the help of the above relations as,

$$\gamma_\pi = \gamma'_p \gamma'_\pi + \sqrt{(\gamma'_p)^2 - 1} \sqrt{(\gamma'_\pi)^2 - 1} \cdot \cos \theta' \qquad \ldots\ldots(4.28)$$

$$\gamma'_\pi = \gamma'_p \gamma_\pi - \sqrt{(\gamma'_p)^2 - 1} \sqrt{(\gamma_\pi)^2 - 1} \cdot \cos \theta \qquad \ldots\ldots(4.29)$$

Expressing γ_π explicitly as a function of the distribution angle in the LS, we get

$$\gamma_\pi = \frac{1}{F^2 + 1} \left| \frac{\gamma'_\pi}{\gamma'_p} \left\{ (\gamma'_p)^2 + F^2 \right\} \pm \sqrt{\left\{ (\gamma'_p)^2 - 1 \right\} \left\{ (\gamma'_\pi)^2 - 1 \right\} \left\{ 1 - (m^2 - 1)F^2 \right\}} \right. \qquad \ldots\ldots(4.30)$$

where the positive sign applies if $\theta \leqslant \pi/2$
and the negative sign applies if $\theta > \pi/2$.

The maximum energy $\gamma_{\pi\,max}$ that a pion can acquire for a given energy of the primary proton and angle of emission is, therefore, given by

$$\gamma_{\pi\,max} = \frac{1}{F^2 + 1} \left| \frac{\gamma'_{\pi\,max}}{\gamma'_p} \left\{ (\gamma'_p)^2 + F^2 \right\} + \sqrt{\left\{ (\gamma'_p)^2 - 1 \right\} \left\{ (\gamma'_{\pi\,max})^2 - 1 \right\} \cdot \sqrt{1 - (m^2 - 1)F^2}} \right. \qquad \ldots(4.31)$$

where $\gamma'_{\pi\,max}$ is given by (4.4)

So far, we have considered a pion of given energy γ_π and found the muon energy spectra arising from the decay of this monoenergetic pion. However, the limits of the pion energies ($\gamma_{\pi 1}, \gamma_{\pi 2}$) capable of contributing to the muon flux at a given muon energy can also be calculated. From

kinematic considerations we obtain

$$\gamma_{\pi 1} = k\,\overline{\gamma_{\mu}} - k_1 \sqrt{\overline{\gamma_{\mu}^2} - 1} \qquad \ldots\ldots (4.32a)$$

and

$$\gamma_{\pi 2} = \begin{cases} \gamma_{\pi\,max} & \text{if, } k\,\overline{\gamma_{\mu}} + k_1\sqrt{\overline{\gamma_{\mu}^2} - 1} > \gamma_{\pi max} \\ k\,\overline{\gamma_{\mu}} + k_1\sqrt{\overline{\gamma_{\mu}^2} - 1} & \text{if, } k\,\overline{\gamma_{\mu}} + k_1\left(\gamma_{\mu}^2 - 1\right)^{1/2} < \gamma_{\pi max} \end{cases} \qquad \ldots\ldots (4.32\ b)$$

Having obtained $(\gamma_{\pi 1}, \gamma_{\pi 2})$ the limits of the pion energy

relevant for a given muon energy $\overline{\gamma_{\mu}}$, we can now get an expression for η_{μ}

We have estimated earlier that in the $\pi - \mu$ decay process

$$d^3 n_{\mu} = \frac{G(\gamma_p, \gamma_{\pi}, \theta)}{\overline{\gamma_{\mu 2}} - \overline{\gamma_{\mu 1}}}\ d\gamma_{\pi}\,dw_{\mu}\,d\overline{\gamma_{\mu}} \qquad \ldots\ldots (4.33)$$

gives the number of muons in the energy interval $d\overline{\gamma_{\mu}}$ due to parent pions

in the energy interval $d\gamma_{\pi}$ and moving within the solid angle dw_{π}

(since $dw_{\mu} = dw_{\pi}$ by eqn. (4.15)).

In order to obtain the total number of muons produced in the

energy interval $d\overline{\gamma_{\mu}}$ and within the solid angle dw_{μ} we must integrate

the above expression over the pion energy range $d\gamma_{\pi}$. Thus,

$$d^2 n_{\mu} = d\overline{\gamma_{\mu}}\,dw_{\mu} \int_{\gamma_{\pi 1}}^{\gamma_{\pi 2}} \frac{G(\gamma_p, \gamma_{\pi}, \theta)\,d\gamma_{\pi}}{\triangle} \qquad \ldots\ldots (4.34)$$

However, by definition of η_{μ} we have

$$\eta_{\mu} = \frac{1}{n_{\mu}}\ \frac{d^2 n_{\mu}}{d\overline{\gamma_{\mu}}\,dw_{\mu}} \qquad \ldots\ldots (4.35a)$$

or

$$\eta_{\mu} = \frac{1}{n_{\mu}} \int_{\gamma_{\pi 1}}^{\gamma_{\pi 2}} \frac{G(\gamma_p, \gamma_{\pi}, \theta)\,d\gamma_{\pi}}{\triangle} \qquad \ldots\ldots (4.35b)$$

Now, since the pion production by pions is negligible in the low energy

range of our interest, the number of muons become equal to the number

of pions. Thus,

$$n_{\mu} = N_{\pi} \qquad \ldots\ldots (4.36)$$

and

$$N_\pi = \int_1^{\gamma'_{\pi max}} \frac{dN_\pi}{d\gamma'_\pi} \, d\gamma'_\pi, \qquad \ldots\ldots(4.37a)$$

therefore,

$$n_\mu = \int_1^{\gamma'_{\pi max}} \frac{dN_\pi}{d\gamma''_\pi} \, d\gamma'_\pi \qquad \ldots\ldots(4.37b)$$

where $\dfrac{dN_\pi}{d\gamma'_\pi}$ is given by (4.3). This integral can be solved analytically and hence, n_μ can be evaluated as a function of γ_p.

The pions between the angles θ and $\theta + d\theta$ in the LS and in the energy interval (γ_π, $\gamma_\pi + d\gamma_\pi$) come from a solid angle dw'_π in the CMS. Thus, we can also put

$$d^2 n_\pi = dw'_\pi \frac{dN_\pi}{4\pi} \qquad \ldots\ldots(4.38)$$

Since we assume that the pions are produced with isotropic angular distribution in the CMS.

We have earlier noted that the angles of emission in the LS and CMS are related by the eqn. (4.25)

$$F = \gamma'_p \tan\theta = \frac{\sin\theta'}{\cos\theta' + m}$$

This can conveniently be written as

$$\cos\theta' = \frac{-mF^2 \pm \sqrt{1-(m^2-1)F^2}}{1 + F^2} \qquad \ldots\ldots(4.39)$$

θ' is a function of θ and γ'_π only since γ'_p is a constant for a given primary energy nucleon-nucleon collision.

From the eqns. (4.25) and (4.26) it is seen that the transformation

$$d\gamma'_{\pi} \, dw'_{\pi} = \left| \frac{\partial(\gamma'_{\pi}, w')}{\partial(\gamma_{\pi}, w)} \right| \, d\gamma_{\pi} \, dw_{\pi} \qquad \ldots\ldots (4.40)$$

can be written in the form

$$d\gamma'_{\pi} \, dw'_{\pi} = \left| \frac{\partial \gamma'_{\pi}}{\partial \gamma_{\pi}} \cdot \frac{\partial(\cos\theta')}{\partial(\cos\theta)} \right| \, d\gamma_{\pi} \, dw_{\pi} \qquad \ldots\ldots (4.41)$$

Splitting this expression into the two factors we get

$$d\gamma'_{\pi} = \left| \frac{\partial \gamma'_{\pi}}{\partial \gamma_{\pi}} \right| \, d\gamma_{\pi} \qquad \ldots\ldots (4.42)$$

and

$$dw'_{\pi} = \left| \frac{\partial(\cos\theta')}{\partial(\cos\theta)} \right| \, dw_{\pi} \qquad \ldots\ldots (4.43)$$

For the solid angle element we put

$$dw'_{\pi} = 4\pi P \, dw_{\pi} \qquad \ldots\ldots (4.44)$$

therefore,

$$P = \frac{1}{4\pi} \frac{\partial(\cos\theta')}{\partial(\cos\theta)} \qquad \ldots\ldots (4.45)$$

The value of P depends upon the value of m. However, Brunberg (1958) has shown that a small change in the value of m from unity results in a very small change in the value of P. Therefore, we will be using the values of P corresponding to $m \leqslant 1$.

From (4.39) we obtain

$$\frac{\partial(\cos\theta')}{\partial(\cos\theta)} = \frac{\pm F\gamma'_p \left[m \pm \sqrt{1-(m^2-1)F^2} \right]^2}{\sin\theta \cos^2\theta (1+F^2)^2 \left\{ 1-(m^2-1)F^2 \right\}^{1/2}} \qquad \ldots\ldots (4.46)$$

here the (+) sign applies if, $\theta \leqslant \pi/2$

and the (−) sign applies if, $\theta > \pi/2$

Thus, we obtain

$$P = \frac{F \gamma_p' \left[m + \sqrt{1-(m^2-1)F^2} \right]^2}{4\pi \sin\theta \cos^2\theta (1+F^2)^2 \left\{ 1-(m^2-1)F^2 \right\}^{1/2}} \quad \ldots\ldots(4.47a)$$

if $\theta \lesssim \pi/2$

$$P = -\frac{F \gamma_p' \left[m - \sqrt{1-(m^2-1)F^2} \right]^2}{4\pi \sin\theta \cos^2\theta (1+F^2)^2 \left\{ 1-(m^2-1)F^2 \right\}^{1/2}} \quad \ldots\ldots(4.47b)$$

if $\theta > \pi/2$

writing $\quad dN_\pi = \dfrac{dN_\pi}{d\gamma_\pi'} \cdot \dfrac{\partial \gamma_\pi'}{\partial \gamma_\pi} \cdot d\gamma_\pi \qquad\qquad \ldots\ldots(4.48)$

the equations (4.14), (4.38), (4.44) and (4.48) yield

$$G = P \frac{dN_\pi}{d\gamma_\pi'} \cdot \frac{\partial \gamma_\pi'}{\partial \gamma_\pi} \qquad\qquad \ldots\ldots(4.49)$$

also $\quad \gamma_\pi' = \gamma_p' \gamma_\pi - \sqrt{(\gamma_p')^2 - 1} \sqrt{\gamma_\pi^2 - 1} \cdot \cos\theta \qquad \ldots\ldots(4.50)$

$$\frac{\partial \gamma_\pi'}{\partial \gamma_\pi} = \gamma_p' - \sqrt{(\gamma_p')^2 - 1} \cdot \frac{\gamma_\pi}{\left\{ \gamma_\pi^2 - 1 \right\}^{1/2}} \cos\theta \quad \ldots(4.51)$$

From (4.3), (4.47 a), (4. 47 b), (4.49), (4.50) and (4.51) we arrive at

an expression which gives G as a function of γ_π, γ_p and θ.

Thus, we have described the method for solving π_μ. By putting

in the limits ($\gamma_{\pi 1}$, $\gamma_{\pi 2}$) according to (4. 32 a) and (4. 32 b) we get

π_μ as a function of γ_p, θ and $\overline{\gamma_\mu}$. The final expression being quite

complicated has not been shown here.

4.3   The survival probability of the muons

Let us consider an atmospheric layer bounded by (z'', z'' + dz'') z being

the linear height above sea level and let P_s denotes the probability that

a muon produced at z above z'' survives to reach z''. The probability

dP_d that the muon will decay in $(z'', z'' + dz'')$ is given by

$$dP_d = \frac{P_s \, (-dz'')}{(\beta_\mu'' c) \cdot \mathcal{T}_\mu''} \qquad \ldots\ldots (4.52)$$

The sign (") denotes the values at the actual level. Also,

$$\mathcal{T}_\mu'' = \overline{\gamma_\mu''} \cdot \mathcal{T}_{\mu o} \qquad \ldots\ldots (4.53)$$

where $\mathcal{T}_{\mu o}$ is the mean life of a muon at rest. Since

$$P_d = 1 - P_s \qquad \ldots\ldots (4.54)$$

we get

$$dP_s = P_s \frac{dz''}{\beta_\mu'' c \cdot \mathcal{T}_\mu''} \qquad \ldots\ldots (4.55)$$

If l is the scale height of the atmosphere then according to the assumption made about the atmosphere

$$\frac{dz''}{l} = -\frac{dx''}{x''} \qquad \ldots\ldots (4.56)$$

Integrating (4.55) we get

$$\ln P_s = \int_x^{x_o} \frac{-l \, dx''}{c \, \overline{\mathcal{T}_{\mu o} \beta_\mu''} \, \overline{\gamma_\mu''} \, x''} \qquad \ldots\ldots (4.57)$$

therefore,

$$P_s(E_\mu, \alpha_s, x) = \exp\left[-\frac{1}{c \, \mathcal{T}_{\mu o}} \int_x^{x_o} \frac{dx''}{x'' \left\{ \overline{\gamma_\mu''}^2 - 1 \right\}^{1/2}} \right] \ldots (4.58)$$

where

$$\overline{\gamma_\mu''} = \gamma_\mu + \frac{dE_\mu/dx}{\cos\alpha_s \, m_\mu c^2} (x_o - x'') \qquad \ldots\ldots (4.59)$$

4.4   Integration limits for the evaluation of the coupling constants

Eqn. (4.12) can be evaluated numerically to obtain the differential intensity of muons at a particular depth in a given direction, where π_μ is evaluated from eqn. (4.35b) and n_μ is given by eqn (4.37b).

To obtain the integral intensity of muons at a particular place we must integrate the differential spectrum over all muon energies. Thus, if we put the solid angle element,

$$dw_p = \sin \alpha_p \; d\alpha_p \; d\phi_p \qquad \ldots (4.60)$$

then we get the integral intensity of muons as,

$$N_\mu = \int_{E_{p1}}^{E_{p2}} dE_p \int_{E_{\mu 1}}^{E_{\mu 2}} dE_\mu \int_0^{\gamma_2} d\alpha_p \int_0^{2\pi} d\phi_p \int_0^{x_0} dx \int_{\gamma_{\pi 1}}^{\gamma_{\pi 2}}$$

$$\psi \; (E_p, \; E_\mu, \; \alpha_p, \; \phi_p, \; x, \gamma_\pi) d\gamma_\pi \qquad \ldots (4.61)$$

where limits $\gamma_{\pi 1}$ and $\gamma_{\pi 2}$ are chosen by (4.32 a) and (4.32 b). By putting different values of x_0 the muon flux at different atmospheric depths can be evaluated. Here $E_{\mu 1}$ is the minimum energy required by a muon to traverse the telescope absorber.

Muon differential energy spectrum at higher energies cannot be evaluated with great accuracy by the method described above because some of the assumptions made earlier do not hold in the high energy range. However, high energy muon contribution is less for sea level muon telescopes and also for measurements at moderate depths. $E_{\mu 2}$ was chosen as 50 GeV. Therefore, the error caused by inaccuracies in high energy muon range is likely to be less.

E_{p1} should be chosen from the cut-off rigidity corresponding to incident (primary) direction at a given place. However, it was found that the major contribution to the secondary flux comes from primary directions very close to the secondary direction, i.e. the secondary particles retain the direction of the parent primaries in most of the cases. Also, we found by putting E_{p1} appropriate to the secondary direction (α_s, ϕ_s) the error incurred is insignificant. E_{p2} was chosen as 1000 GeV. Though for higher primary energies the accuracy cannot be claimed to be high, nevertheless, the contribution from higher energies declines quite fast. Furthermore, it must be kept in mind that the purpose of the present calculation was to get the estimates of the coupling constants and hence, we are interested only in the relative contribution at different energies. Thus, the errors caused by high energy part is likely to be less.

Before deriving coupling constants, we must also remember (as first pointed out by Pal and Tandon, 1964) that at any latitude nearly 26% of the primary nucleons are alphas (or equivalents) and have a cut-off of only at $E_c/2$, where E_c is the cut-off for protons (in terms of momentum per nucleon). Therefore, dN_μ/dE_p are evaluated first for different values of E_p. Then, the effective contribution from a given energy is obtained by

$$\left(\frac{dN_\mu}{dE_p}\right)_{eff.} = 0.74 \left(\frac{dN_\mu}{dE_p}\right)_{E_p} + 0.26 \left(\frac{dN_\mu}{dE_p}\right)_{E_p/2} \qquad \ldots\ldots (4.62)$$

Effective contributions thus obtained are then integrated from E_{p1} to E_{p2} (where E_{p1} and E_{p2} are chosen as explained earlier) to get the total muon flux for a narrow angle telescope located at a given place and looking in a particular direction. Coupling constants, corrected for the contribution of heavies are then obtained by expressing the effective

contributions obtained from (4.62) as a percentage of the total muon flux.

Correction for the contribution of heavies is essential in (a) calculating the latitude effect as obtained by latitude surveys (b) obtaining the azimuth effect (the east-west effect) and (c) comparing the coupling constants obtained theoretically with those derived from experimental data.

4.5   Discussion of the theoretical model

4.5.1   The interaction mean free path

The attenuation length of primary nucleons in the atmosphere, λ, was taken as 120 g cm^{-2} which is in agreement with the values obtained by many workers from the experimental data.

We have assumed earlier that the primaries interact once with the target nuclei in the atmosphere which is equivalent of replacing the nucleonic cascade with a single interaction process. Thus, it becomes essential to introduce the concept of the effective interaction mean free path to account for the contributions from those primaries which interact more than once in the atmosphere.

Åström calculated the muon flux at sea level for different values of L and compared the results thus obtained with the measured muon spectra. The best fit gave L = 120 g cm^{-2}. Incidentally, this value is in good agreement with the attenuation mean free path of primaries in the atmosphere as mentioned earlier.

Furthermore, L can be changed if so desired without affecting the coupling constants because the effect of changing L is merely to change the intensity of muons.

4.5.2   The multiplicity and the inelasticity

The power law dependence for the multiplicity has widely been used

$$M(\gamma_p) \propto \gamma_p^{0.25} \quad . \qquad \ldots\ldots (4.63)$$

However, we have chosen the mean value of the multiplicity according to Bradt et al. (1950) which is given by eqn (4.2)

$$M(\gamma_p) = C_1 (\gamma_p I^2)^{C_2} \quad .$$

In this relation the mean value of the inelasticity is given explicitly.

Åström has shown that the disagreement between the multiplicities according to (4.2) for $I = 0.8$ and $I = 0.6$ and those according to (4.63) is not very important over the energy range of our interest.

Different values of the inelasticity I, and the constants C_1 and C_2 in the multiplicity relation (4.2) were used by Åström to calculate the sea level muon spectra. A comparison of the results thus obtained with the measured spectra gave the following best fit values for the above quantities.

$$I = 0.6 \qquad \ldots\ldots (4.64)$$

and

$$M(\gamma_p) = 3.33 (\gamma_p I^2)^{0.32} \quad \text{if,} \ \gamma_p I^2 \leq 11.4 \qquad \ldots\ldots (4.65 \ a)$$

$$M(\gamma_p) = 2.61 (\gamma_p I^2)^{0.42} \quad \text{if,} \ \gamma_p I^2 > 11.4 \qquad \ldots\ldots (4.65 \ b)$$

4.5.3   The pion production spectrum and the angular distribution in the CMS

The secondary pion spectrum was chosen according to the cut Camerini formula

$$\frac{dN_\pi}{d\gamma'_\pi} = \begin{cases} A_\pi(E_p) \cdot \dfrac{\sqrt{(\gamma'_\pi)^2 - 1}}{(\gamma'_\pi)^3} & \text{if, } \gamma'_\pi \leq \gamma'_{\pi\,max} \\ 0 & \text{if, } \gamma'_\pi > \gamma'_{\pi\,max} \end{cases} \quad \ldots (4.66)$$

It is evident from the relation defining π_μ that the quantity $A_\pi(E_p)$ need not be known because it gets cancelled in the equation (4.35 a). $\gamma'_{\pi max}$, the maximum possible energy with which pions could emerge, was calculated according to eqn. (4.4).

We assumed that the pions produced in the CMS are isotropic which agrees very well with many measurements for moderate primary energies (< 100 GeV). Also, it can be shown that the sea level muon spectrum is not very sensitive to an anisotropic distribution. Thus, the simplifying assumption of isotropy is justified.

4.5.4 Atmospheric and geomagnetic effects

The pions after their production decay almost immediately and their corresponding mean free paths are ≤ 1 km for the energies with which we are concerned. We have neglected the pion interactions with atmospheric nuclei because most of the π – mesons are produced in a layer where the atmospheric density is low. The pion energy losses due to ionization have also been neglected for the same reasons.

On the other hand, the energy losses of the muons recorded deep in the atmosphere are quite appreciable. For muon energies upto few GeV the ionization losses are most important. The ionization losses vary slowly with the muon energy if the kinetic energy is greater than 0.1 GeV. Since, the maximum variation of the energy losses is not very important for a muon reaching sea level with a kinetic energy of 0.1 GeV, the energy

dependence of the ionization losses is neglected and the mean value of 2.2 MeV g^{-1} cm^2 for the energy loss per unit atmospheric depth is used in the calculations.

The atmosphere was assumed to be static and isothermal. However, the effective temperature of the lower atmosphere does vary during seasons producing slight variation in the cosmic ray intensity. In our calculations we have used the value of the scale height $1 \approx 6.53$ km in accordance with $T_{eff} = -50^{\circ}C$.

Brunberg has estimated the geomagnetic deflection of the secondaries and the angular deflection for mesons reaching sea level with a kinetic energy of 0.1 GeV estimated by him comes out to be about 11°, and if the energy of the mesons reaching sea level is 1 GeV, the corresponding deflection would be about 6°.

The maximum effect of scattering of the muons is about 10° if the muons lose about 2 GeV energy from the production level to sea level. This has rather a small effect on the angular distribution of the muons.

Further, meson telescopes have opening angles of the order of $10-20^{\circ}$. Thus, the scattering and geomagnetic deflection should produce a second order effect in the measured spectra. We have, therefore neglected these effects without introducing any significant error.

COMPARISON WITH EXPERIMENTAL DATA

5.1   Latitude and azimuth effect

In chapter IV we have described in detail the method of calculating the coupling functions applicable to muon monitors. A number of parameters are used in these calculations which could suitably be adjusted to give good results in agreement with the experimental data. Some of these parameters, such as (L, λ, I), were adjusted by Åström after a detailed study. Implications of changing some of these parameters have also been discussed earlier.

We can check our method of calculation upto 15 GV with the latitude effect data and upto 25 GV with the azimuth effect data at the equator. The experimental data available so far for such comparisons are (a) the latitude effect data at sea level by Carmichael and Bercovitch (1969), (b) the latitude effect data at 312 g cm^{-2} by Webber and Quenby (1959), (c) the azimuth effect data at sea level (Ahmedabad) at 42.5° zenith (present investigation), (d) the azimuth effect data at Makerere (1200 meters above sea level) at 30° zenith angle by Mathews and Sivjee (1967), (e) the azimuth effect data at Timboroa (2700 meters above sea level) at 43.5° zenith angle by Mathews and Sivjee (1967).

The locations (Makerere and Timboroa), where the azimuth effect studies (d), (e) were carried out, were at such altitudes that the muons travelling at angles of 30° and 43.5° to the vertical respectively will traverse the same amount of air as vertically travelling muons at sea level.

We have tried out different values of B and γ in the primary cosmic ray spectrum $N = A(B + E)^{-\gamma}$ and obtained the counting rates. In all, nine combinations were tried with B = 0, -1, -2 and γ = 2.5,

2.6 and 2.7. The counting rates thus obtained for each combination of B and $\sqrt{}$ for each of the five cases mentioned above are then compared with the experimental results.

In the case of latitude effect of vertical muons at sea level and at 312 g cm^{-2} good agreement with the experimental data is obtained for (i) B = -1, $\sqrt{}$ = 2.6 and (ii) B = 0, $\sqrt{}$ = 2.7. These results are shown in Fig. 5.1. On the other hand in the case of azimuth effect data at 42.5°, 30° and 43.5° zenith angles the good agreement is possible only for B = 0, $\sqrt{}$ = 2.5. The comparison of the calculated and the experimental data is shown in Figs. 5.2 and 5.3.

There seems to be some source of error for this peculiar behaviour i.e. vertical muon latitude effect at sea level and at 312 g cm^{-2} showing good agreement for B = -1, $\sqrt{}$ = 2.6 and B = 0, $\sqrt{}$ = 2.7 values and azimuth effect data showing good agreement with B = 0, $\sqrt{}$ = 2.5. However, it must be noted that whereas the vertical muon latitude effect data at sea level is taken from Carmichael and Bercovitch (1969), which is corrected for atmospheric temperature effect, the latitude effect data at 312 g cm^{-2} taken from Webber and Quenby (1959) could not be corrected for atmospheric temperature effect. Therefore, in the latter case a part of the latitude effect at 312 g cm^{-2} may be due to atmospheric temperature effect itself.

We then compared the latitude effect data at sea level and at 312 g cm^{-2} with the calculated effect for B = 0, $\sqrt{}$ = 2.5 and the results are shown graphically in Fig. 5.4. It is to be noted that the calculated latitude effect at 312 g cm^{-2} comes out to be less than the experimentally obtained value, which is to be expected in view of the above discussion about temperature correction. Therefore, it may be concluded
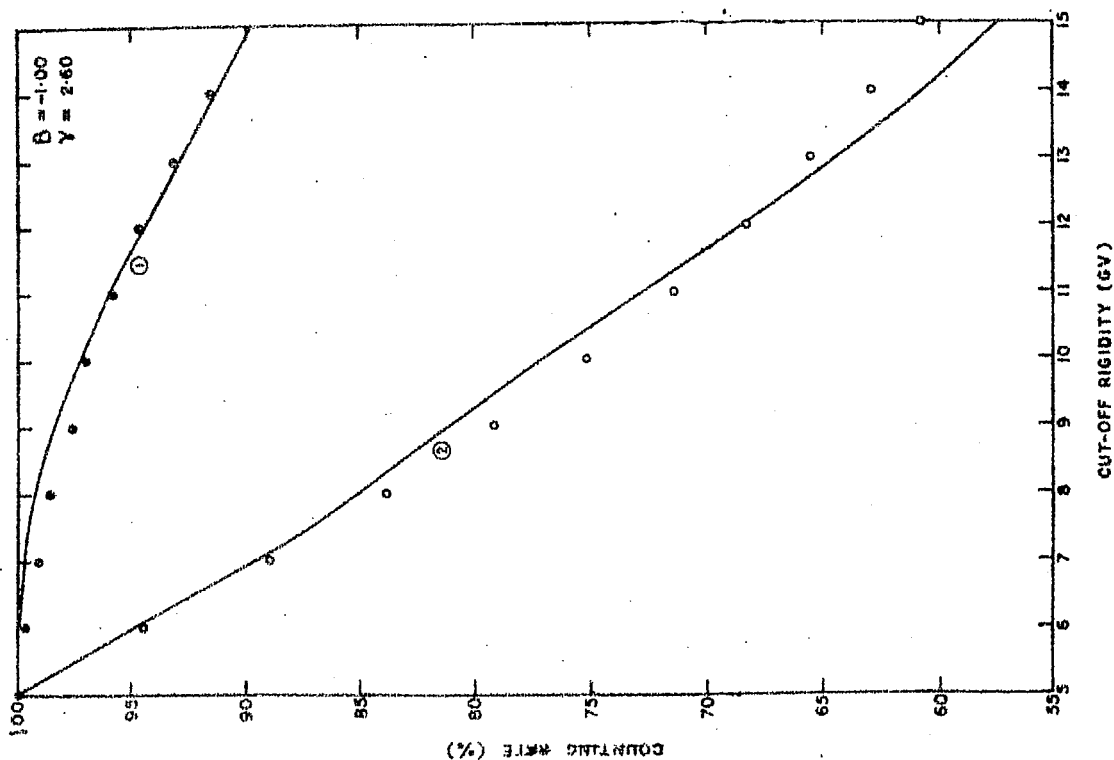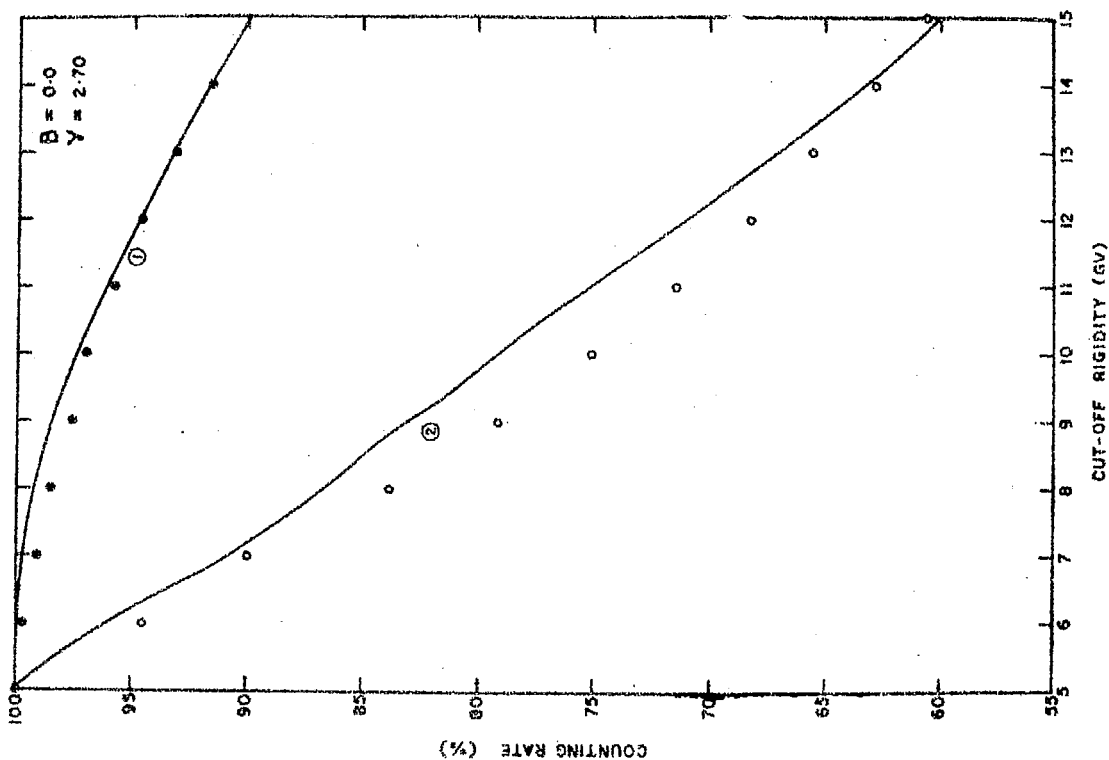
Fig. 5.1 Comparison of calculated and observed latitude effects for the muon component. Open circles represent experimental values given by Webber and Quenby (1959) at 312 g cm⁻². Closed circles represent experimental values given by Carmichael and Bercovitch (1969) at sea level. Continuous curves give calculated rates. 1. at sea level. 2. at 312 g cm⁻². Parameters are the constant B and the exponent γ of the primary spectrum (eqn. 4.1). (a) For B = -1.00, γ = 2.60, (b) For B = 0.00, γ = 2.70.
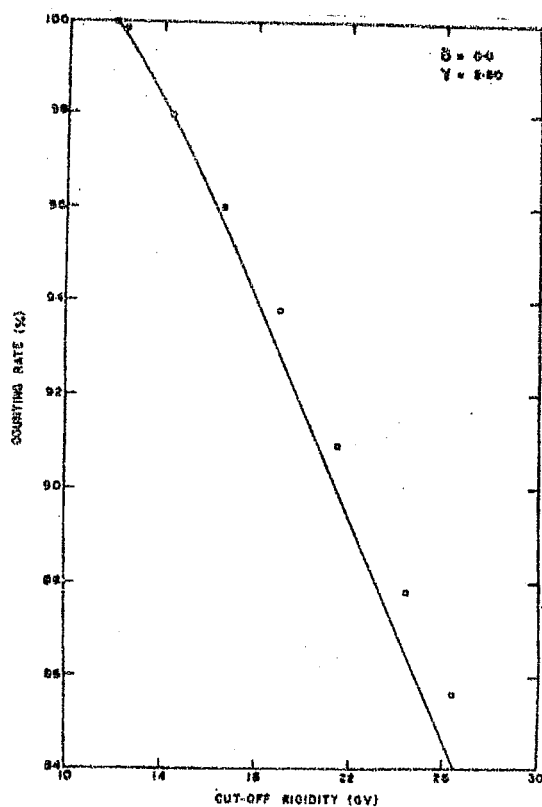
Fig. 5.2 Comparison of predicted and observed azimuthal effect at Ahmedabad. Open circles represent experimental values obtained with meson telescopes inclined at 45° to the zenith. Continuous curve gives calculated rates for B = 0.0 and γ = 2.50.
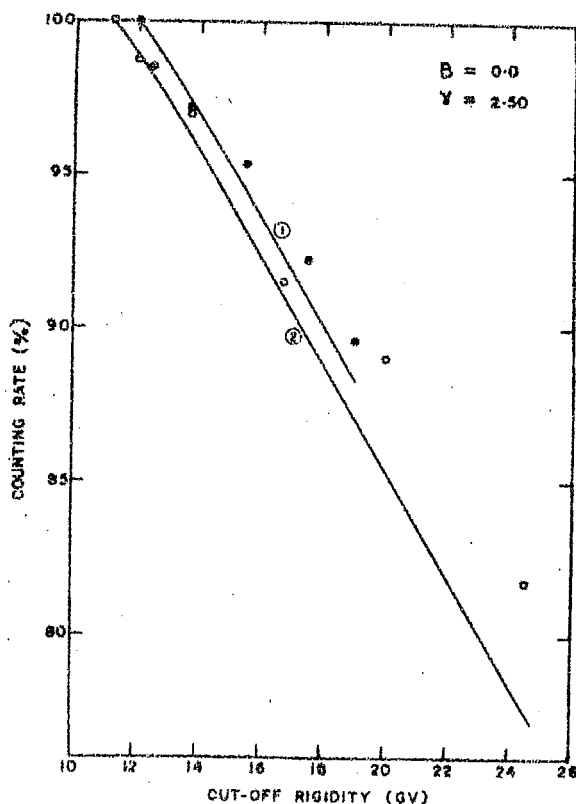
Figure 5.3 Comparison of predicted and observed azimuth effects. Continuous curves give calculated rates. Experimental points are those given by Mathews and Sivjee (1967).

● at 1200 meters above sea level at 33° zenith angle and curve numbered (1) calculated.

O at 2700 meters above sea level at 47° zenith angle and curve numbered (2) calculated.
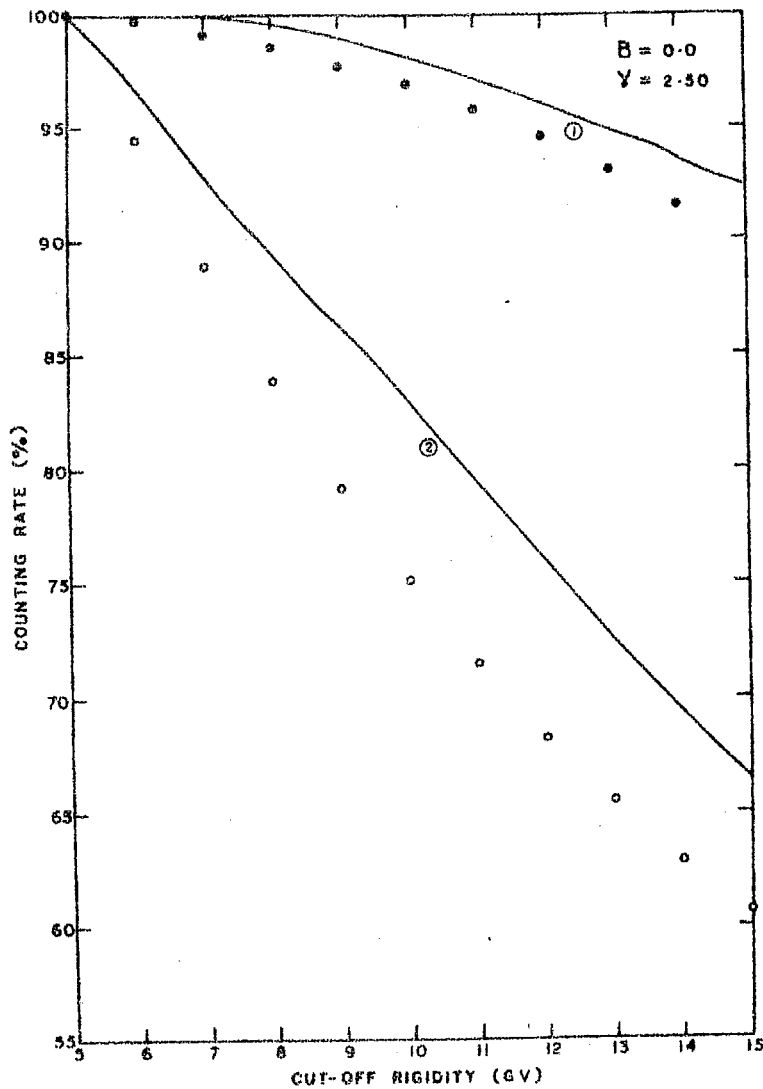
Fig. 5.4   Comparison of calculated and observed latitude
           effects for the muon component. Open circles
           represent experimental values given by Webber
           and Quenby (1959) at 312 g cm^{-2}.   Closed circles
           represent experimental values given by Carmichael
           and Bercovitch (1969) at sea level.   Continuous
           curves give calculated rates. 1. at sea level.
           2. at 312 g cm^{-2}.   For B = 0.00, γ = 2.50.
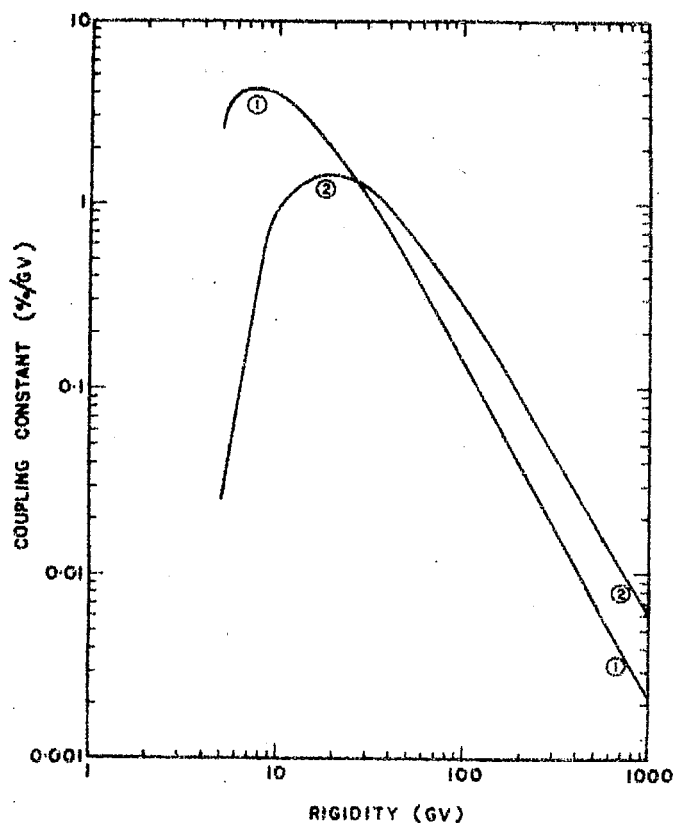
Fig.5.5 Theoretically derived
coupling constants applicable
to muon monitors pointing to
zenith. For   B = 0.0, γ= 2.50.
(1) at 312 g cm^{-2},
(2) at sea level.
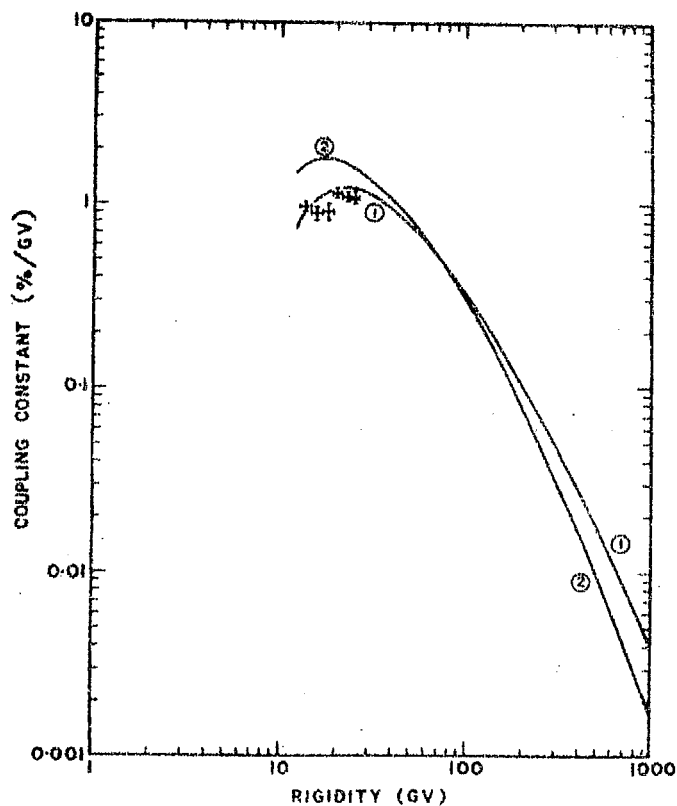
Fig. 5.6   Theoretically derived
coupling constants applicable to
muon monitors inclined to zenith.
B = 0.0, γ= 2.50.
(1) at sea level at a zenith
    angle of 45^{0}.
(2) at 1200 meters above sea level
    at a zenith angle of 33^{0}.
    Experimental points (with
    error bars) are obtained from
    the azimuth effect study at
    Ahmedabad.

that for $B = 0$, $\sqrt{} = 2.5$ the calculated results compare very well
with the experimental data.

5.2 Coupling constants

Coupling constants for muon monitors are evaluated using eqn.4.62
for the case $B = 0$, $\sqrt{} = 2.5$. In Fig. 5.5 coupling constants are shown
for muon monitors pointing to zenith at 312 g cm^{-2} (curve 1) and at sea
level (curve 2). Both these curves are normalized such that at 5 GV
rigidity the counting rate is 100.

In Fig. 5.6 theoretically calculated coupling constants are shown
for muon monitor at sea level (Ahmedabad) at a zenith angle of 45° (curve 1)
and at 1200 meters above sea level at a zenith angle of $33^{\bullet}$ (curve 2).
Both these curves are normalised such that at 12 GV rigidity the counting
rate is 100. In the same Figure the coupling constants derived from the
azimuth effect study at Ahmedabad are also shown for comparison.

The coupling constants at a zenith angle of 43.5^O and at 2700 meter
above sea level were also calculated and were found to be almost similar
to those shown by curve 2 in Fig. 5.6 and hence are not shown here.

C H A P T E R - VI

CONCLUDING REMARKS

An experiment to study the azimuthal variation of cosmic ray muon intensity has been conducted at Ahmedabad with the help of two independent triple coincidence G.M. counter telescopes. Coupling constants, which play a vital role in connecting the variations in the secondary intensity observations to the corresponding variations in the primary intensity, can be obtained experimentally upto 15 GV from latitude effect data. However, azimuth effect data can be used to obtain coupling constants beyond 15 GV.

The azimuth effect recorded with telescopes inclined at the same zenith angle but in different azimuths also make the correction due to atmospheric temperature effect (which even otherwise may not be applied adequately) unnecessary. The shape of the response curve for sea level muon detectors in the range 10-25 GV is of vital importance. Hence, the azimuth effect data assume greater significance. Unfortunately, the azimuth effect data available before this investigation started lacked the consistency and were found to be inadequate for the derivation of coupling constants.

Two identical independent telescopes were used to compare the results obtained with these telescopes in the same direction. An accuracy of better than 0.4% was obtained for intensity recorded in each of the fourteen directions studied experimentally. Comparison of the results showed that both the telescopes worked satisfactorily during the whole period of operation. These observations were utilized to derive coupling constants. Coupling constants thus derived from experimental observations are presented and their implications discussed.

Having obtained azimuth effect accurately an attempt was made to derive latitude and azimuth effects theoretically using an appropriate model. The model proposed by Åström (1966) for the calculation of the sea level muon spectrum in zenith direction was used with appropriate changes for muon flux calculations in inclined directions. The correction for the fact that 26% of the primary nucleons (in the form of alphas and heavies) have a cut-off only at half the value of that for protons (in terms of momentum per nucleon), has also been incorporated in our calculations.

The experimental data available so far to check the validity of our method of calculations are (a) the latitude effect data at sea level by Carmichael and Bercovitch (1969), (b) the latitude effect data at 312 g cm^{-2} given by Webber and Quenby (1959), (c) the azimuth effect data at sea level (Ahmedabad) at 42.5° zenith (present work), (d) the azimuth effect data at Makerere (1200 meter above sea level) at 30° zenith by Mathews and Sivjee (1967) and (e) the azimuth effect data at Timboroa (2700 meter above sea level) at 43.5° zenith by Mathews and Sivjee (1967).

We tried to fit all the above mentioned experimental data by taking different combinations of B and γ in the primary spectrum $N = A(B + E)^{-\gamma}$. In all, nine combinations with $B = 0, -1, -2$ and $\gamma = 2.5, 2.6, 2.7$ were tried. For inclined directions (i.e. the azimuth effect) $0, 2.5$ combination for B, γ fitted the experimental data most satisfactorily while for latitude effect (at sea level and at higher altitude) $0, 2.7$ and $-1, 2.6$ combinations fitted the experimental data well. None of the combinations fitted all the experimental data very well.

We suspect that this may be due to the latitude effect data at 312 g cm^{-2} being uncorrected for atmospheric temperature variation. It is shown that 0, 2.5 combination gave the best fit for all the available data. Coupling constants are calculated for different zeniths and atmospheric depths and the theoretical curves obtained are presented.

It is hoped that the method developed in the present investigation would be useful for many investigators in this field to calculate the coupling constants at various zenith angles and at various atmospheric depths within the limits imposed by the various assumptions.

The determination of the charge ratio of cosmic ray muons has also been of considerable importance because of its utility in the understanding of the parent particle producing nuclear interactions. The information on multiplicities and nature of particles created in these collisions can be obtained from the knowledge of charge ratio. This becomes specially more significant at very high energies which are not accessible by the accelerators available presently. However, the rapidly falling primary cosmic ray spectrum makes the statistically significant observations rather difficult. Unfortunately, charge ratio data is not available for all energy ranges with appreciable accuracy.

An experiment employing the method of delayed coincidences was conducted at Ahmedabad to obtain the charge ratio in the low energy range (i.e. $<$ 1 GeV). Plastic scintillators were used as detectors. The same apparatus could provide information about the integral intensity of vertical muons, the differential momentum spectrum and the mean life of muons besides the charge ratio. The results obtained from this experiment are listed below.

(1)   The integral intensity of vertical muons of momentum greater than 320 MeV/c as obtained is $(7.01 \pm 0.03) \times 10^{-3}$ cm^{-2} s^{-1} sr^{-1} which is 3.3% less than the value obtained by Allkofer et al. (1968). The higher cut-off rigidity at Ahmedabad adequately explains this reduction of intensity. Integral intensities at other momenta are also in agreement with other measurements.

(2)   The differential intensity of vertical muons obtained for the momentum range (0.2 – 0.8 GeV/c) is presented together with other measurements.

(3)   The mean life of muons which is also obtained from this experiment served as a check on the satisfactory operation of the instrument. The mean life thus obtained comes out to be 2.2185 ± 0.0135 μs which is in good agreement with the values obtained by other workers.

(4)   The results of charge ratio experiment in the momentum range (0.2 – 0.8 GeV/c) are shown. The charge ratio thus obtained is nearly unity in the momentum range studied which is expected on the basis of theoretical considerations. It is shown that the results are in good agreement with similar measurements performed near geomagnetic equator.

R E F E R E N C E S

Åström K.   1966   Ark. Fys. 33, 1

Ahluwalia H.S. and
Ericksen J.H.   1971   J. Geophys. Res. 76, 6613

Allkofer O.C. and
Clausen K.   1970   Acta Phys. Acad. Sci. Hung.
29, Suppl.2, 689

Allkofer O.C. and
Dau W.D.   1972   Phys. Letters 38B, 439

Allkofer O.C.,
Andresen R.D. and
Dau W.D.   1968   Can. J. Phys. 46, S301

Allkofer O.C.,
Dau W.D. and
Jokisch H.   1970   Phys. Letters 31B, 606

Allkofer O.C.,
Carstensen K. and
Dau W.D.   1971 a   Phys. Letters 36B, 425

Allkofer O.C.,
Carstensen K.,
Dau W.D.,
Fähnders E.,
Heinrich W. and
Jokisch H.   1971 b   Proc. 12th Int. Conf. Cosmic
Rays (Hobart), 4, 1319

Appleton I.C.,
Hogue M.T. and
Rastin B.C.   1971   Nucl. Phys. B26, 365

Ascoli G.   1950   Phys. Rev. 79, 812

Ashton F. and
Wolfendale A.W.   1963   Proc. Phys. Soc. 81, 593

Ashton F.,
Mackeown P.K.,
Ramana Murthy P.V.,
Pattison J.B.M. and
Wolfendale A.W.   1963   Phys. Letters 6, 259

Aurela A.M.,
Mackeown P.K. and
Wolfendale A.W.   1966   Proc. Phys. Soc. 89, 401

Ayre C.A.,
Hamdan M.A.,
Holroyd F.W.,
Hume C.J.,
Nandi B.C.,
Thompson M.G.,
Wells S.C.,
Whalley M.R. and
Wolfendale A.W.
1971 a   Proc. 12th Int. Conf. Cosmic
          Rays (Hobart),4, 1309

Ayre C.A.,
Hamdan M.A.,
Hume C.J.,
Thompson M.G.,
Wells S.C.,
Whalley M.R. and
Wolfendale A.W.
1971 b   Proc. 12th Int. Conf. Cosmic
          Rays (Hobart), 4, 1364.

Barlow J.,
Booth P.S.L.,
Carroll L.J.,
Court G.R.,
Davies J.D.,
Edwards D.N.,
Johnson R.G. and
Wormald J.R.
1964   Proc. Phys. Soc. 84, 239

Barrett P.H.,
Bollinger L.M.,
Cocconi G.,
Eisenberg Y. and
Greisen K.
1952   Rew. Mod. Phys. 24, 133

Bateman B.J.,
Cantrell W.G.,
Durda D.R.,
Duller N.M.,
Green P.J.,
Jelienk A.V.,
Nagy T.A. and
Sheldon W.R.
1971   Phys. Letters 36B, 144

Bedewi F. EL. and
Goned A.
1971   J. Phys. A.4, 660

Benecke J.,
Chou T.T.,
Yang C.N. and
Yen E.
1969   Phys. Rev. 188, 2159

Bergeson H.E.,
Keuffel J.W.,
Larson M.O.,
Martin E.R. and
Mason G.W.

1967   Phys. Rev. Letters 19, 1487

Bhattacharyya D.P.   1970   Z. Physik. 234, 17

Bjorken J.D.,
Pakvasa S.,
Simmons W. and
Tuan S.F.

1969   Phys. Rev. 184, 1345

Blackett P.M.S.   1937   Proc. Roy. Soc. 159A, 1

Bradt H.L. and
Peters B.

1948   Phys. Rev. 74, 1828

Bradt H.L. and
Peters B.

1950 a   Phys. Rev. 77, 54

Bradt H.L. and
Peters B.

1950 b   Phys. Rev. 80, 943

Bradt H.L.,
Kaplon M.F. and
Peters B.

1950   Helv. Phys. Acta 23, 24

Brooke G. and
Wolfendale A.W.

1964   Proc. Phys. Soc. 83, 843.

Brunberg E.Å.   1958   Ark. Fys. 14, 195

Caldiroli P. and
Loinger A.

1950   Nuovo Cimento 7, 1

Camerini U.,
Lock W.O. and
Perkins D.H.

1952   Progress in Cosmic Ray Physics
Vol.I, North-Holland Publishing
Co., Amsterdam, 1

Camerini U.,
Davies J.H.,
Franzinetti C.,
Lock W.O.,
Perkins D.H. and
Yekutieli G.

1951   Phil. Mag. 42, 1261

Carmichael H. and
Bercovitch M.

1969   Can. J. Phys. 47, 2073

Carmichael H., Shea M.A. and Peterson R.W.	1969 a	Can. J. Phys. 47, 2057
Carmichael H., Bercovitch M., Steljes J.F. and Magidin M.	1969 b	Can. J. Phys. 47, 2037
Cini M. and Wataghin G.	1950	Nuovo Cimento 7, 135
Conversi M.	1950	Phys. Rev. 79, 749
Cooke D.J. and Fenton A.G.	1971	Proc. 12th Int. Conf. Cosmic Rays (Hobart) 3, 923
Crookes J.N. and Rastin B.C.	1971	Proc. 12th Int. Conf. Cosmic Rays (Hobart) 4, 1325
Daniel R.R. and Stephens S.A.	1966	Proc. Ind. Acad. Sci. 63A, 275
De A.K., Ghosh P., Mitra S., Bhattacharya P.C. and Das A.K.	1972	Phys. Rev. D5, 1068
Dorman L.I.	1957	Cosmic Ray Variations, State Publishing House, Moscow.
Dorman L.I., Kovalenko V.A., Milovidova N.P. and Chernov S.B.	1970	Acta Phys. Acad. Sci. Hung. 29, Suppl. 2, 359
Feinberg G. and Lederman L.M.	1963	Ann. Rev. Nucl. Sci. 13, 431
Feynman R.P.	1969	Phys. Rev. Letters 23, 1415
Finch H.P. and Leaton B.R.	1957	Monthly Notices Roy. Astro. Soc. (Geophysical Suppl.), 7, 314
Flint R.W. and Nash W.F.	1970	Acta Phys. Acad. Sci. Hung. 29, Suppl. 4, 263
Fonger W.H.	1953	Phys. Rev. 91, 351

Frazer W.R., Poon C.H., Silverman D. and Yesian H.J.	1972	Phys. Rev. D5, 1653
Fukui S., Kitamura T. and Murata Y.	1955	J. Phys. Soc. Japan 10, 735
Fukui S., Kitamura T. and Murata Y.	1957	J. Phys. Soc. Japan 12, 854
Greisen K.	1942	Phys. Rev. 61, 212
Hagedorn R. and Ranft J.	1968	Suppl. Nuovo Cimento 6, 169
Hayman P.J. and Wolfendale A.W.	1962	Proc. Phys. Soc. 80, 710
Jones H.	1939	Rev. Mod. Phys. 11, 235
Judge R.J.R. and Nash W.F.	1963	Proc. Int. Conf. Cosmic Rays (Jaipur) 6, 68
Kamiya Y., Kawaguchi S. and Iida S.	1971	Proc. 12th Int. Conf. Cosmic Rays (Hobart) 4, 1354
Kane R.P.	1962	J. Geophys. Res. 67, 1295
Kane R.P. and Rao U.R.	1958	Proc. Ind. Acad. Sci. 47A, 30
Kane R.P. and Rao U.R.	1960	Current Science 29, 425
Kasper J.E.	1960	J. Geophys. Res. 65, 39
Keuffel J.W., Osborne J.L., Bolingbroke G.L., Mason G.W., Larson M.O., Lowe G.H., Parker J.H., Stenerson R.O. and Bergeson H.E.	1970	Acta Phys. Acad. Sci. Hung. 29, Suppl. 4, 183

Kitamura Y. and Minakawa O.	1953	Progr. Theoret. Phys. Kyoto, 10, 239
Kodama M., Kondo I. and Wada M.	1957	J. Sci. Res. Inst. Tokyo 51, 138
Kondo I., Kodama M. and Makino T.	1963	Proc. Int. Conf. Cosmic Rays, (Jaipur) 2, 386
Krimsky G.F., Krivoshapkin P.A. and Skripin G.V.	1965	Proc. 9th Int. Conf. Cosmic Rays (London) 1, 503
Krishnaswamy M.R., Menon M.G.K., Narasimham V.S., Kawakami S., Kino S. and Miyake S.	1968	Phys. Letters 27B, 535
Lal D., Pal Y. and Peters B.	1953	Proc. Ind. Acad. Sci. 38, 398
Lockwood J.A. and Webber W.R.	1967	J. Geophys. Res. 72, 3395
Mackeown P.K. and Wolfendale A.W.	1966	Proc. Phys. Soc. 89, 553
Mackeown P.K., Said S.S., Wdowczyk J. and Wolfendale A.W.	1965	Proc. 9th Int. Conf. Cosmic Rays (London) 2, 964
Maeda K.	1964	J. Geophys. Res. 69, 1725
Mathews T.	1963	Phil. Mag. 8, 387
Mathews T. and Sivjee G.G.	1967	Can. J. Phys. 45, 1643
McCracken K.G.	1962	J. Geophys. Res. 67, 423
Meyer P and Simpson J.A.	1955	Phys. Rev. 99, 1517
Neher H.V.	1951	Phys. Rev. 83, 649

Neher H.V.	1952	Progress in Cosmic Ray Physics Vol.I, North-Holland Publishing Co., Amsterdam, 243
Pal Y.	1971	Private Communication
Pal Y. and Peters B	1964	Mat. Fys. Medd. Dan. Vid. Selsk. 33, No. 15
Pal Y. and Tandon S.N.	1964	Private Communication
Peacock D.S.	1970	Acta Phys. Acad. Sci. Hung. 29, Suppl. 2, 189
Pomerantz M.A.	1970	J. Franklin Inst. 290, 207
Puppi G.	1956	Progress in Cosmic Ray Physics Vol. III, North-Holland Publishing Co., Amsterdam, 339
Quenby J.J. and Webber W.R.	1959	Phil. Mag. 4, 90
Quenby J.J. and Wenk G.J.	1962	Phil. Mag. 7, 1457
Rose D.C., Fenton K.B., Katzman J. and Simpson J.A.	1956	Can. J. Phys. 34, 968
Rossi B.	1948	Rev. Mod. Phys. 20, 537
Rossi B.	1952	High energy particles, Prentice Hall, N.Y.
Rossi B., Sands M. and Sard R.F.	1947	Phys. Rev. 72, 120
Rothwell P. and Quenby J.	1958	Suppl. Nuovo Cimento 8, 249
Sands M.	1948	Phys. Rev. 74, 1237
Shamos M.H., Levy M.G. and Lowen I.S.	1948	Phys. Rev. 74, 1237
Shapiro M.M. and Silberberg R.	1970	Ann. Rev. Nucl. Sci. 20, 323

Shea M.A., Smart D.F. and McCracken K.G.	1965	J. Geophys. Res. 70, 4117
Sheldon W.R., Cantrell W.G., Duller N.M., Cambou F., Vedrenne G., Bazer – Bachi R., Marc A. ST. and Barouch E.	1970	Acta Phys. Acad. Sci. Hung. 29, Suppl. 4, 209
Simpson G. and Mathews T.	1972	Preprint, University of Calgary, Canada.
Simpson J.A., Fonger W.H. and Treiman S.B.	1953	Phys. Rev. 90, 934
Simpson J.A., Fenton K.B., Katzman J. and Rose D.C.	1956	Phys. Rev. 102, 1648
Sitte K.	1961	Handbuch der Physik (Springer-Verlag, Berlin) Vol. 46/1, 157
Sternheimer R.M.	1956	Phys. Rev. 103, 511
Stockel C.T.	1969	J. Phys. A2, 639
Störmer C.	1955	"The Polar Aurora", Clarendon Press, Oxford
Treiman S.B.	1952	Phys. Rev. 86, 917
Vallarta M.S.	1961	Handbuck der Physik (Springer-Verlag, Berlin) Vol. 46/1, 88
Waddington C.J.	1960	Progr. Nucl. Phys. 8,1
Webber W.R.	1958	Suppl. Nuovo Cimento 8, 532
Webber W.R.	1967	Handbuch der Physik (Springer-Verlag, Berlin) Vol. 46/2, 181
Webber W.R. and Quenby J.J.	1959	Phil. Mag. 4, 654
Yeivin Y.	1955	Nuovo Cimento 2, 658